ISTANBUL TECHNICAL UNIVERSITY ★ EARTHQUAKE ENGINEERING AND DISASTER MANAGEMENT INSTITUTE

SEISMIC SIMULATION OF DAMAGED REINFORCED CONCRETE SCHOOL BUILDINGS

M.Sc. THESIS

Doruk UÇAK

Department of Earthquake Engineering and Disaster Management

Earthquake Engineering Programme

SEPTEMBER 2019

ISTANBUL TECHNICAL UNIVERSITY ★ EARTHQUAKE ENGINEERING AND DISASTER MANAGEMENT INSTITUTE

SEISMIC SIMULATION OF DAMAGED REINFORCED CONCRETE SCHOOL BUILDINGS

M.Sc. THESIS

Doruk UÇAK
(802151207)

Department of Earthquake Engineering and Disaster Management

Earthquake Engineering Programme

Thesis Advisor: Assoc. Prof. Dr. Reşat Atalay OYGUÇ

SEPTEMBER 2019

İSTANBUL TEKNİK ÜNİVERSİTESİ ★ DEPREM MÜHENDİSLİĞİ VE AFET YÖNETİMİ ENSTİTÜSÜ

HASAR ALMIŞ BETONARME OKUL BİNALARININ SİSMİK SİMÜLASYONU

YÜKSEK LİSANS TEZİ

Doruk UÇAK
(802151207)

Deprem Mühendisliği ve Afet Yönetimi Anabilim Dalı

Deprem Mühendisliği Programı

Tez Danışmanı: Doç. Dr. Reşat Atalay OYGUÇ

EYLÜL 2019

Doruk UÇAK, an M.Sc. student of ITU Institute of Earthquake Engineering and Disaster Management student ID 802151207, successfully defended the thesis entitled "SEISMIC SIMULATION OF DAMAGED REINFORCED CONCRETE SCHOOL BUILDINGS", which he prepared after fulfilling the requirements specified in the associated legislations, before the jury whose signatures are below.

Thesis Advisor : Assoc. Prof. Dr. Reşat Atalay OYGUÇ ....
Istanbul Technical University

Jury Members : Prof. Dr. Tülay Aksu ÖZKUL ....
Istanbul Technical University

Asst. Prof. Dr. Gökçe TÖNÜK ....
MEF University

Date of Submission : October 10th, 2019
Date of Defense :   September 12th, 2019

To my mother and father,

FOREWORD

TABLE OF CONTENTS

ABBREVIATIONS

AFAD   **:** Disaster and Emergency Management Presidency
ADRS   **:** Acceleration displacement response spectra
Acc.   **:** Acceleration
App.   **:** Appendix
BPF   **:** Band pass filter
CCS   **:** Construction Control and Supervising Law
DAP   **:** Displacement based adaptive pushover
EEDMI   **:** Earthquake Engineering and Disaster Management Institute of Istanbul Technical University
ELSA   **:** European Laboratory for Structural Assessment
ESS   **:** Error sum-of-squares
EQ   **:** Earthquake
FAP   **:** Force based adaptive pushover
FFA   **:** Fourier frequency analysis
GIS   **:** Geographic Information Systems
ITU   **:** Istanbul Technical University
KOERI   **:** Kandilli Observatory and Earthquake Research Institute of Boğaziçi University
MDOF   **:** Multiple degree of freedom
SA   **:** Spectral acceleration
SD   **:** Spectral displacement
SDOF   **:** Single degree of freedom
SRSS   **:** Square root of the sum of the squares
STD   **:** Standard deviation

LIST OF TABLES

SEISMIC SIMULATION OF DAMAGED REINFORCED CONCRETE SCHOOL BUILDINGS

SUMMARY

Detailed site investigation studies of 2011 Van Earthquake have provided valuable information about the aftermath of the event. Using the field reports, two irregular reinforced concrete school buildings located near Van, Turkey were examined in this study, in an attempt to predict the possible damage in such buildings by re-creating the scenario digitally using non-linear analysis methods and degrading material models.

One of the buildings that were studied was found by the field teams as totally collapsed and the other one with substantial damage. It was evident that both buildings have experienced the consequences of bad engineering practice. Insufficient shear capacity and small column sections coupled with poor workmanship and poor quality materials contributed to the damage.

Using ZEUS-NL, a non-linear analysis tool created by the University of Illinois; pushover, adaptive pushover and time-history analyses were conducted. In order to model the buckling and fracture of rebars, a modified Menegotto-Pinto model was implemented. The concrete model that was used degrades in strength and stiffness under cyclic loads. In order to follow a stochastic approach, 7 hazard-compatible earthquake records were used in the analyses. Records were amplified to match the design spectrum (Max Sa: 1.0g, Ta: 0.12s, Tb: 0.6s) by using a series of iterations.

Pushover and adaptive pushover methods were useful in order to determine the shear capacity of both buildings. Adaptive pushover produced a more convervative result, governing the shear capacity. For sake of simplicity, time-history analyses were only conducted on the weaker directions of both buildings. In all 7 cases, shear capacity of buildings were exceeded. Plastic hinge development was mostly present in the first and second story of both buildings. Both buildings have exceeded the allowable interstory drift of 0.5%.

The first section gives introductory information on the Van Earthquake of 2011 as well as the literature review that was of utmost importance for this study.

Second section is about strong ground motion data and their applicability in certain cases. Strong ground motion simulations, synthetic records, PGA-scaling methods are discussed. Seismicity of Van Province is also discussed in this section as well as field investigation reports. In addition, strong ground motion record set that has been used for this thesis study is revealed.

Third section discusses the theoretical and practical background of non-linear static and non-linear dynamic analysis. Types of analyses and their scientific reasoning are discussed.

Fourth section covers material properties and material models that are used in structural analysis. Differences between degrading and non-degrading models and the history of development of advanced material models are revealed.

Fifth section is the explanation of methods of analytical study of this thesis. Analysis methods that were implemented are discussed in this section

Sixth section is about results of the analytical study. Aside from the results, this section also contains a discussion of results section where findings of the study are examined.

Seventh section is the conclusion where the study is summarized and the overall outcome of the study is discussed.

HASAR ALMIŞ BETONARME OKUL BİNALARININ SİSMİK SİMÜLASYONU

ÖZET

2011 Van Depremi ardından yapılan saha inceleme çalışmaları detaylı ve önemli bilgiler sağlamaktadır. Bu çalışmada, saha inceleme çalışmalarından yola çıkarak Van Merkez İlçesi'nin yakınında bulunan iki düzensiz betonarme okul binası doğrusal olmayan analiz yöntemleri ve azalımlı malzeme modelleri kullanarak modellenmiş, bu iki binada oluşan hasar simüle edilmiştir.

İncelenen yapılardan biri bir ilköğretim okulu olup saha ekipleri tarafından çökmüş halde bulunmuştur. Diğeri ise ciddi hasar gören fakat yıkılmamış halde bulunan bir kurs binasıdır. Her iki yapının da kötü mühendislik uygulamaları sebebiyle hasar gördüğü tespit edilmiştir. Yetersiz kesme yük kapasitesi, özensiz işçilik, kalitesiz malzeme kullanımı ve yetersiz kolon boyutları hasarda etkili olan faktörler olarak öne çıkmıştır.

Bu tez kapsamında, Illinois Üniversitesi tarafından geliştirilen ZEUS-NL adlı bir doğrusal olmayan analiz yazılımı kullanılarak, itme, uyarlamalı itme ve zaman-tanım aralığı analizleri yapıldı. Donatıların bükülme ve kırılmalarını modellemek için güncellenmiş bir Menegotto-Pinto modeli uygulandı. Kullanılan beton modeli, çevrimsel yükler altında dayanım ve rijitlik seviyesinde azalıma izin vermektedir. Stokastik bir yaklaşım izlenerek analizlerde birbiriyle benzer özellikli 7 deprem kaydı kullanılmıştır. Kayıtlar, bir dizi iterasyon kullanılarak tasarım spektrumuna (Max Sa: 1.0g, Ta: 0.12s, Tb: 0.6s) uyacak şekilde büyütülmüştür.

Her iki binanın kayma kapasitesini belirlemek için itme ve uyarlamalı itme yöntemleri kullanılmıştır. Uyarlamalı itme, itme analizine kıyasla daha konservatif bir sonuç üretmiştir. Analizleri sadeleştirme adına, zaman tanım aralığı analizleri yalnızca binaların zayıf yönlerinde gerçekleştirildi. 7 depremin tümünde binaların kesme yük kapasitesi aşıldı. Plastik mafsal gelişimi, her iki binanın birinci ve ikinci katında daha fazla oluştu. Her iki binada da izin verilen % 0,5'lik göreli kat ötelemesi limiti aşıldı.

İlk bölüm, 2011'in Van Depremi hakkında tanıtım bilgileri ve bu çalışma için son derece önemli olan literatür taramasını sunmaktadır.

İkinci bölüm kuvvetli yer hareketi verileri ve verilerin uygulanabilirliği ile ilgilidir. Kuvvetli yer hareketi simülasyonları, sentetik kayıtlar, PGA ölçeklendirme yöntemleri tartışılmıştır. Van depreminin ve bölgenin sismik durumunun ayrıntıları da bu bölümde paylaşılmaktadır.

Üçüncü bölümde, doğrusal olmayan statik ve doğrusal olmayan dinamik analizlerin teorik ve pratik arka planı tartışılmaktadır. Analiz türleri ve bilimsel gerekçeleri tartışılmaktadır.

Dördüncü bölüm, malzeme özelliklerini ve yapısal analizde kullanılan malzeme modellerini kapsar. Azalımsal ve klasik modeller ile ileri malzeme modellerinin gelişim süreci ve aralarındaki farklardan bahsedilmektedir.

Beşinci bölüm, bu tezin analitik çalışma yöntemlerinin açıklamasıdır. Uygulanan analiz yöntemleri bu bölümde ele alınmıştır.

Altıncı bölüm analitik çalışmanın sonuçlarnı paylaşmaktadır. Elde edilen sonuçların yanı sıra, bu bölüm çalışmanın bulgularının incelendiği bir alt başlığı da içermektedir.

Yedinci bölüm çalışmanın özetlendiği ve çalışmanın genel sonucunun tartışıldığı bölümdür.

1. INTRODUCTION

On 23rd of October 2011, a Mw 7.1 earthquake has struck Van, Turkey. The earthquake caused severe damage in the region, collapsing 58 buildings and affecting 18,464 others. Local authorities have reported 644 casualties in addition to 1966 injured and 251 rescued victims (EEDMI, 2011). According to a report published by KOERI (2011), 2.223 aftershocks have occurred, which include 104 shocks with magnitudes between 4.0 and 5.0, and 7 shocks with magnitudes between 5.0 and 6.0. Figure 1.1 shows the epicenter and epicentral distances of the Van earthquake of October 23.
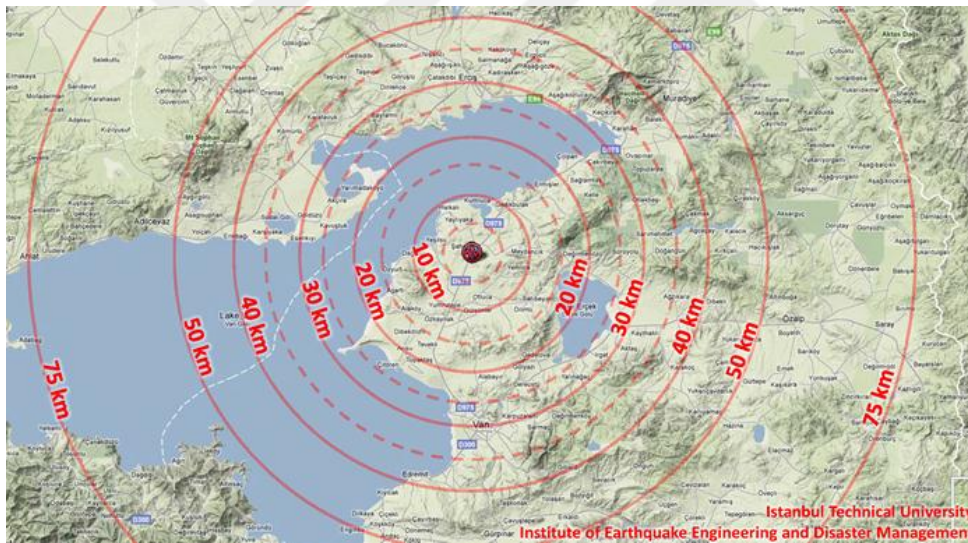
Figure 1.1 :   Epicentral disctances of Van Earthquake. (EEDMI, 2011).

Several articles reveal that most of the building stock in the region had been built before Construction Control and Supervising Law of 2011 (CCS) was put in effect, making the quality of construction dubious (Taskin et. al, 2013)(Di Sarno et. al, 2013). Field reconnaissance studies report that use of low-grade and inadequate materials was common in the region. Workmanship is reported to be poor as well, including incorrect use of stirrups and sloppy concrete mixtures. Figure 1.2 shows large pebbles used as aggregate in concrete.

1

Figure 1.2 : Pebble use in concrete mixtures in Van region (Taskin et. al 2013; Yazgan et. al, 2016).

Field teams have also reported inadequate outer concrete cover and poor anchorage as well. Stirrups were hooked 90 degrees throughout the region which provide nearly no confinement.

About one-third of the building stock was considered aseismically designed as they were completed before 1980s (Oyguc et. al, 2018). Soft stories, high torsional flexibilities, strong beam-weak column connections, short column effects and inadequately spaced buildings were reported in site investigation reports (Oyguc, 2015)(Yazgan et. al (2016)(Taskin et. al 2014)(Di Sarno et. al 2012). Figure 1.3 shows buildings with faulty seismic designs.

Figure 1.3 : Soft story situation and inadequate separation between adjacent buildings in Van Province (EEDMI Reconnaissance Photos, 2011)

Turkish Earthquake Code has been revised for seven times since 1947 (AFAD). Therefore, seismic design procedures were in place long before the year 2011. However, it was common among contractors to take out structural elements from the designs, mainly to cut costs. An elementary school in the town of Gedikbulak, Van was a result of such contractor negligence. According to reports, the contractor has purposely skipped building some of the shear walls that were in the original design. The school building had collapsed in the main shock on 23rd of October, due to lack of shear capacity and high torsional flexibility (Yazgan et. al 2016; Bal et. al 2015).

Figure 1.4 : Elementary school buildings of same design. Left: Construction conforming to the original design (EEDMI report). Right: Collapse due to missing shear walls (Yazgan et. al, 2016).

Field reports have shown that newly constructed buildings in the region have only seen slight damage (Yazgan et. al 2016).

Inadequate structural engineering practice and sloppy construction techniques have resulted in the catastrophe that happened during the main shock. Thousands of people have suffered the consequences and hundreds were killed during and after the main shock.

1.1 Purpose of Thesis

Advances in technology make it possible to solve complex problems accurately and with ease. Nowadays, most personal computers are powerful enough to analyze 3-D models beyond their elastic range. With that in mind, engineering professionals throughout the world are being encouraged to use inelastic analysis procedures. Non-linear analysis is a robust way to assess the behavior of structures when they are pushed beyond elastic range. Major earthquakes put a greater seismic demand than elastic capacity of most engineered structures (Deierlein et. al, 2010). Therefore, engineers need to keep inelastic behavior in check, especially in the seismically active regions such as Turkey.

Despite its necessity and ever-growing computer technology, non-linearity is still a challenge from an engineering perspective. Non-linear analysis is an iterative process where the computer searches for a solution that is close enough to the engineer. Iterations follow modeled material stress-strain curves as well as changes in structural geometry. Inelastic range is supposed to be a representation of the real world where an infinite number of variables take place simultaneously. Since computers cannot deal with too many unknowns, analyses need to be idealized while keeping major aspects of non-linear behavior.

One of the idealized parameters of non-linear analysis is plastic hinging. For sake of simplicity, engineers often allow plastic behavior on predetermined locations along members (concentrated hinge). That is a time saving approach for properly engineered structures. However, it is an unfavorable method for performance analysis of existing buildings. Deierlein et. al (2009) state that concentrated plastic hinging approach can underestimate strength loss due to buckling and non-linearity. Newer and more robust computational methods can detect plasticity along entire lengths of structural members, giving results that are more realistic. On the other hand, material models have a major role in non-linear analysis. Most structural analysis software use simple, non-degrading material models that are almost too idealized. However, field reconnaissance photos of Van earthquake show many instances of material degradation in the form of buckled or fractured rebars, deep cracks on concrete, and failed column-beam connections. It is evident that those buildings have had altered seismic responses after a certain time into the earthquake,

due to changes in material properties and section geometry. It is a well-known fact that cyclic loads can cause strength and stiffness degradation. Therefore, technically it would make better sense to implement degrading material models to simulate seismic behavior of buildings that have already been damaged.

This study investigates the effectiveness of degrading material models by conducting seismic simulation of two reinforced concrete school buildings that were heavily damaged by the Van earthquake of October 23, 2011.

1.2 Problem Statement

Numerous field investigation reports and seismic analysis studies were published following the 2011 Van earthquake. Seismic analysis of buildings from the field reports have been conducted mostly using a straightforward approach. Due to distance related issues, using the real Van earthquake record directly is likely to cause a decrease in the response of analyzed structures. For the same reason, some of the characteristics of the earthquake are probably not accounted for in the Van earthquake record. That hypothesis raises the question of whether there could be a more suitable way to simulate the Van earthquake. In addition to the problem with the earthquake record itself, field investigation reports of Van earthquake reveal a widespread occurrence of failing steel bars, and concrete sections. These findings are often overlooked in structural analysis. It would make better sense to account for those findings as they can make a significant change in the response of analyzed structures.

Several studies focus on the abovementioned problems. Oyguc, Oyguc and Tonuk (2018) have studied buildings that were damaged in the 2011 Van earthquake. They mention that the only available strong ground motion record do not represent the actual shock due to far-field effects. Instead, they have used a set of six selected records, fitted to the NEHRP target acceleration spectrum. The selection was conducted using the hazard-compatibility criteria published by Tönük et. al (2014) with the help of a coordinate-based spatial distribution of simulated PGA, PGV and SA values of the Van region by Zengin and Cakti (2014). Zengin and Cakti (2014) have published an isometric map of the Van Earthquake with simulated PGA, PGV, and SA values providing the reader with precise strong ground motions for specific coordinates. Following the strong ground motion record selection, the two buildings

of interest have analyzed using static adaptive pushover, and dynamic time-history analysis.

In the article, Oyguc, Oyguc, and Tönük (2018) state that both buildings (A and B) were designed and build aseismically with no shear walls. Both buildings were built according to the TEC of 1975. According to the study, adaptive pushover procedure can provide more conservative results compared to static pushover analysis as it considers irregularity effects. They have calculated weights of the structure A and B as 11,157 kN and 7,465 kN, respectively using the G+nq equation. For the dynamic time-history analysis, they have applied the selected set of earthquake records by assuming a 5% constant damping ratio and neglecting second order effects. They have ran a total of 48 analyses, analyzing both directions of buildings using the two components of the strong ground motions. In the study, they have plotted base shear versus roof drift in order to visualize the dissipated energy. Through those plots, Oyguc, Oyguc and Tonuk have shown that the simulation results represent the in-situ condition of the buildings A and B. They also have stated that the dynamic time-history results are in good correlation with the adaptive pushover analysis results, in terms of hysteretic behavior.

Oyguc, Oyguc and Tonuk (2018) conclude that the results correlate well with the in-situ condition of the studied buildings, as both buildings have exceeded the 0.5% inter-story drift ratio limit, both buildings have experienced residual story drift, and both buildings have behaved inelastically.

Kappos et. al (2007) have published a study that is similar to Oyguc, Oyguc, and Tonuk (2008), that was done for a seismic risk analysis of Athens. Study uses simulated near-field strong ground motions through stochastic and deterministic methods.

Abdelnaby (2014) have coded a degrading steel model and a degrading concrete model into a non-linear analysis tool called ZEUS-NL. His version of material models has yielded significantly greater responses in structures during aftershocks, due to degrading materials properties. The model incorporates bar buckling and fracture, and strength losses of concrete.

2. STRONG GROUND MOTION EVALUATION

2.1 Van Earthquake

Province of Van is located in the Turkish-Iranian plateau, where Eurasian and Arabian plates are colliding (Dewey et al., 1986). The collusion creates a north-south convergence at a rate of 23mm/yr (Reilinger et. al, 2006). The region is surrounded by several fault systems such as the Bitlis-Zagros Fault Line, the North Anatolian Fault line, and the East Anatolian Fault Line. According to Elliot et al. (2013), the northward movement of the Van region is significantly slower at a rate of 5 mm per year. This slow movement is an indication of strain accumulation near Lake Van (Konca, 2015). Van region experiences significant earthquakes periodically, such as the magnitude 7.5 earthquake of Çaldıran in 1976.

The most recent major earthquake in Van occurred on October 23, 2011. Moment magnitude 7.1 main shock was followed by thousands of aftershocks, including a M_L 5.7 shock that was strong enough to cause additional damage in the region. Strong ground motion records of the earthquake are given in Figure 2.1.
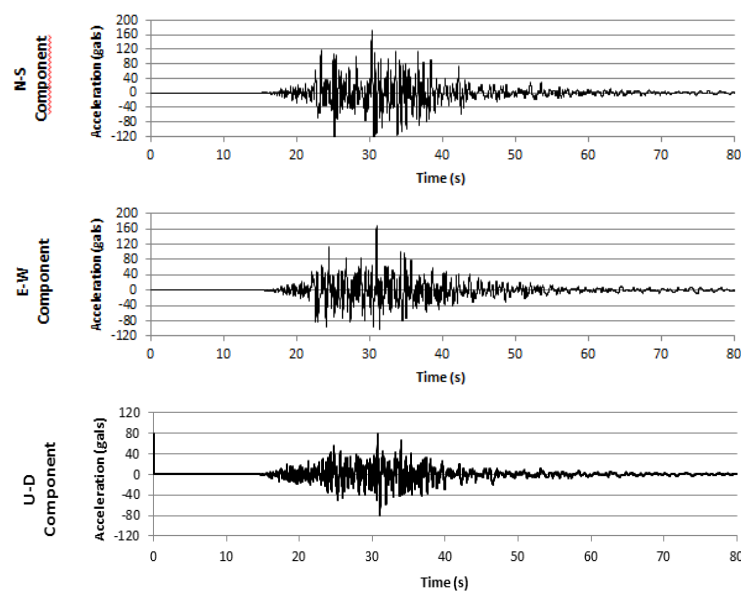
Figure 2.1 : Accelerogram of October 23, 2011 Van Earthquake.

The main shock was detected by 22 strong ground motion stations in Turkey and 11 stations in Iran (Zengin and Cakti, 2014). Turkish stations that are operated by AFAD are shown in Figure 2.1.

Figure 2.2 : AFAD's strong ground motion recording stations that detected the October 23, 2011 Van earthquake (Zengin and Cakti, 2014).

Unfortunately, the strong ground motion recording station near the epicenter was temporarily out of service at the time of the main shock. Peak ground motion values recorded by the closest available ground motion recording station is given in Table 2.1

Table 2.1 : PGA values of Van earthquake recorded by Van-Muradiye station #6503 (AFAD)

North-South	East-West	Up-Down
178.5 gals	169.5 gals	79.5 gals

AFAD's Muradiye strong ground motion station (6503) is located approximately 40 kilometers north-east of the epicenter which is quite far to represent the earthquake accurately. Furthermore, given the intensity near the epicenter, peak accelerations recorded by the station are quite low. Figure 2.2 shows intensity contour map of the main shock generated by ELER software (KOERI, 2011). An area with a diameter of approximately 20 kilometers have experienced VIII (severe) intensity, while a greater area experienced VII on the Modified Mercalli Intensity Scale (MMIS). Level VIII is defined as "Slight damage in specially designed structures;

considerable damage in ordinary substantial buildings with partial collapse. Great damage in poorly-built structures. Fall of chimneys, factory stacks, columns, monuments, walls. Heavy furniture overturned.". The definition fits the aftermath of the Van earthquake well. However, PGA of 178.5 gals would not create that much motion.
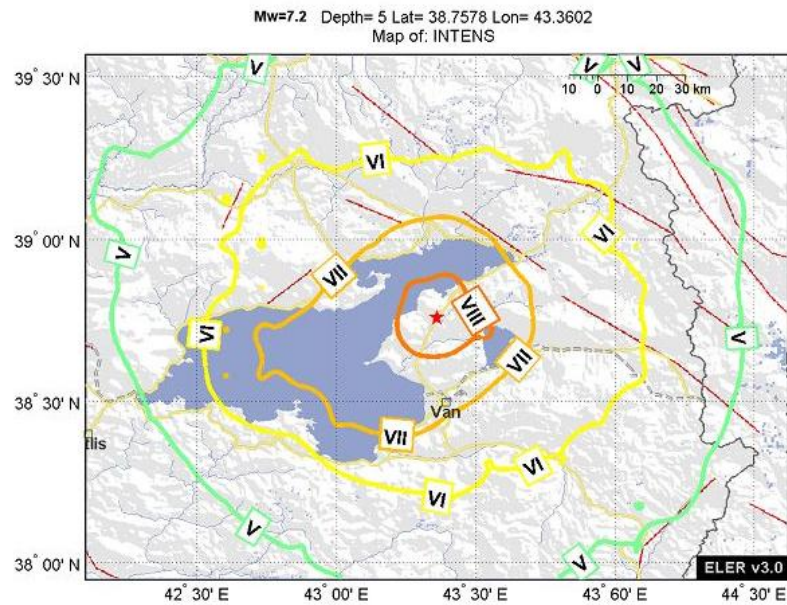
Figure 2.3 : Intensity shake map generated by ELER v3.0 by KOERI (Press Release 2011)

As a result, in order to make sensible further analyses, simulated accelerograms would have to be used.

According to KOERI (2011), PGAs recorded by stations within 200 kilometers of the epicenter are in good agreement with simulated PGA values. Therefore, it is possible to use simulated data for regions that are close to the epicenter. Figure 2.4 shows the correlation between recorded PGAs and simulated PGAs. The graph shows that near the epicenter peak ground acceleration should be in the range of approximately 0.6g-0.4g.
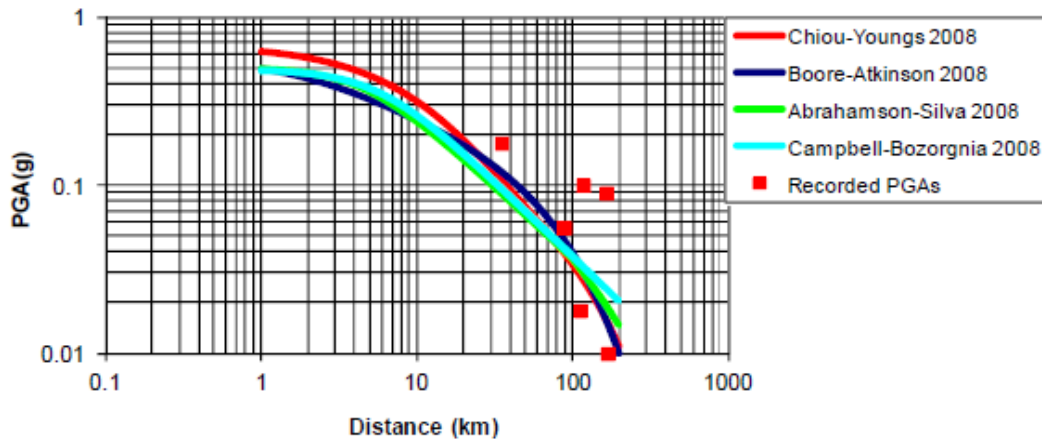
Figure 2.4 : Comparison of recorded PGAs and simulated PGAs (KOERI, 2011).

2.2 Strong Ground Motion Selection

Tectonic activities are monitored and studied by researchers extensively. Despite a constant supply of seismic data, earthquake is still not a fully understood phenomenon due to the chaotic nature of the Earth.

Each earthquake has unique characteristics, such as fault-mechanism, frequency content, local site conditions, and shear wave velocity. Researchers can determine those characteristics only after an earthquake has happened. Even then, it is a challenge to create computer models of observed seismic behavior.

Van earthquake was recorded by a distant strong ground motion station. Hence, it is not a viable option to use the record for seismic analyses. Kappos et. al (2007) report that near-field strong ground motions can be simulated in cases of data unavailability using stochastic and deterministic methods, together. Oyguc, Oyguc, and Tonuk (2018) have used a similar approach for Van earthquake combining stochastic method with NEHRP record selection and PGA scaling methods.

2.3 Record Synthesis Methods

There are two ways of generating simulated strong ground motion: empirical and stochastic methods. Empirical approach strongly depends on stable regressions of a large data set of magnitudes, distances and source mechanism using Green's Equations (Massa et. al, 2008). The objective is to generate a design earthquake

signal using empirical formulas created by incorporating as many data points as possible. Stochastic approach do not depend on datasets, instead it requires input parameters. The goal is to generate a design earthquake that fits into a description.

Motazedian and Atkinson (2005) state that stochastic approach results in a more realistic representation of earthquakes, due to resultant signal's complexity in high frequencies. On the other hand, other research show empirical approach resonates with near-fault ground motions due to its low frequency content (Pitarka et. al 2000). Both methods have pros and cons regarding intended use and outcomes.

2.3.1 Empirical strong ground motion method

Empirical approach is often used in tectonically active regions where earthquakes happen frequently. A large data set is collected and then processed in order to create attenuation relations (Douglas, 2005). Those relations are then used to create a design accelerogram using synthetic signal generators (Hutchings et. al, 2012; Fahjan et. al, 2014).
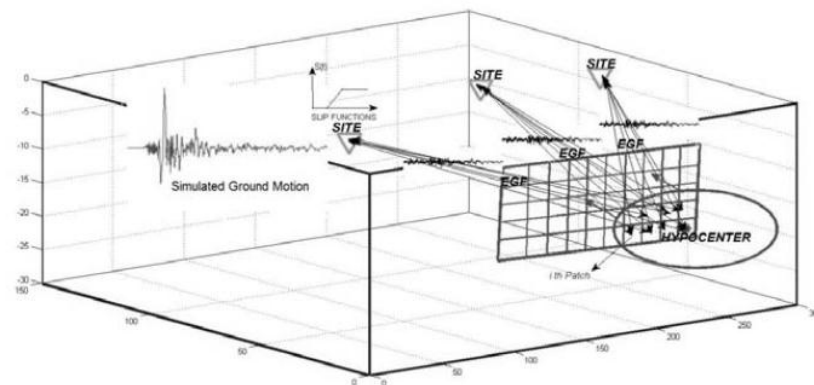
Figure 2.5 : Empirical strong ground motion method in generating design earthquake (Fahjan et .al, 2014).

According to research, efficacy of empirical approach depends on the information available on source and path characteristics, site effects, and the return period, fault mechanism, hanging wall effect and site response (Abrahamson and Silva (1997); Douglas (2005)). As shown in Figure 2.5, empirical methods use site characteristics at monitoring stations and project those into the target site. Keeping that in mind, empirical approach is best when site and path characteristics are homogenous between the source and target areas.

11

2.3.2 Stochastic strong ground motion method

Stochastic methods do not need a data set in order to simulate an earthquake. Only parametric and functional descriptions are needed to generate a design seismic signal. Those input parameters are entered into special software, such as EXSIM, to generate synthetic ground motion signals. Figure 2.6 shows the overview of stochastic approach..

Target ground motion's amplitude spectrum is combined with a random phase spectrum in order to account for high frequency content of earthquake signals.
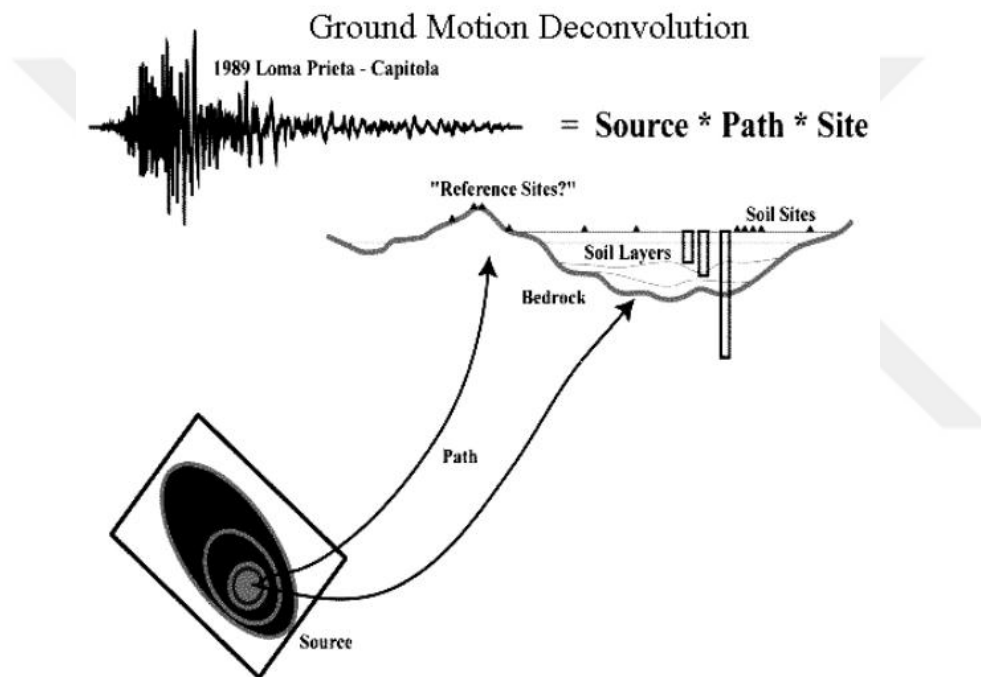
Figure 2.6 : Overview of stochastic approach (Boore, 2004)

Boore et. al (2003) reports that this method is best for simulating major earthquakes where no strong ground motion records are available in the region. Parameters used in generation of ground motion include, moment magnitude, hypocenter location, strike and dip angle, fault dimensions, slip distribution, stress drop, shear-wave velocity, density, site amplification, and distance-dependent duration (Sun et. al, 2018)

According to Sun et. al (2018), synthetics can be used in an area to simulate strong ground motion, in a coordinate sensitive manner. Researchers have created successful simulations of earthquakes using finite-fault stochastic methods (Kappos et. al 2009; Zengin and Cakti, 2013).

2.4 Simulations of Van Earthquake

Zengin and Cakti (2013) have created synthetic simulations of Van earthquake of October 23 around the epicenter. They have divided the region into approximately 2500 grids with dimensions of 5 kilometers by 5 kilometers. For each grid, they have generated a synthetic earthquake record using stochastic finite fault method.

Finite-fault method is an improved version of stochastic point-source method. In finite-fault method a large fault is divided into N sub-faults, where each sub-fault is considered as a small point-source. Contribution of each sub-fault to the ground motion is calculated by the point source method. Then they are combined at the observation point. Figure 2.7 shows correlation between observed and simulated pseudo-acceleration response spectra using stochastic finite-fault method. Two response spectra are in good agreement, which justifies the use of this method in strong ground motion simulation.
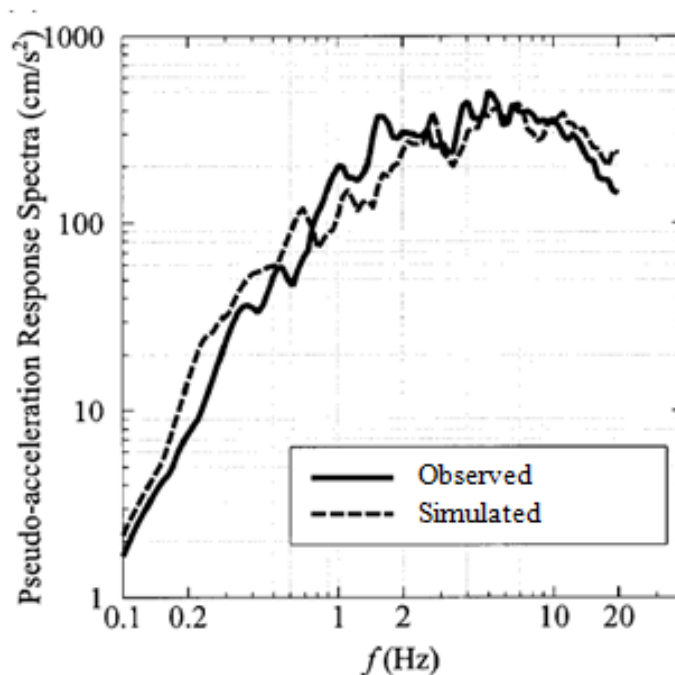

Figure 2.7 : Correlation between 1994 Northridge earthquake and stochastic finite-fault method (Motazedian and Atkinson, 2005).

Zengin and Cakti (2013) used fault geometry, slip distribution, rupture velocity, and stress drop for simulation of Van earthquake. For coordinate sensitive adjustments, path effects including regional quality factors have been used in the input parameters

13

to simulate realistic site-specific acceleration time history. Accurate synthetic generation of S-waves strongly depends on quality factor, spectral decay functions, and shear wave velocity. Hence, Zengin and Cakti (2013) used local geomorphology studied by Zor et. al (2007) regarding crustal attenuation of the Turkish plateau. Following signal generation, Zengin and Cakti (2013) calibrated the signals using observed strong ground motion data of the Van earthquake using misfit function in frequency domain.

In their study (2013), Zengin and Cakti revealed that synthetic signals they created using finite-fault method are in good agreement with the ground motion recording station 6503, as shown in figure 2.8 and 2.9. Given that it is the closest available station, it is safe to say that their synthetic records are well calibrated, and can be used in further analyses.
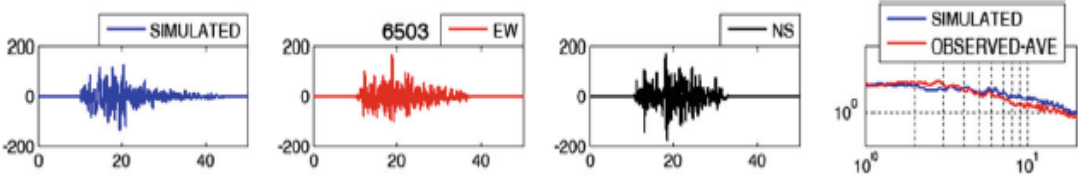
Figure 2.8 : Simulated and observed accelerograms and Fourier amplitude spectra of Van earthquake at station 6503 (Zengin and Cakti, 2013).
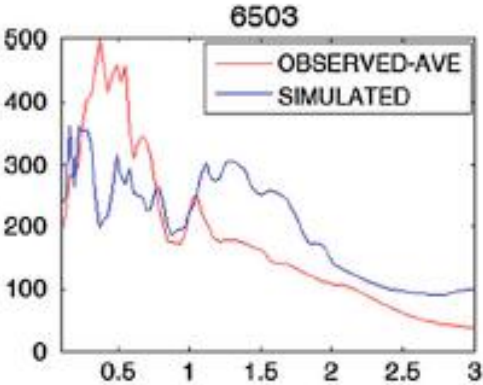
Figure 2.9 : Simulated and observed response spectra at station 6503 (Zengin and Cakti, 2013).

Following successful calibration of synthetic site-specific signals, Zengin and Cakti (2013) created spatially assigned synthetic signals of the epicentral region. Figure 2.10 shows simulated PGA values of synthetic acceleration time histories. Results

show a PGA of 400 to 600 gals near the hypocenter. Results coincide with the PGA values from KOERI (2011) simulations as shown in Figure 2.4.
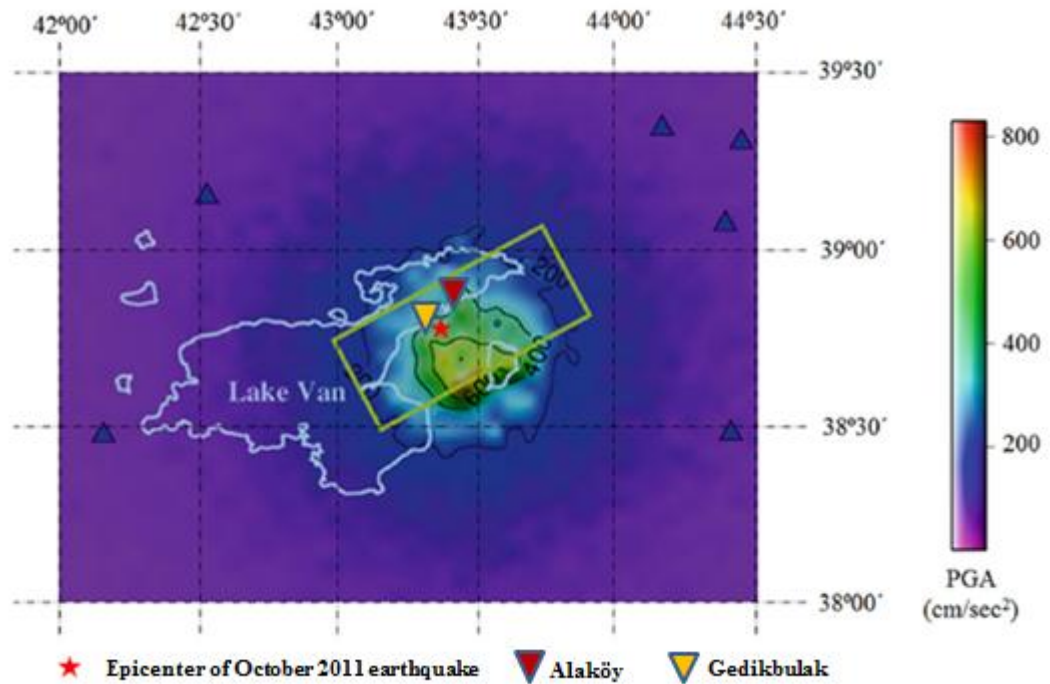
Figure 2.10 : Contour map of simulated PGA values of Van region for 2011 Van Earthquake. Epicenter is marked on the fault plane. Zengin and Cakti (2013).

Zengin and Cakti (2014) have also created a peak response-acceleration contour map for the region. Using site-specific parameters, PRA values (T=0.3s) have reached up to 1500 gals near the hypocenter. Figure 2.11 shows contour map of PRA values of the region.

Figure 2.11 : Peak response acceleration spectra (PRA) (Zengin and Cakti, 2013).

2.5 Amplitude Scaling Procedures

Source and path characteristics are unique to each earthquake. Regardless of the simulation method of choice, it is almost impossible to account for every aspect of a particular earthquake. Hazard studies use determi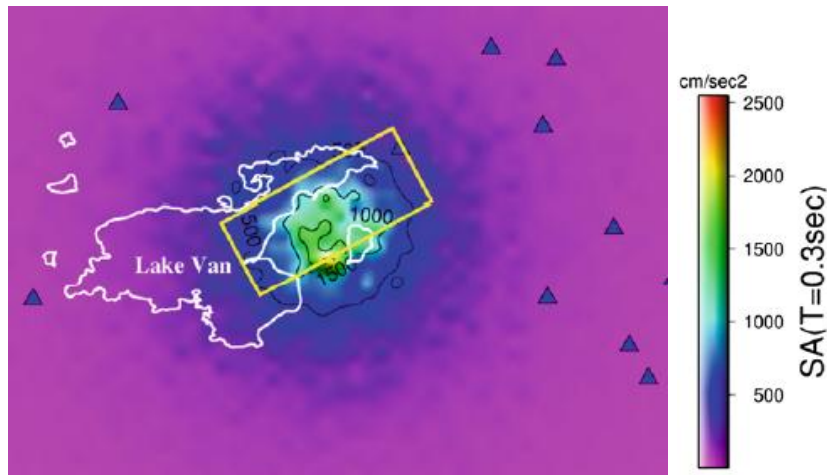nistic or probabilistic approaches in order to create site compatible design earthquakes. Ansal and Tönük (2007) have shown that response histories change drastically when considering a few hazard-compatible strong ground motion records, compared to a deterministic approach. Tönük et. al (2013) state that in order to cover uncertainty associated with earthquakes, a representative number of strong motion acceleration records need to be considered when creating design earthquakes. Selected earthquakes need to undergo a scaling procedure in order to achieve consistency. Fahjan (2008) reports three methods that can be used for record scaling: an empirical time-domain scaling method, a multiple earthquake time-domain scaling method, and a frequency-domain scaling method. The empirical method depends on regression of multiple strong ground motion data and using that to calculate a scale factor. Multiple-earthquake method guidelines selection of a set of hazard-compatible strong ground motion records and have those fit a target spectrum. Lastly, frequency-domain scaling method scales the selected records by altering their frequency content in order to fit a target spectrum. The result is nearly perfect; however, altered frequency content can negatively affect the site-specific characteristics.

Tönük et. al (2013) conducted a comparison study using different scaling methods for input strong ground motion set used in 1D site response analyses. They have compared a PGA scaling method, an optimized PGA scaling method, and a frequency domain spectrum scaling method. PGA scaling method applies the same amplification factor to all earthquake records. On the contrary, optimized PGA scaling method uses an iteration process where each earthquake in the data set is assigned a different scaling factor. Figure 2.12 shows comparison of PGA scaling and optimized PGA scaling methods.
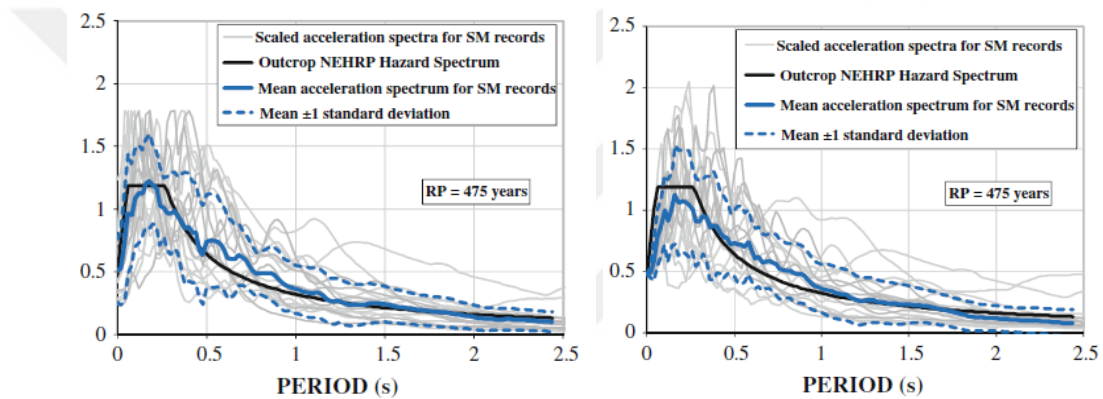
Figure 2.12 : Left: Optimized PGA scaling based on iterative processes. Right: PGA scaling of strong ground motion set (Tönük et. Al, 2013).

As shown in Figure 2.12, optimized PGA scaling method gives slightly better results. The mean acceleration spectrum in PGA scaling method does not exceed the target spectrum. Optimized PGA scaling method, on the other hand, fulfills that criterion. Tönük et. al (2013) report that their preferred method of strong ground motion scaling is the iteration based best-fitting mean-spectrum approach.

2.6 Strong Ground Motion Selection Criteria

Correct selection of strong ground motion is crucial. Frequency content of strong ground motions can greatly alter dynamic response of structures. Structures with high ductility, high irregularity, and dominant higher-modes are affected the most (Bommer and Acevedo, 2004).

Researchers report that the selection criteria for strong ground motion are: earthquake magnitude, site classification, fault mechanism, source distance, duration, shear-wave velocity, and PGA range. It is also recommended to use PEER database to search for earthquake records that match a target NEHRP (2003) spectrum. (Bommer and Acevedo, (2004); Tönük et. al (2013)).

2.7 Strong Ground Motions Used in This Study

Upon careful searching, seven hazard-compatible earthquakes were selected considering following criteria: magnitude range, PGA range, source distance, fault mechanism, and average shear wave velocity. PGA values were obtained from Zengin and Cakti (2013). The selected earthquakes were then scaled to fit the NEHRP design spectrum. As shown in figure 2.13, the best fit was achieved using the optimized PGA scaling method, which was published by Tönük et. al (2014). The process achieves the best fit by scaling the mean spectrum of selected records, through amplifying strong ground motion records individually by corresponding scale factors. Set of selected hazard-compatible strong ground motions are given in Table 2.2.
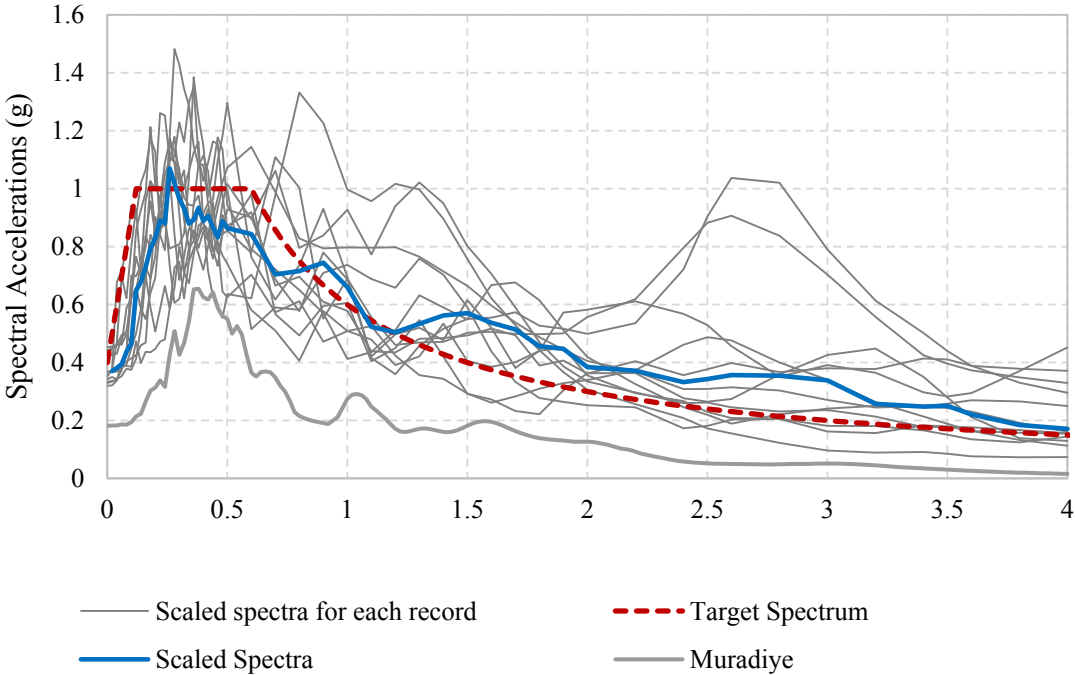

Figure 2.13 : Spectra scaling guidelined by Tonuk et. al (2014)

Table 2.2 : Earthquakes that were selected for dynamic time-history analysis.

Earthquake Name	Magnitude	Mechanism	Rjb (km)	Rrup (km)	Vs30 (m/sec)	Initial-search Scale Factor
Tabas Earthquake	7.35	Reverse	24.07	28.79	324.57	2.4601
Landers Earthquake	7.28	Strike slip	23.62	23.62	353.63	1.1937
Cape Mendocito Earthquake	7.01	Reverse	16.64	19.32	387.95	0.837
El Mayor-Cucapah Earthquake	7.20	Strike slip	14.8	17.32	242.05	1.1798
Darfield Earthquake	7.00	Strike slip	19.89	19.89	198	0.9915
Darfield Earthquake	7.00	Strike slip	18.4	18.4	194	1.1223
Darfield Earthquake	7.00	Strike slip	18.73	18.73	263.2	0.9751

3. REVIEW of NON-LINEAR ANALYSIS METHODS

Non-linearity is a concept that contains uncertainties. It requires computer iterations to calculate the next data point on the force-deformation curve. There are a number of non-linear analysis methods available today. Non-linear analysis methods can be separated into two main types: Non-linear static and non-linear dynamic. Static methods use static forces or displacements applied incrementally to capture the force-deformation curve, independent of time. Dynamic methods apply cyclic loads onto the structure, such as seismic accelerations, that lasts for a duration of time.

According to FEMA (2005) static and dynamic procedures deviate from each other due to following factors: inaccuracies in the equal displacement approximation in the short period range, P-delta effects and instability, static load vector assumptions, strength and stiffness degradation, multi-degree of freedom effects, and soil-structure interaction effects. According to Antioniou and Pinho (2004), non-linear static procedures only consider material strength and strain relationship, leaving out other sources of energy dissipation such as kinetic energy, effects of damping, and effect of time duration. Iervolino et. al (2006) reports that time duration does not affect displacement ductility; however, it affects other demand parameters such as hysteretic ductility, and equivalent number of cycles. Elnashai and Papanikolaou (2004) report similar differences of static and dynamic non-linear analysis procedures. As a conclusion, dynamic analysis methods are more realistic, but static analysis methods are more practical. Hence, researchers are working towards improving non-linear static procedures in order to achieve results that are more realistic.

The most popular type of non-linear static analysis is pushover analysis. According to Papanikolaou (2000), pushover analysis has no theoretical background. However, researchers continue to create better versions in order to get as close to dynamic analysis as possible. Below, different types of non-linear static methods are

explained. All methods include applying lateral forces to structures, but they follow different paths in calculating response of the structure.

3.1 Concept of Pushover Analysis

According to Papanikolaou (2000), conventional pushover analysis is an incremental-iterative solution of a set of equilibrium equations. Iterations continue until convergence is reached between external forces and lateral displacements. The resistance and stiffness of the structure is updated at every load step until user-defined failure.

Pushover analysis is first used by Gulkan and Sozen (1974). They have created an equivalent SDOF model of an MDOF system, monitoring post-yield stiffness, yield strength and ultimate strength. Since then, pushover methods have been improving. Saiidi and Sozen (1984), published a pushover method for MDOF systems, followed by Fajfar and Fischinger (1988).
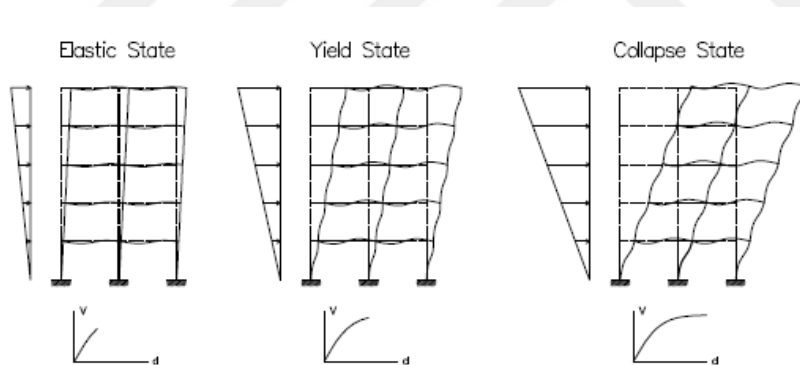

Figure 3.1: Stages in non-linear static procedures (Papanikolaou, 2000).

In pushover analysis, application method of lateral forces is key. In the original version of pushover analysis, external forces can have a uniform or triangular distribution between floor levels. Later on, new studies were published on lateral force distribution, incorporating mode shapes into the force equilibrium (Fajfar, 2000).

Sasaki et. al (1998) have published a method in displacement combination of SDOF systems with respect to modal characteristics. The method proposes using mode-shapes of the structure, in order to account for structures dynamic response. As

shown in figure 3.2, the method is a fundamental part of modern pushover procedures.
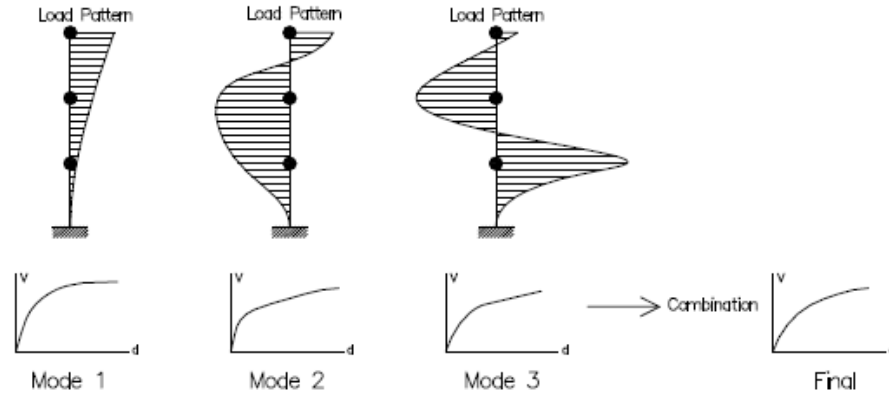

Figure 3.2: Mode combination method proposed by Sasaki et. al (1998).

Bathe (1982) formulated iterative process for calculation of out of balance forces as following:

$$\Delta U = [K_T]^{-1} \cdot (\lambda P_0 - P^e)$$ **(3.1)**

ΔU: calculated displacement increment within an iteration

K_T: current tangent stiffness matrix

λ: load factor withinthe corresponding load increment

P_0: initial load

P^e: equilibrated load of the previous iteration

$$P^* = \sum \int_V B^T \cdot \sigma_{NL} \cdot dV$$ **(3.2)**

B is the strain-displacement matrix of each element.

σ_{NL} is the element non-linear stress vector determined using its material

characteristics.

23

Equation of motion can be expressed as in the equation 3.3 below:

$$\underline{M}\ddot{x} + \underline{C}\dot{x} + \underline{K}x = -\underline{M}\mathrm{I}\,\ddot{x}_g \qquad \textbf{(3.3)}$$

M: Mass matrix

C: Damping matrix

K: Stiffness matrix

$\ddot{x}$: Acceleration

$\dot{x}$: Velocity

x: Displacement

$\ddot{x}_g$: Ground acceleration

Pushover method solves the equation of motion as follows:

$$X = \Phi\, x_1 \qquad \textbf{(3.4)}$$

Displacement matrix of the system is denoted by X. Φ is the modal displacement vector, and x_1 is the top displacement of the MDOF system.

MDOF system is converted into an equivalent SDOF system by a coefficient x* as in equation 3.5.

$$x^* = \frac{\Phi^T M\, \Phi}{\Phi^T M\, 1}\, x_1 \qquad \textbf{(3.5)}$$

Plugging equation into equation 3.3:

$$\Phi^T M 1 \ddot{x}^* + \Phi^T C \Phi \frac{\Phi^T M\, \Phi}{\Phi^T M\, 1} \dot{x}^* + \Phi^T Q = -M^* \ddot{x}_g \qquad \textbf{(3.6)}$$

Equation 3.6 then becomes:

$$M^* \ddot{x}^* + C^* \dot{x}^* + Q = -M^* \ddot{x}_g \qquad \textbf{(3.7)}$$

Equation 3.7 is the equation of motion of the equivalent SDOF system.

Papanikolaou (2000) have reported several drawbacks of conventional pushover analysis. These drawbacks include the inability of pushover analysis to consider seismic demand of structures, considering only lateral strength neglecting duration and cumulative energy dissipation, and not accounting for modal properties, which lead to period elongation altering the spectral amplification.

3.1.1 Adaptive Pushover

Papanikolaou (2000) has proposed a new method known as adaptive pushover, in which modal properties are updated at every load increment. The new method also considers spectral amplification and fiber models.
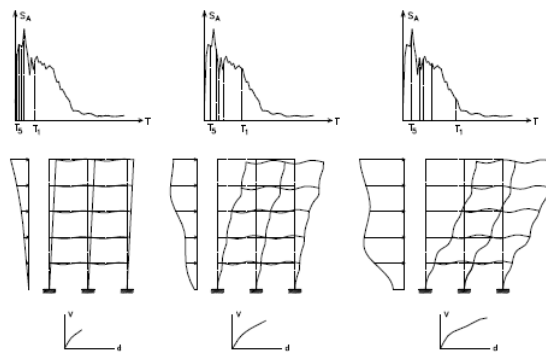
Figure 3.3: Period elongation in adaptive pushover analysis (Papanikolaou, 2000).

A software called INDYAS, later referred to as ZEUS-NL, created by Papanikolaou (2000) runs the iterations in the following order:

- Application of lateral forces

- Extraction of mass and tangent stiffness matrices

25

- Elimination of the restrained degrees of freedom

- Static condensation of the massless degrees of freedom

- Eigenvalue solution - Calculation of natural periods and mode shapes

- Response spectrum calculation from record integration

- Load pattern definition and modal combinations

- Load pattern normalization and re-application

One of the most important aspects of adaptive pushover is its ability to incorporate spectral acceleration. Spectral acceleration of the corresponding fundamental period of the structure is plugged into the modal load formula as in equation 3.8.

$$F^i_j = v^i \, \phi_j{}^i \, m_j \, S^i_A \tag{3.8}$$

v^i denotes modal participation factor of mode i as in equation 3.9,

$$v^i = \frac{\Phi^i M \, \delta}{\Phi^{i^T} M \, \Phi^i} \tag{3.9}$$

F^i_j denotes the force acting on the structure in the ith mode, referring to the j degree of freedom.

m_j is lumped mass on the j degree of freedom

S^i_A denotes the spectral acceleration of mode i. S_A equals 1 when spectral acceleration is not used.

Adaptive pushover has been a well-researched method since its introduction. Elnashai et. al (2005) have compared adaptive and conventional versions of pushover analysis. They have used incremental dynamic analysis (IDA) as a control data. Results in figure 3.4 show that method that gave closest results to IDA was adaptive pushover with spectral acceleration.
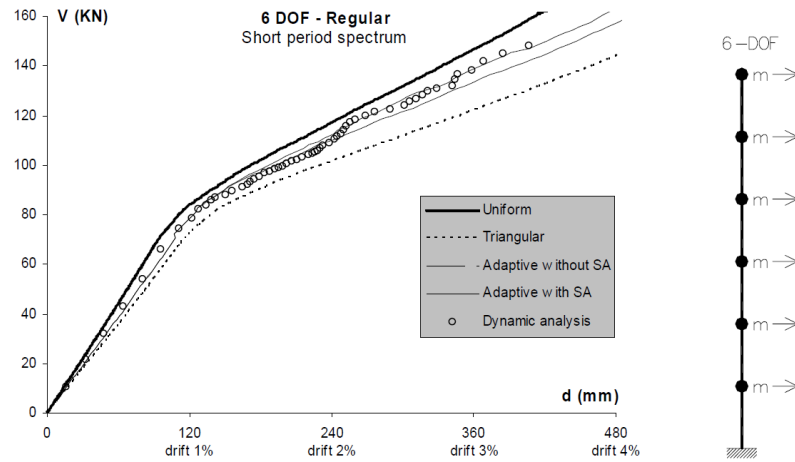
Figure 3.4: Capacity curve comparison of pushover analyses against IDA (Elnashai et. al 2005).

Oyguc (2011) have compared capacity curves of conventional, story shear based non-adaptive and story shear based adaptive pushover. As shown in figure 3.5, adaptive pushover resulted in a lower capacity compared to other two types of pushover analyses.
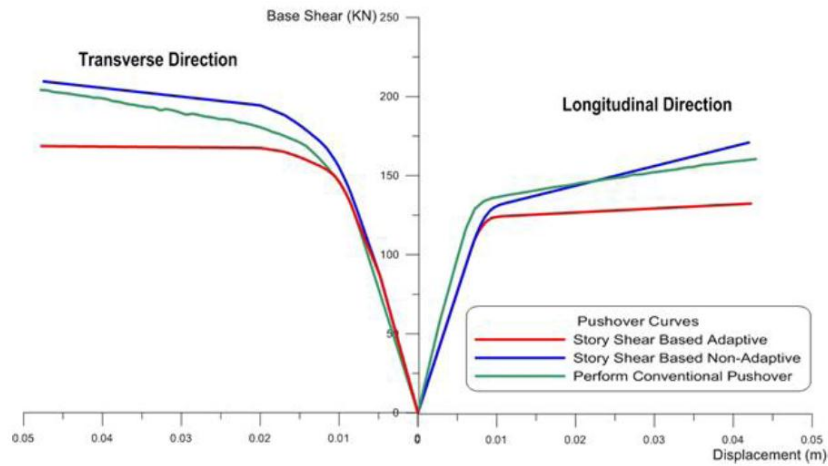

Figure 3.5: Capacity curve comparison of pushover analyses against IDA (Oyguc 2011).

Oyguc (2011) did not consider P-delta effects; however, results show that conventional pushover method overestimates capacity by 20%, in irregular buildings.

3.1.2 Modal pushover analysis

Modal pushover analysis is an extension of early versions of pushover analysis. MPA contains dynamic aspects of structures. Analysis uses response spectra and combination of inertia force distribution of modes in order to calculate total seismic demands of structures (Chopra and Goel, 2002). MPA procedure can be summarized as follows:

1. Compute natural frequencies and mode shapes for elastic vibrations.

2. Lateral forces are applied at the center of mass at each floor level, for every mode. Develop base shear vs. displacement curve using lateral response of structure.

3. Idealize base shear vs. displacement curve as bilinear or trilinear curve, and convert it to force-deformation curve. Calculate effective modal mass for each mode.

4. Calculate displacements using response history analysis.

5. Determine total dynamic response using mode combination methods SRSS or CQC.

3.1.3 Energy based pushover analysis

In pushover analysis roof displacement is used to plot the capacity curve. According to Montes et. al (2008) roof displacements increase disproportionately as the lateral loads increase. Their proposed methodology includes using absorbed energy instead of roof displacement. Montes et. al (2008) state that some designs can have roof displacements that do not represent the total response correctly. Figure 3.6 shows different types of frames. Type a is a moment frame where roof displacement is a good indicator of total response. Roof displacements of type b and c; however, may not represent the force-deformation interaction well.
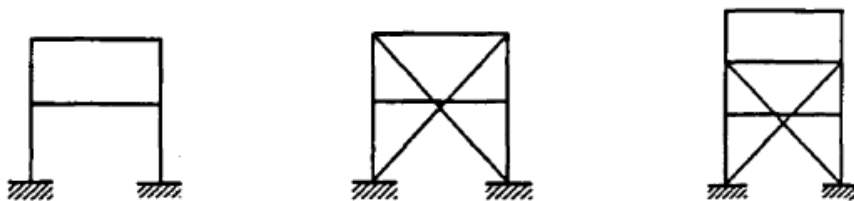

Figure 3.6:   Types of frames a, b, c (Mendes et. al, 2008).

Mendes et. al (2008) conclude that substantially large errors were determined for a three-story moment-resistent frame after 4% of roof displacement.

3.1.4 Direct displacement based pushover

Priestley (2000) states that non-linear static procedures overestimate the inelastic response and that elastic stiffness should follow another line shown in figure 3.7. In their study, Priestley lists deficiencies of the pushover concept as the following:

1. Two buildings designed to same design code may experience a different seismic response, even though they are subject to same ductility factors.

2. Iterative design is needed in order to account for force reduction-factor discrepancy with design codes.

3. If capacity design is required, there seems little benefit from the additional complexity of 3-D modal analysis.

4. Design based on force-reduction factors provides an inadequate representation of torsional effects, underestimating the torsional response for ductile torsionally unrestrained systems.

5. Strain as a damage indicator is a poor concept as depicted in point 1 above.

6. Force-based design requires the specification of initial stiffness of structural members.

Priestley (2000) proposed a new method on force-based analysis considering a better characterization of stiffness. Design base shear is a function of effective stiffness and design displacement. Effective stiffness is calculated using equation 3.10.

$$T_e = 2\pi \sqrt{\frac{M_e}{K_e}} \qquad\qquad \textbf{(3.10)}$$
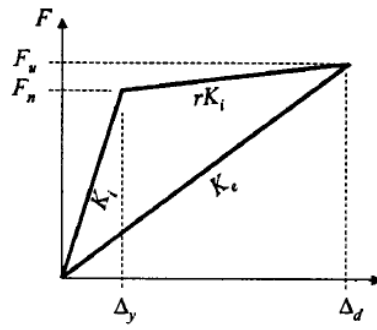
Figure 3.7: Force-deformation curve with effective stiffness (Priestley, 2000).

3.1.5 N2 method

N2 method was proposed by Fajfar (2000) in order to include seismic demand of buildings in pushover analysis. The method is formulated in the acceleration-displacement format. The main difference between capacity spectrum method and N2 method is that, N2 method uses inelastic spectra instead of elastic spectra with equivalent damping and vibration period. According to Fajfar (2000) results of N2 method are reasonably accurate, given that the building oscillates mostly in the first mode.Fajfar (2000) concludes that N2 method yields similar results of FEMA-273 and ATC-40. Easy-to-implement nature of the N2 method makes it a better choice than the American versions of pushover analysis.

Fajfar (2000) presents the N2 method in 8 simple steps.

Step 1. Transformation of the elastic demand spectra to acceleration-displacement format using the following equation:

$$S_{de} = \frac{T^2}{4 \pi^2} S_{de} \tag{3.11}$$

Step 2. Apply pushover analysis to create force-deformation relationship of the MDOF system.

Lateral loads are calculated as follows:

$$\mathbf{P} = p \, \mathbf{\Psi} = p \, \mathbf{M} \, \mathbf{\Phi} \tag{3.12}$$

P denotes the lateral load vector in equation 3.12. The distribution of lateral loads is denoted by **Ψ**, which is product of mass matrix **M** and assumed mode shape **Φ**.

$$P_i = p\, m_i\, \varphi_i \tag{3.13}$$

Equation 3.13 defines forces of each story.

Step 3. In N2 method seismic demand is determined using a response spectrum. Equation 3.5 denotes the starting point of such concept.

$$M\ddot{U} + R = M\,\mathbf{1}\,a \tag{3.14}$$

U and **R** denote displacement and internal force vectors. **M** is mass matrix, **1** is a unit vector and a is the ground acceleration.

Assuming that mode shape **Ψ**, the displacement vector **U** can be defines as in equation 3.15.

$$U = \Phi\, D_t \tag{3.15}$$

And since internal forces should be equal to external forces due to statics **P** is equal to **R** (3.7)

By plugging in formulas 3.7, 3.12 and 3.13 into formula 3.14, formula 3.16 is obtained.

$$\Phi^T M\, \Phi\, \ddot{D}_t + \Phi^T M\, \Phi\, p = -\Phi^T\, M\,\mathbf{1}\,a \tag{3.16}$$

Cancelling out $\Phi^T\, M\,\mathbf{1}$ on each side in equation 3.16, equation of motion of an equivalent SDOF system is obtained as in 3.17.

$$m^*\, \ddot{D}^* + F^* = -m^*\,a \tag{3.17}$$

m* denotes the equivalent mass of the SDOF system. Equation 3.18 defines m*.

$$m^* = \mathbf{\Phi}^T \mathbf{M} \, \mathbf{1} = \sum m_i \, \Phi_i \tag{3.18}$$

Equivalent displacement and forces can be denoted by D* and F*.

$$D^* = \frac{D_t}{\Gamma} \tag{3.19}$$

$$F^* = \frac{V}{\Gamma} \tag{3.20}$$

Base shear of the MDOF system is given in equation 3.21

$$V = \sum P_i = \mathbf{\Phi}^T \mathbf{M} \, \mathbf{1} \, p = p \sum m_i \, \Phi_i = pm^* \tag{3.21}$$

In equation 3.19 and 3.20, displacement and base shear of MDOF system are divided by a modal participation factor Γ. Γcontrols the transformation from MDOF to SDOF model.

$$\Gamma = \frac{\mathbf{\Phi}^T \mathbf{M} \, \mathbf{1}}{\mathbf{\Phi}^T \mathbf{M} \, \mathbf{\Phi}} = \frac{\sum m_i \Phi_i}{\sum m_i \Phi_i^2} = \frac{m^*}{\sum m_i \, \Phi_i^2} \tag{3.22}$$

Equations 3.19 and 3.20 are mainly used in the creation of equivalent force-deformation curve of SDOF system. N2 method uses a graphical procedure in order to bilinearize the V-D curve. N2 method assumes zero post-yield stiffness. The reason is the reduction factor is defined as the ratio of the required elastic strength to the yield strength. The influence of moderate strain hardening is embedded in the demand spectra.

Elastic period of the idealized bilinear system T* is determined as:

$$T^* = 2\pi \sqrt{\frac{m^* D_y{}^*}{F_y{}^*}} \tag{3.23}$$

32

Finally, the capacity diagram of equivalent SDOF system can be transformed into AD format by dividing F* by m*, resulting in equivalent acceleration of the system.

4. Calculate reduction factor R_μ

$$R_\mu = \frac{S_{ae}(T^*)}{S_{ay}} \qquad (3.24)$$

S_{ae} denotes the spectral acceleration where radial line of bi-linearized capacity curve intersects the elastic spectra. S_{ay} is defined as the spectral acceleration of bi-linearized capacity curve at yield point. Figure 4.5 shows S_{ae} and S_{ay}, S_d, S_{de}, T^*, D_d^*, and D_y^* on the demand spectra.
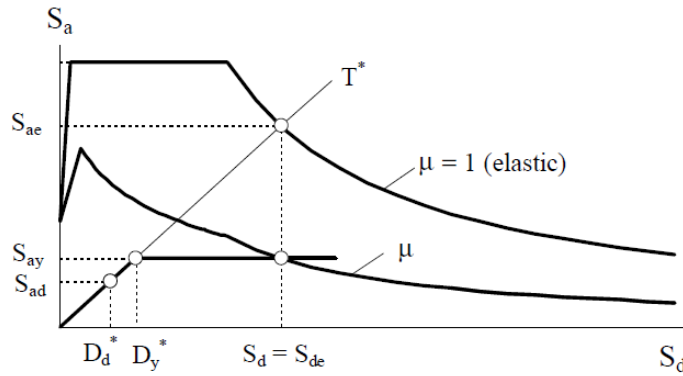
Figure 3.8: N2 method's elastic and inelastic demand spectra versus capacity diagram (Fajfar, 2000).

If the elastic period of the system is smaller than T_C then ductility demand μ is calculated as follows:

$$\mu = (R_\mu - 1)\frac{T_C}{T^*} + 1 \qquad T^* < T_C \qquad (3.25)$$

μ equals R_μ when T* is smaller than T_C.

Step 5 and 6. Transformation of SDOF system back to MDOF system.

Maximum S_d is transformed into D_t which represents the maximum top displacement of the MDOF system.

3.2 Dynamic Analysis

Dynamic analysis incorporates energy dissipation and duration aspects into the analysis. Contrary to strain energy, dissipated energy cannot be recovered. According to Elnashai and Di Sarno (2015), energy can only be absorbed by irreversible deformations. Therefore, dynamic analysis can reveal more information than static analysis. Also, dynamic analysis can impose characteristics of an earthquake on to the model building. Figure 3.9 shows a brief graphical summary of dynamic seismic analysis.

$$m[\ddot{u}_g(t) + \ddot{u}_r(t)] + c\,\dot{u}_r(t) + k\,u_r(t) = 0$$

$$\boxed{m\ddot{u}_r(t) + c\,\dot{u}_r(t) + k\,u_r(t) = -m\ddot{u}_g(t)}$$
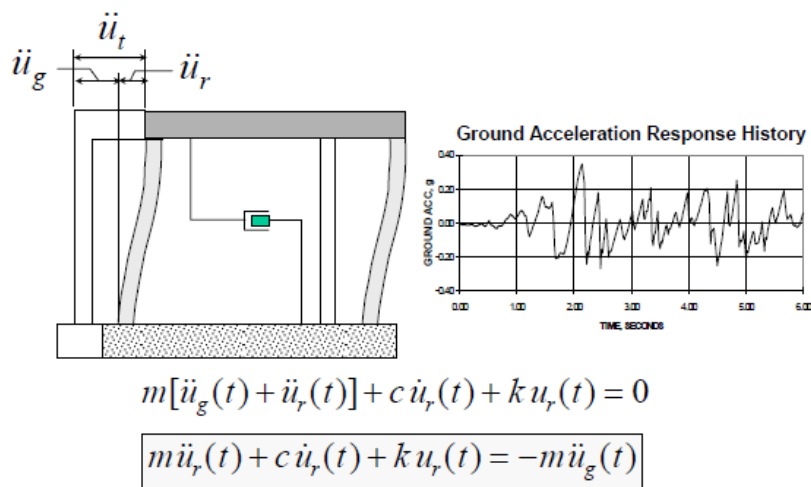
Figure 3.9:   FEMA 451 Design example

Dynamic analysis uses direct integration methods to solve equation of motion under dynamic loading. There are four types of direct integration methods. Fourier transform, Duhamel integration, piecewise exact, and Newmark techniques. All methods are numerical; however, Newmark's method can relate to in-elastic behavior better than the others can. It can also be applied to elastic systems as well.

Equation of motion is defined as:

$$m\ddot{u} + c\dot{u} + ku = -m\ddot{u}_g$$

(3.26)

Dividing both sides by **m** and making following substitutions will result equation 3.29.

34

$$\frac{c}{m} = 2\xi\omega \qquad\qquad (3.27)$$

$$\frac{k}{m} = \omega^2 \qquad\qquad (3.28)$$

$$\ddot{u}_r(t) + 2\xi\omega \dot{u}_r(t) + \omega^2 u_r(t) = -\ddot{u}_g(t) \qquad\qquad (3.29)$$

ξ denotes damping ratio of the system, which is assumed as 5% for most buildings.

ω denotes free vibration frequency of the system. It can be expressed as $T = 2\pi / \omega$

$\ddot{u}_g$ denotes ground acceleration.

Equation of motion is solved for accelerations in terms of displacements, velocities, and applied forces. All parameters are a function of time. At each time increment Δt stiffness matrix of the whole structure is updated. Hence, analysis takes more time than static analysis.

Newmark (1959) have proposed a procedure to for the solution of structural dynamics. According to the article, new procedure can consider any type of dynamic loading due to shock, impact, vibration, earthquake, or blasts. With the added coefficients γ and β and solving for velocity and displacements of the equation of motion results in equation 3.30 and 3.31:

$$\dot{u}_{i+1} = \dot{u}_i + \left[(1-\gamma)\Delta t \right]\ddot{u}_i + (\gamma\Delta t)\ddot{u}_{i+1} \qquad\qquad (3.30)$$

$$u_{i+1} = u_i + (\Delta t)\dot{u}_i + \left[(0.5-\beta)(\Delta t)^2 \right]\ddot{u}_i + \left[\beta(\Delta t)^2 \right]\ddot{u}_{i+1} \qquad\qquad (3.31)$$

γ and β denotes participation factors to control weight of acceleration in velocity and displacement at the end of time interval Δt.

At any time acceleration of the system equals equation 3.32.

$$a = \frac{(P - R)}{M} \qquad\qquad (3.32)$$

Assuming β equals zero, the general procedure is as follows:

1. Assume values of acceleration of each mass at the end of the interval.

2. Compute the velocity and displacement of each mass at the end of the interval using equations 3.19 and 3.20.

3. Compute resisting forces R, which are holding the structural framework in the deflected configuration.

4. Re-calculate acceleration using applied loads (P) and resisting forces (R) at the end of time interval Δt from equation 3.32.

5. Compare derived acceleration with assumed acceleration. If they are different, start from step 1 with a closer assumption of acceleration.

Newmark (1959) suggests using γ and β as 0.5 and 0.25, respectively; in order to damp high frequencies at the end of time interval Δt. If γ is taken greater than 0.5, there will be a significant amount of numerical damping present in results. If it is taken as zero, then the results will involve self-excitement of the structure arising solely from numerical integration.

4. REVIEW of MATERIAL MODELS

Material model is a mathematical representation of the expected behavior of a given material in response to an applied load (Thompson, 2017). Models are created through optimization of force-deformation curves with respect to laboratory data. Behavior of the structure depends heavily on force-deformation curves, and physical properties. Response analysis requires realistic material models that incorporate all the important phenomena including energy dissipation (Takeda et. al, 1970; Ibarra et. al, 2004).

Material testing is often done under cycling loads, resulting in compression and tension. Loading and unloading phases measure the material's strength and ductility. During cyclic loading a phenomenon called hysteresis that occurs due to accumulating dissipated energy. Hysteresis in material science is defined as the material's ability to restore energy with respect to former deformations (Erberik, 2010).
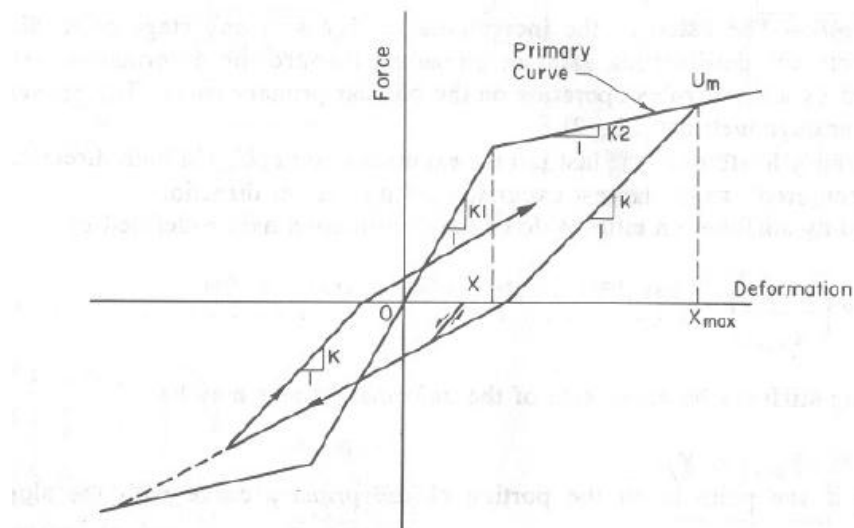
Figure 4.1: Graphical representation of Q-model (Saiidi and Sozen, 1970).

Ever since MDOF models' need for hysteretic material simulations began, need for greater computing power has been introduced. In figure 4.1 Saiidi and Sozen (1970) proposed a "low-cost", meaning less required computing power, hysteresis model.

The model treats an MDOF structure as an SDOF oscillator. However, since greater computing power has become more available, local plasticity started to attract more attention. Ibarra et. al (2005) states that local monitoring is just as important as global, as local collapse may induce a total collapse of the structure through damage propagation.

Local in-elastic monitoring of MDOF systems is done through the use of plastic hinges. Plastic hinge is a yield zone that occurs at points of maximum bending moment, such as in the middle or at support joints of beam or column elements. Maximum moment regions of fixed-end beams can be seen in figure 4.2.
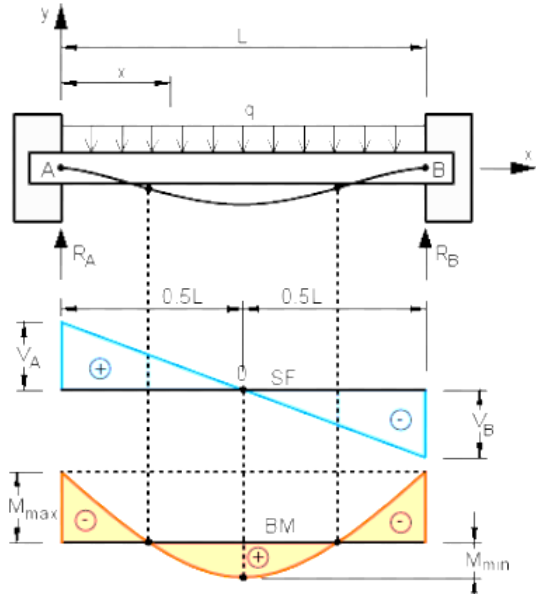
Figure 4.2:   Free-body diagram of a fixed-end supported beam.

In traditional structural analysis, plastic hinges are assigned on pre-determined locations on beam and column elements. That is a viable solution; however, concentrated plasticity can underestimate strength loss due to buckling and non-linearity (Deierlein et. al, 2009).

Newer software are able to compute distributed plasticity in order to achieve realistic results. Finite element hinge model can calculate in-elasticity along the member's length, as well as, within the hinge location. Figure 4.3 shows the difference between several hinge models.
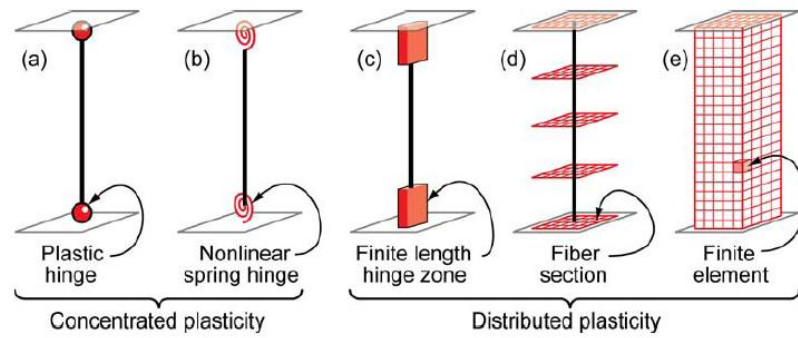
Figure 4.3:   Types of plastic hinges used in finite element analysis (Deierlein, 2009).

In most structural FEA analysis, assigned hinges undergo a significantly idealized capacity curve, as shown in figure 4.4.
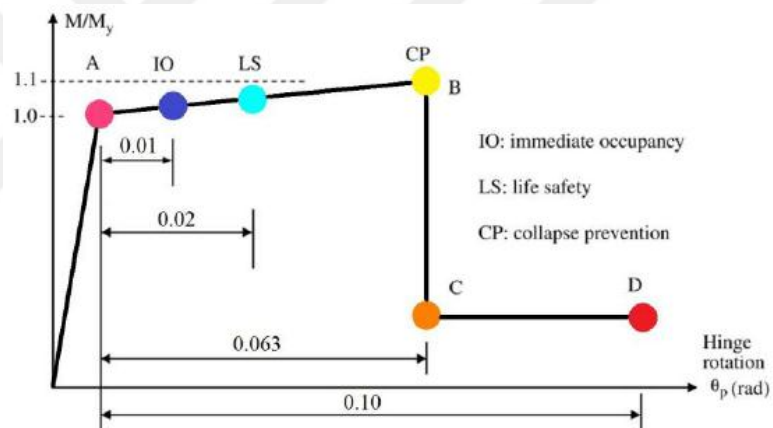
Figure 4.4:   Hinge behavior model in SAP 2000.

Concentrated and idealized hinge behavior yields faster results, but they are far from reality.

Different material models are available today in order to simulate in-elastic behavior of elements. A well-known and popular concrete model was proposed by Mander et. al (1988). The model considers effect of confinement in stress-strain relationship under monotonic compression loading as shown in figure 4.5.
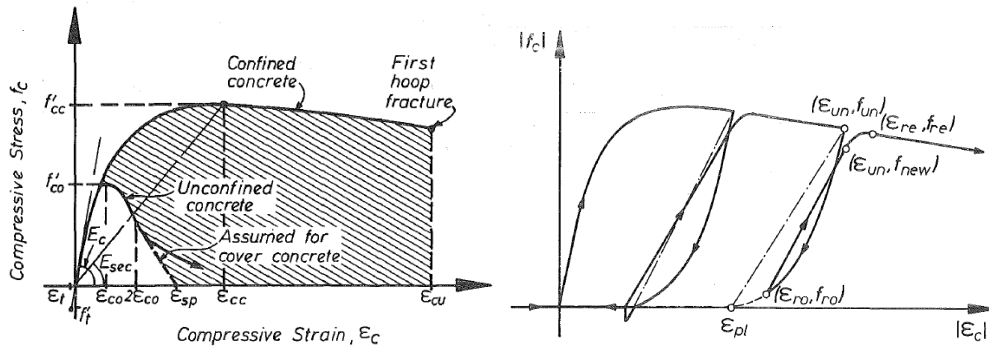
Figure 4.5: Left: Mander model for confined and un-confined concrete sections. Right: Concrete cross section under cyclic loading (Mander et. al, 1988).

Longitudinal compressive stress f_c is given by equation 4.1.

$$f_c = \frac{f'_{cc}\, xr}{r - 1 + x^r}$$ (4.1)

f'_{cc} denotes compressive strength of confined concrete.

$$x = \frac{\varepsilon_c}{\varepsilon_{cc}}$$ (4.2)

ε_c denotes longitudinal compressive concrete strain.

$$\varepsilon_c = \varepsilon_c \left[1 + 5 \left(\frac{f'_{cc}}{f'_{co}} - 1 \right) \right]$$ (4.3)

As suggested by Richart et. al (1928), f'_{co} and ε_{co} , the unconfined concrete strength and corresponding strain, respectively. Generally, ε_{cc} can be assumed 0.002.

Lee and Fenves (1998) have proposed a concrete model for structures under cyclic loading. The model uses fracture-energy-based damage and stiffness degradation in continuum damage mechanics. They have incorporated two damage variables; one for tension and one for compression. The model considers crack opening and closing that takes place in a macroscopic level, which causes stiffness degradation.
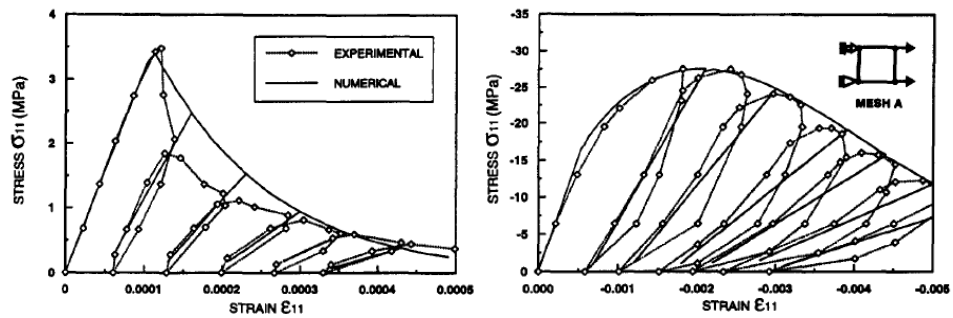
Figure 4.6: Lee and Fenves comparison of numerical data with experimental.
Left: RC section in tension. Right: RC section in compression.

Concrete is a material that performs well under compression. Its ability to dissipate energy under tension is poor. Steel on the other hand, have significantly higher tensional strength. There are a few steel models available today, such as bi-linear steel model, and Menegotto-Pinto models as shown in figure 4.7.
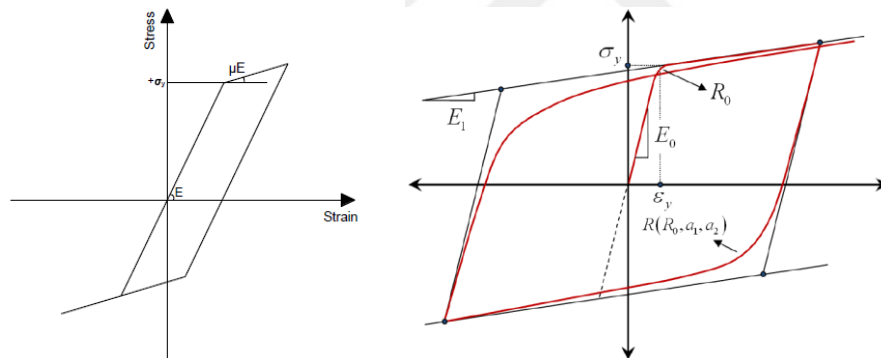
Figure 4.7: Left :bi-linear steel model with kinematic strain hardening. Right: Menegotto-Pinto steel model with isotropic strain-hardening (ZEUS-NL manual).

Steel models differ greatly between each other. Bi-linear model only considers a strain-hardening phase, neglecting any type of degradation. Gomes and Appleton (1997), have developed an advanced steel model that considers buckling, and Bauschinger effects. The model simulates following characteristics of steel:

- Elastic, yielding and hardening branches in the first excursion.

- Reduction of yield stress after a reverse cycle, which increases with the enlargement of the plastic strain component of the last excursion, and decrease of the curvature in the transition zone between the elastic and the plastic branches, also known as Bauschinger effect.

41
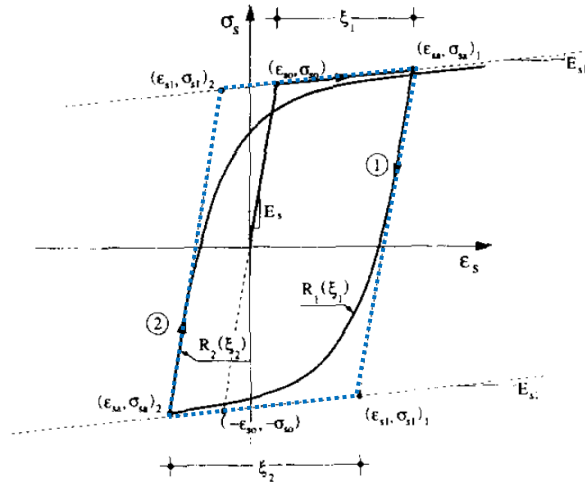
Figure 4.8: Menegotto-Pinto steel model (Gomes and Appleton, 1997). Bilinear envelope is marked with dotted blue line.

The loading and unloading paths are contained in a bilinear envelope, E, defined by equation 4.4.

$$\sigma^*_x = \beta\epsilon^*_x + (1 - \beta) \frac{\epsilon^*_s}{[1 + (\epsilon_s^*)^R]^{1/R}} \tag{4.4}$$

Normalized strain and stress in the first load are obtained by using variables in equation 4.5.

$$\epsilon_s^* = \frac{\epsilon_s}{\epsilon_{so}} \qquad \sigma_s^* = \frac{\sigma_s}{\sigma_{so}} \tag{4.5}$$

In the unloading phase they are obtained by variables in equation 4.6.

$$\epsilon_s^* = \frac{\epsilon_s - \epsilon_{so}}{2\epsilon_{so}} \qquad \sigma_s^* = \frac{\sigma_s - \sigma_{so}}{2\sigma_{so}} \tag{4.6}$$

Curve R defines the Bauschinger curve in load reversal phase.

$$R = R_o - \frac{a_1\xi}{a_2 + \xi} \tag{4.7}$$

R_o, a_1, and a_2 are material constants. ξ is the absolute value of the plastic strain of the last excursion. Gomes and Appleton (1997) state that the response of model was not sensitive to those material constants, but much more on the envelope curve R.

In order to simulate bar buckling, Gomes and Appleton (1997) have considered a simple model of two consecutive stirrups. Visual representation can be seen in figure 4.9. They state that bar buckling only takes place if all concrete layers are crushed.
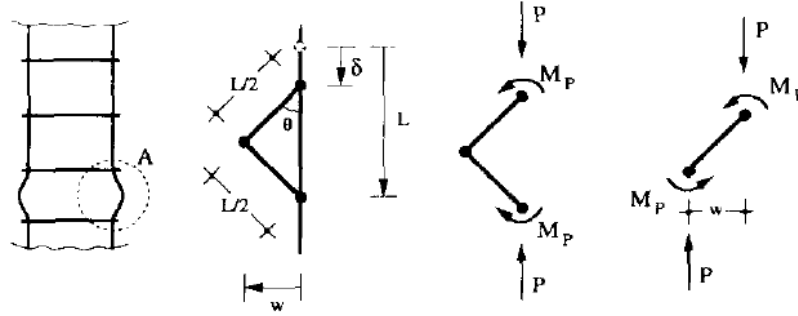
Figure 4.9: Free body diagrams for steel bar buckling (Gomes and Appleton, 1997).

The equilibrium of the buckled reinforcement in the deformed configuration is given by equation 4.8.

$$P = \frac{2M_P}{w} \tag{4.8}$$

w denotes the transverse displacement. Mp denotes plastic moment of the bar. For a circular section without axial load, Mp is given by:

$$M_P = Z_P \sigma_{so} = 0.424\pi R^3 \sigma_{so} \tag{4.9}$$

Zp denotes the plastic modulus of the circular section. The compatibility between the transverse displacement w and the longitudinall displacement δ and the rigid body rotation Θ, is given in equations 4.10.

$$w = \frac{L}{2}\sin\theta \qquad\qquad \delta = L\,(1 - \cos\theta) \tag{4.10}$$

Plugging in equations 4.10 into equation 4.8, yields:

$$P = \frac{2\sqrt{2}M_P}{\sqrt{L}}\,1/\sqrt{\delta} \tag{4.11}$$

43

Considering equations 4.12:

$$\varepsilon_s = \frac{\delta}{L} \qquad\qquad \varepsilon_s = \frac{P}{A_s} \qquad\qquad \text{(4.12)}$$

Equation 4.11 becomes:

$$\sigma_s = \frac{2\sqrt{2}M_P}{\sqrt{L}} \, 1/\sqrt{\varepsilon_s} \qquad\qquad \text{(4.13)}$$

Figure 4.10 shows the steel model that includes effect of buckling. According to Gomes and Appleton (1997), point B has to be found via iterations. Point P is the intersection of buckling curve CD and load reversal curve AB.
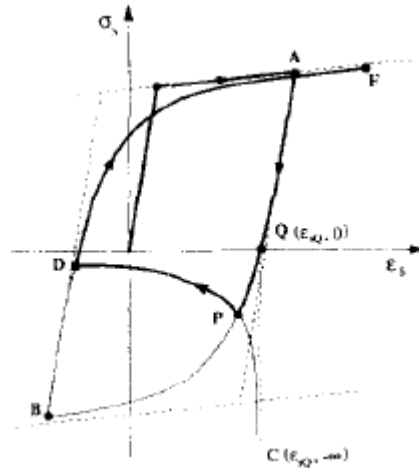
Figure 4.10: Modified Menegotto-Pinto model considering bar buckling (Gomes and Appleton, 1997).

4.1 Degradation

According to FEMA 440, degradation occurs in two ways: cyclic degradation and in-cycle degradation as shown in figure 4.11. Cyclic degradation is defined as a loss of stiffness and strength over following cycles. In-cycle degradation occurs in a loss loss of strength and negative stiffness within a cycle.
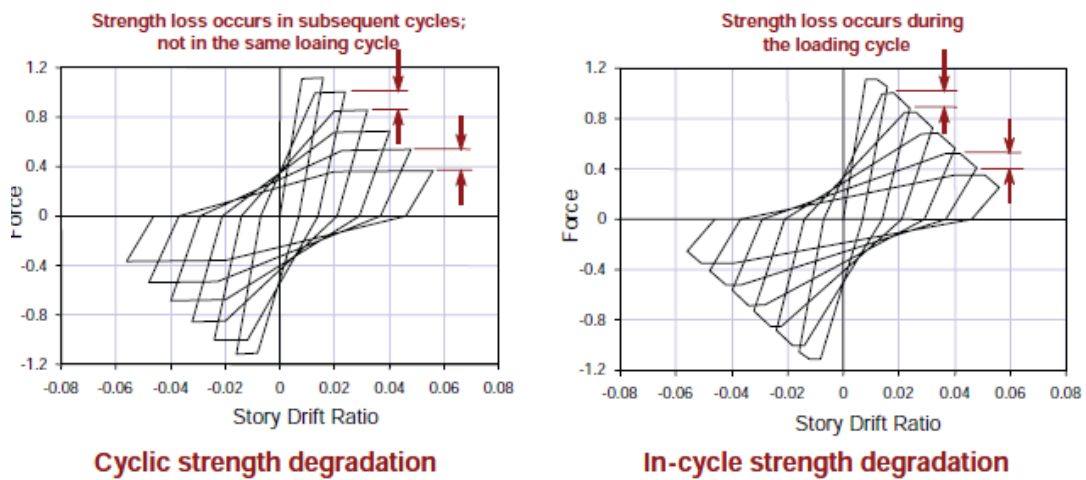
Figure 4.11: Cyclic and in-cycle degredation (FEMA P440A).

According to FEMA P440A, cyclic degradation stiffness degradation in RC components occurs because of cracking, loss of bond, or interaction with high shear or axial stresses. Strength degradation occurs due to strain hardening following yield.

In-cyclic strength degradation occurs following reverse loading or during subsequent loading cycles. According to Park et. al (1987), cyclic strength degradation can also occur in subsequent cycles even if the level of inelastic displacement is not increased. In-cycle strength degradation can be caused by P-delta effects or material non-linearities, such as concrete crushing, shear failure, and steel bar buckling.

Figure 4.12 shows a representation of story drift vs time plot of two test structures that experienced cyclic and in-cycle strength degradation.
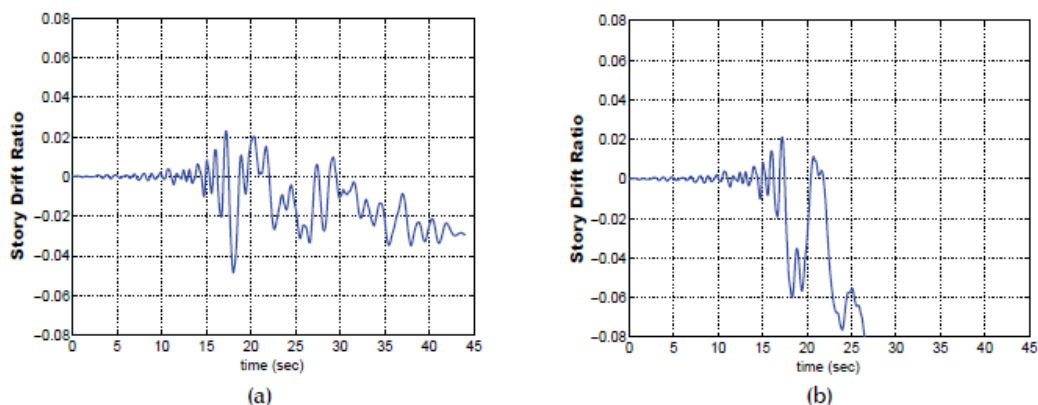
Figure 4.12: Displacement time histories of test structures. Left: Cyclic strength degradation. Right: In-cycle strength degradation (FEMA P440A).

Degrading models consider some of the aspects of materials that are generally overlooked by analysis software, such as strength loss due to hysteresis. A

comparison between these two tiers of material models have been published by Abdelnaby.(2012). He has coded degrading steel and concrete models within a non-linear structural analysis software called ZEUS-NL. Degrading models are often used to analyze multiple earthquake effects; however, as shown on Figure 4.13, a difference occurs after a certain point in time during a single run.
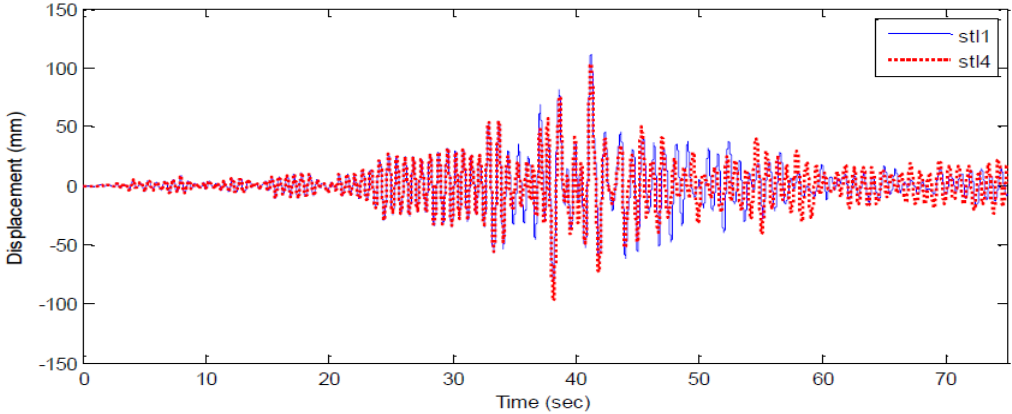
Figure 4.13: Non-degrading bi-linear steel model (stl1) and degrading modified Menegotto-Pinto model (stl4) steel model in dynamic time-history analysis. (Abdelnaby, 2012)
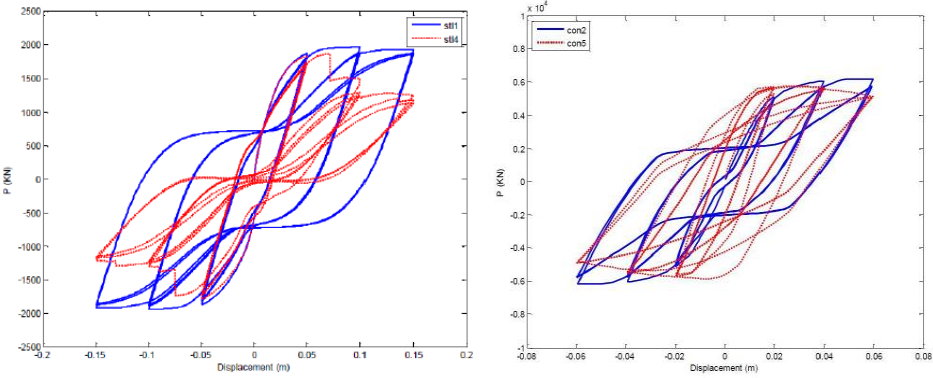
Figure 4.14: Side by side comparison of steel (right) and concrete (left) (Abdelnaby, 2012).

In figure 4.14, both cyclic and in-cycle strength and stiffness degradation occur. Pinching effects are also visible.. The difference occurs because of buckling of bars and bar fracture phenomena that is accounted for in the degrading model (stl4). Figure 4.13 and 4.14 are a result of a 2-D SDOF pier analysis. Considering the

visible difference of the two results, a greater difference would be expected in a much complex 3-D model.

Steel model of Abdelnaby (2012) uses the modified Menegotto-Pinto model with an added bar-fracture feature. According to the model, bar fracture that occurs under large excursions that exceeds ultimate steel strength. If fracture occurs, applied strains will result in zero stresses.
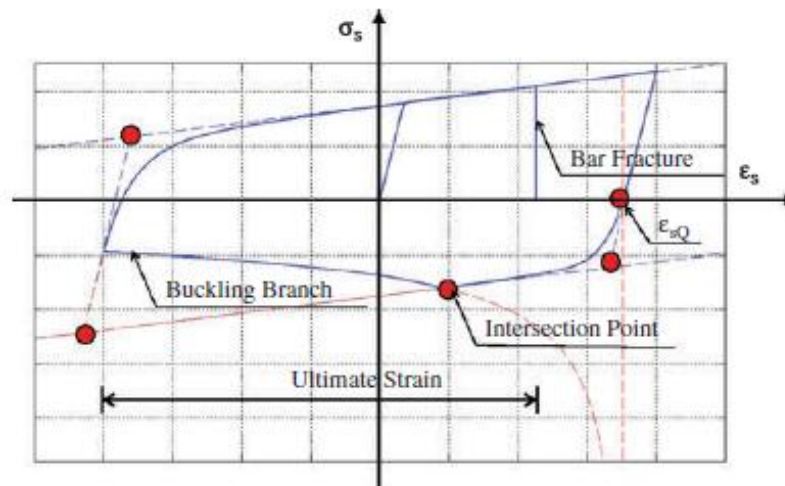
Figure 4.15: Steel Model (Abdelnaby, 2012)

The concrete model coded into the program implements concrete strength loss model proposed by Fenves (1998). As shown in figure 4.16 the concrete model undergoes cyclic stiffness and strength degradation.
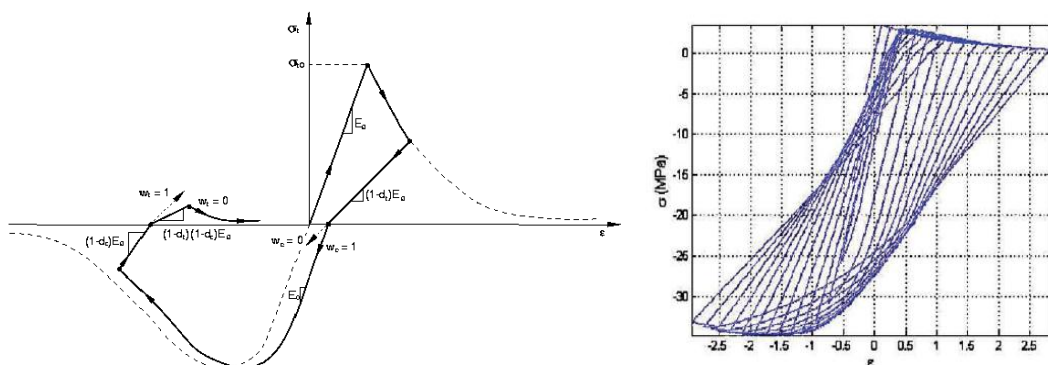
Figure 4.16: Concrete stiffness and strength loss model (Fenves, 1998) and Concrete Model (Abdelnaby, 2012).

47

5. ANALYTICAL STUDY

This section gives in-depth details of the analytical study that was conducted for this thesis. Selected buildings, chosen analysis methods, material models, and other methods are shared. Two buildings that were affected in 2011 Van earthquake have been selected for this study. Gedikbulak Elementary School building which was collapsed and Alaköy school building which was significantly damaged.

As in figure 5.1, analytical study involves eigenvalue analysis, pushover analysis, adaptive pushover analysis, and dynamic time-history analysis. Degrading and non-degrading models were used in the analyses for comparison.

Even though the buildings were analyzed for effects of Van earthquake, seven hazard compatible earthquakes were used in the analyses due to inapplicability of Van strong ground motion record. Selection of the strong ground motion set was made considering simulated PGA values of the region. Dynamic analyses were conducted for each record.
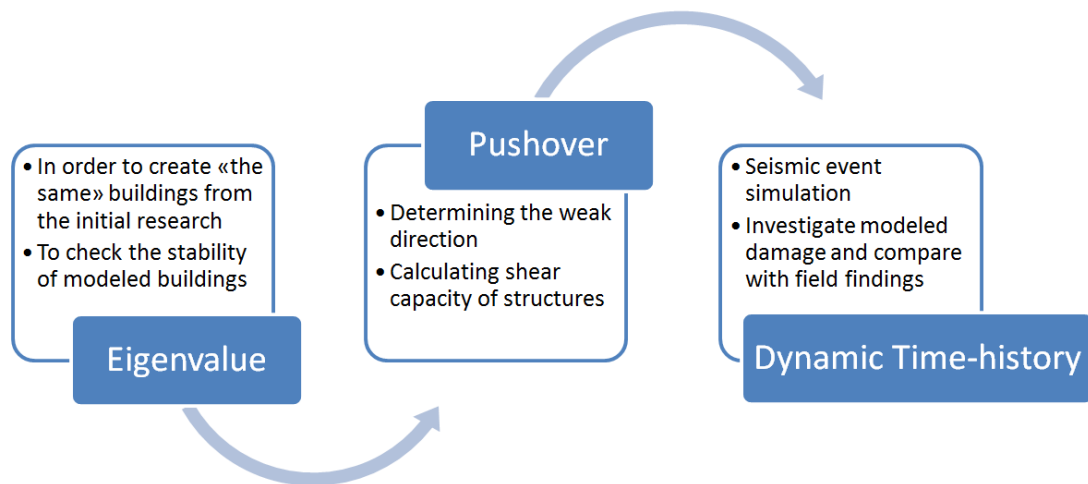
Figure 5.1: Phases of analytical study of this thesis.

5.1 Analysis Software

ZEUS-NL is open-code non-linear structural analysis software that assumes distributed plasticity on members. The software has built-in eigenvalue analysis,

static and adaptive pushover, static time-history and dynamic analysis programs. Cross sections can be built with ease; also, the whole structure can be viewed instantly in 3D. Since the software is open-code, researchers can run their own material model and view the results the same way.
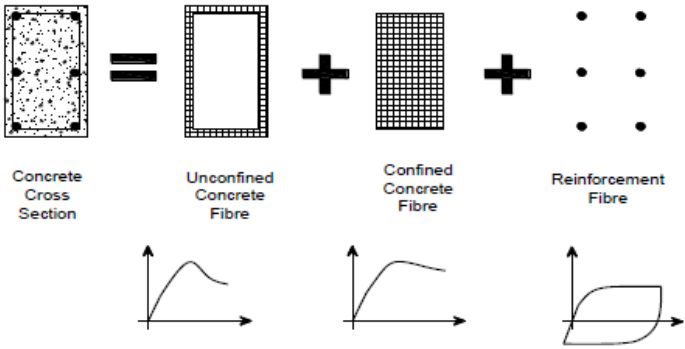
Figure 5.2: ZEUS-NL multi-layered mash approach for cross-section calculation

ZEUS-NL models cross sections by treating them as a multi layered finite mesh as shown in figure 5.2. Unconfined, confined and reinforcement mesh elements are added together to act as one. Since plasticity is spread along the length and depth of the members, analysis takes more time but it is more accurate than other FEM software.

ZEUS-NL lets the user monitor certain sections of the elements. Those monitoring spots are located on top and bottom of the elements in both beam/column-end as in figure 5.3. User can monitor materials at each time step. Material yielding can be monitored using those monitoring points. That way, the user can see whether yielding occurred under tension or compression.
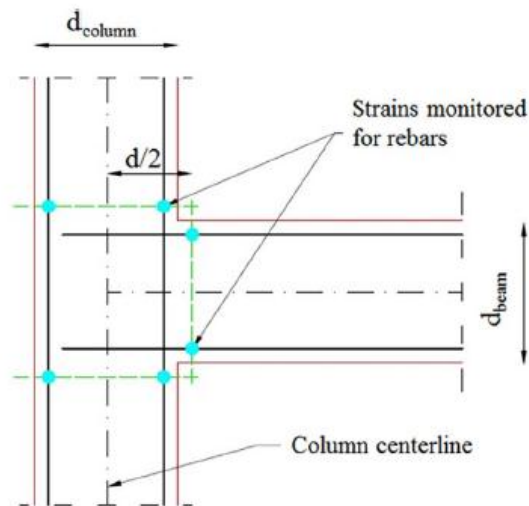
Figure 5.3: ZEUS-NL monitoring spots.

5.2 Structures of Interest

Two structures have been chosen for this study. A 3-story reinforced concrete school building located in Gedikbulak town of Van, Turkey, which collapsed during the October 2011 Van Earthquake; and a 3-story reinforced concrete school building located in town of Alaköy which took substantial damage during the same earthquake but did not collapse. Photos of the buildings are given below in figure 5.4.

Figure 5.4: Gedikbulak and Alaköy school buildings (EEDMI, 2011).

5.2.1 Test structure

In order to calibrate the ZEUS-NL software, SPEAR building of ELSA laboratory was used. SPEAR building has been used by researchers extensively and its analysis data and specifications are easily accessible. According to Stratan and Fardis (2003), the building resembles residential RC buildings that were built in Greece and Mediterranean region, without considering seismic engineering. The structure was designed only for gravity loads with materials from 1970s. Photo of the structure is given in figure 5.5.

Figure 5.5:   Photo of SPEAR building.

SPEAR is a full-scale plan-irregular 3 story test building. Each floor is 3 meters high slab to slab, and the plan dimensions are 10.5 meters by 10 meters, which is shown in figure 5.6. Beam and column cross sections are given in figure 5.7. The specified strength of concrete, f_c, is 25 MPa, and steel yield strength, f_y, is 400 MPa.

The building is irregular in plan, with center of mass and stiffness on different locations as shown in figure 5.8.
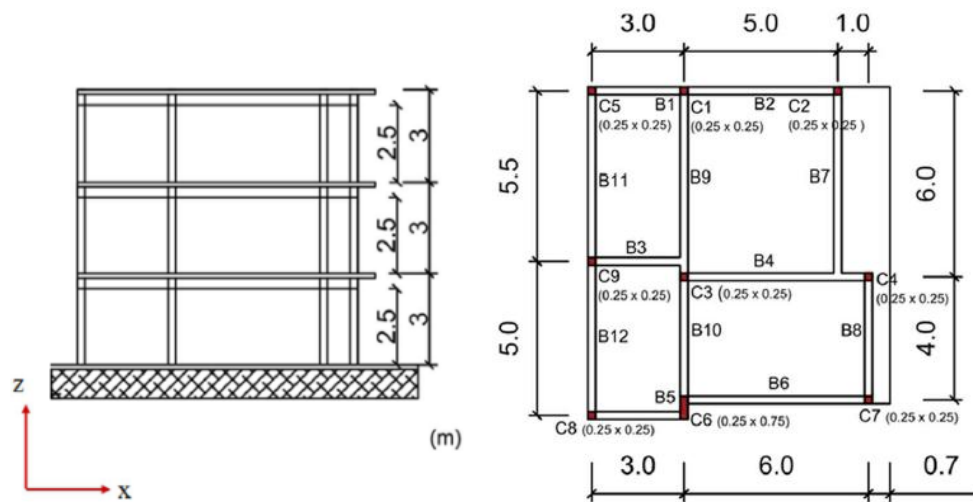
Figure 5.6: Front elevation and horizontal plan of SPEAR building (Oyguc et. al, 2017).
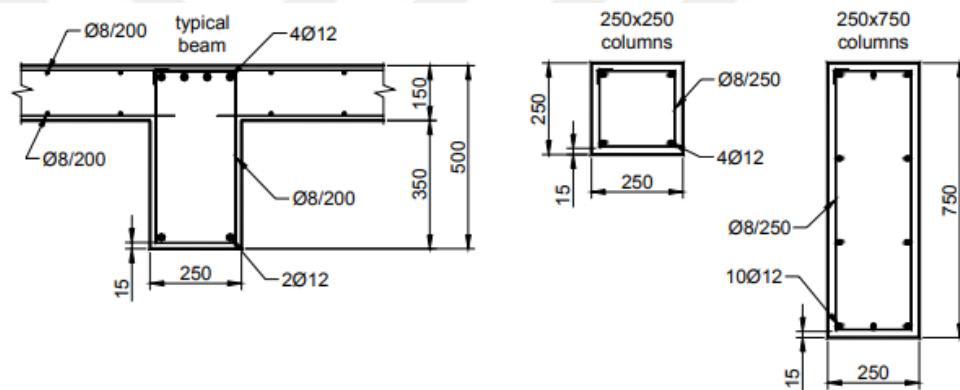
Figure 5.7: Element cross sections of SPEAR (Stratan and Fardis, 2003)

Beams of the building are 25cm by 35 cm with 4 12mm bars. Longitudinal reinforcements on the beam-ends start with 4 12 mm bars on top of beams and 2 12mm bars on the bottom. Columns are 25cm by 25cm except for the shear wall. Longitudinal reinforcements in columns are 12 mm bars placed on each corner. The shear wall is 250mm by 750mm with 10 12 mm diameter bars placed 3 in the short and 4 in long side. Stirrups in all elements are closed with 90-degree angles, which provide no confinement. Concrete cover is 15mm in all elements.
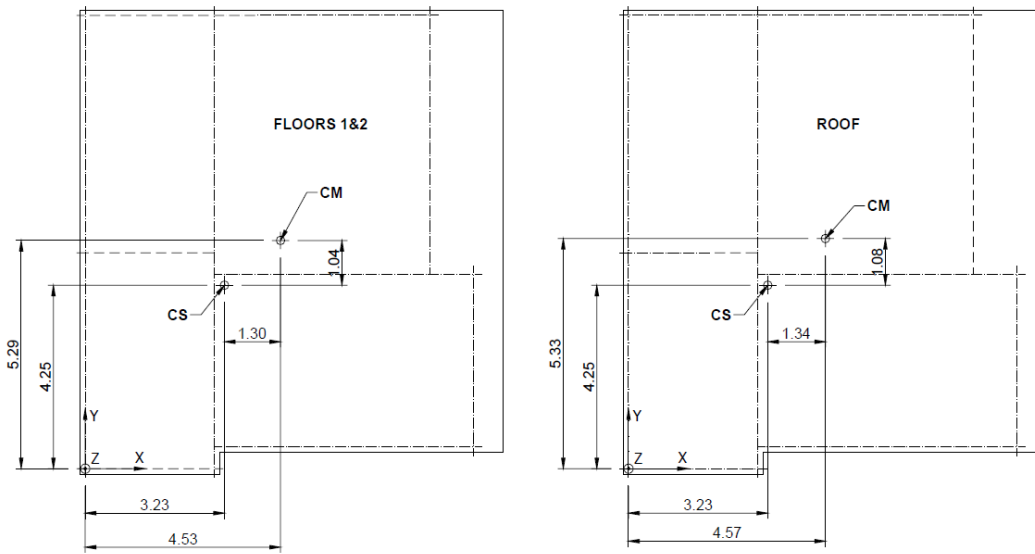
Figure 5.8: Centers of mass and stiffness of SPEAR building (Stratan and Fardis, 2003).

5.2.2 Gedikbulak school building

Gedikbulak school building was an irregular 3-story RC building that collapsed due to 2011 Van earthquake. Each story is 3 meters high, and dimensions vary between the beams and columns. The structure is irregular as the center of mass, center of stiffness, and the center of strength are located of different coordinates along the X-Y plane as shown in figure 5.9. Member cross-sections are given in figure 5.10. Because stirrup use was unsatisfactory, the model assumed that the cross-sections were unconfined.

Strength of concrete and yield strength of steel were estimated as 10 MPa and 400 MPa, respectively (Bal et. al 2015).
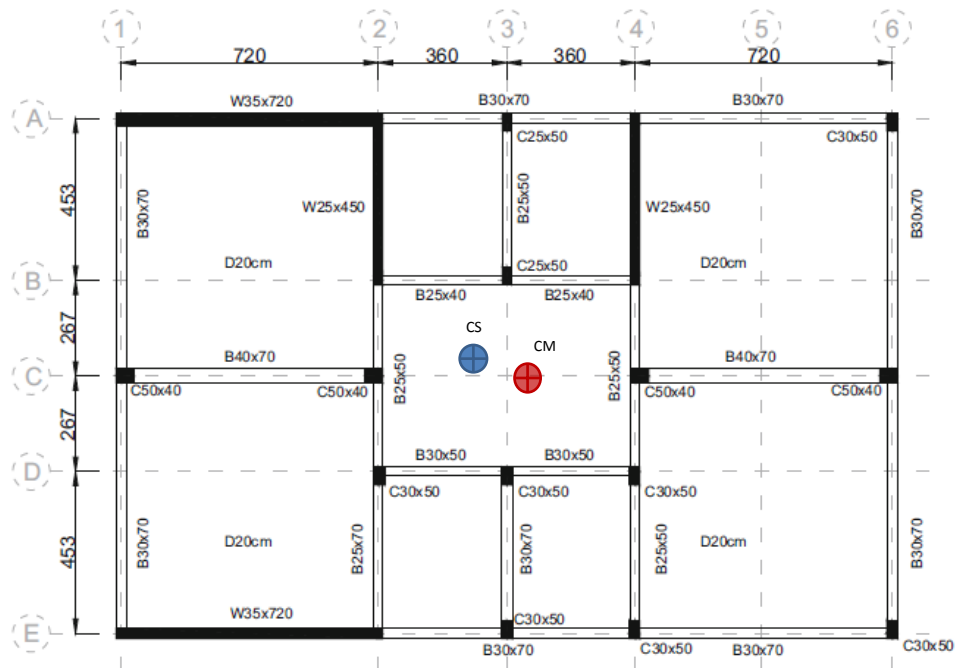
Figure 5.9: Plan of Gedikbulak building (Bal and Symrou, 2016)
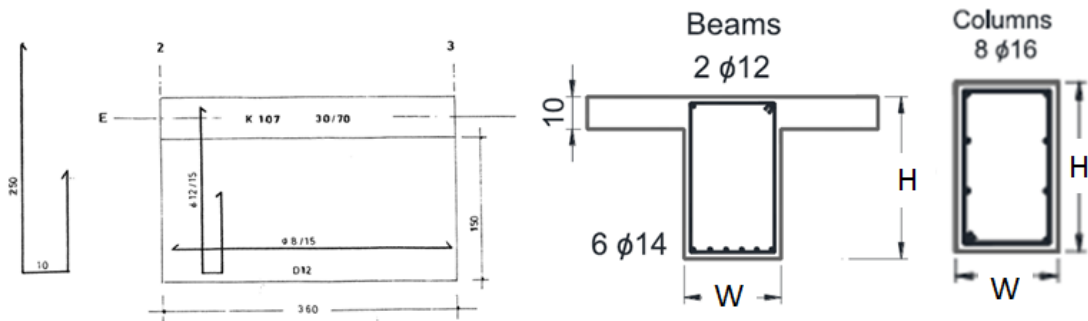
Figure 5.10: Cross-section drawings of Gedikbulak building's members.

As-built specifications of beam and column reinforcements could not be gathered; therefore, simple cross-sections have been used. Shear walls have 12mm diameter bars placed at 15 cm spacing.

5.2.3 Alaköy school building

Alaköy school building was an irregular 3 story RC building that was heavily damaged due to 2011 Van earthquake. Damage can be seen in figure 5.11. The building was investigated by EEDMI field teams after the earthquake and Taşkın et.

al (2014) have conducted a seismic analysis of the building while giving as-built specifications.

Figure 5.11: Photos of Alaköy building from site investigation (Taşkın et. al, 2014; EEDMI, 2011)

Upon investigation Taşkın et. al (2014) have found that the building had two frames and 4 bays and an external enclosed staircase. Bays have varying spans and columns are 2.65 meters tall from slab to slab. Plan geometry of the building is given in figure 5.13.
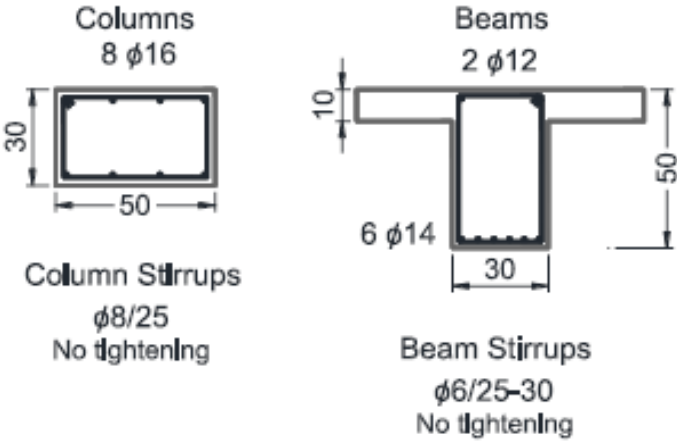
Figure 5.12: Cross-section specifications of Alaköy school building (Taşkın et. al, 2014).

56

Taşkın et. al (2014) note that upon investigation beam and column elements did not have confinement even though stirrups were used. Stirrups were constructed at 90 degrees. Taşkın et. al (2014) report that estimated steel and concrete classes are S220 and C12, respectively.
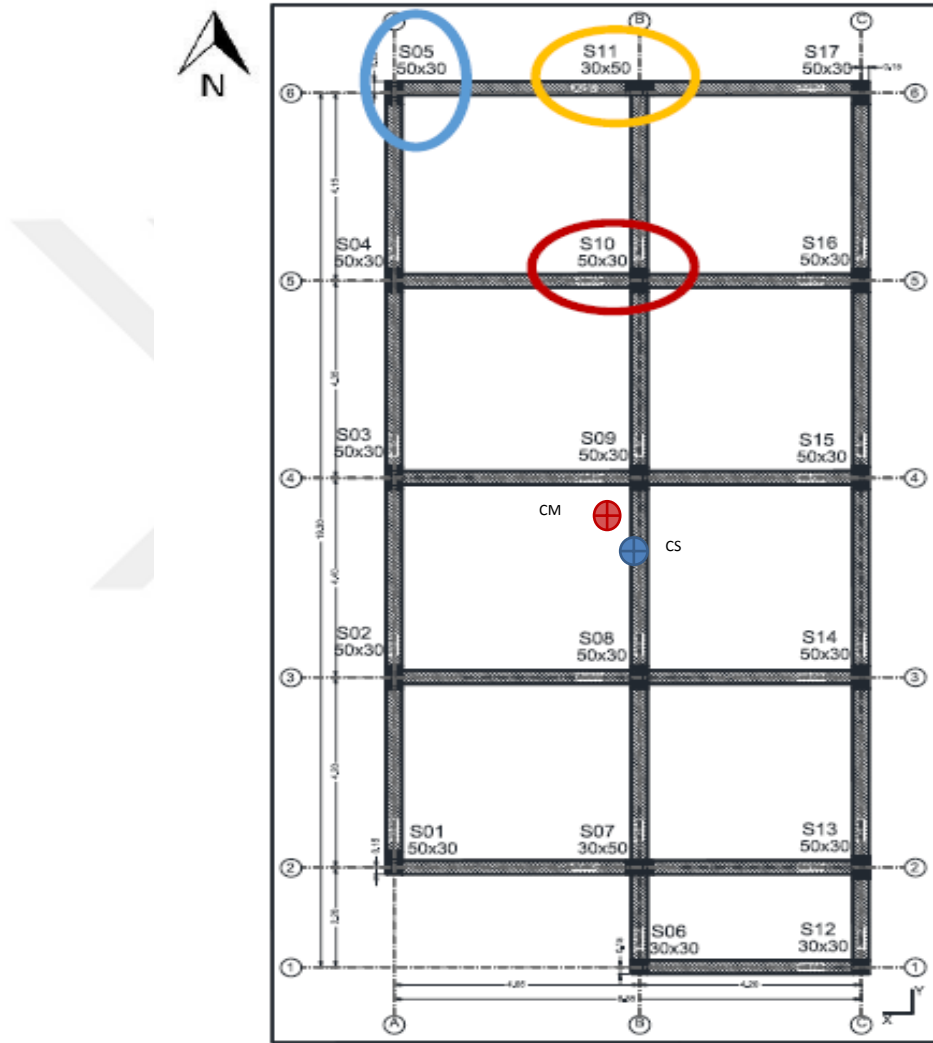
Figure 5.13: Specifications of Alaköy building (Taşkın et al. 2014).

5.3 Computer Models of Structures

5.3.1 SPEAR calibration structure

The SPEAR building was modeled according to past articles that analyzed the building (Fardis et. al, 1998; Jeong et. al, 2004; Papanikolaou, 2005; Oyguc et. al, 2015). The modeling approach is influenced by Oyguc et. al (2015). As shown in figure 5.14, beam elements were divided into multiple sections by assigning a node at 0.15L away from each end, and at every 0.35L for the rest of the beam's length. Masses of each story was assigned to nodes, and distributed according to the respected tributary areas. SPEAR building was used only for calibration purposes. Only eigenvalue analysis was conducted in order to crosscheck periods and the effects of torsion with previous research.
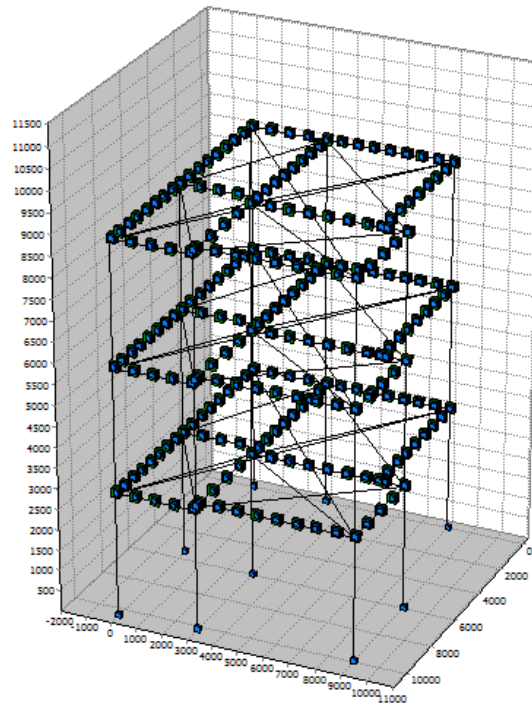
Figure 5.14:   ZEUS-NL model of SPEAR building.

5.3.2 Gedikbulak school building

Gedikbulak building was modeled using ZEUS-NL, a powerful tool for non-linear analysis. The model was built with according to as-built specifications reported by

Bal et. al. (2016). As shown is figure 5.15, modeling of masses and structural elements were done according to Oyguç et. al (2017). Each beam element has been divided into sections, depending on their lengths. The model uses lumped masses for simplicity, as the partitioning nodes were found to be adequate for such analysis. Total mass of the stories were distributed evenly among the nodes. Confinement was not applied due to inadequate in-situ stirrup hook angle. Reinforcements were simplified and placed on the bottom of beams. Reinforcements used specified materials f_y=400 MPa, f_{ck}= 10 MPa as reported by Bal. et. al (2007).
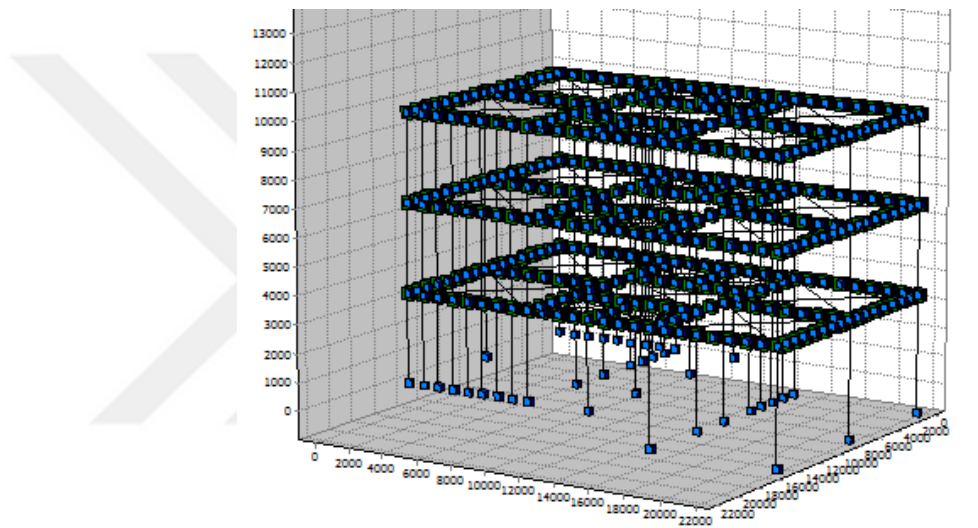
Figure 5.15: ZEUS-NL model of Gedikbulak school building.

Section types vary among columns and beams. The building has 4 shear walls that have different specifications that run from ground to the top. Shear walls were modeled in 9 and 5 equivalent shear walls for W35x720 and W25x450, respectively. Building consisted of four C50x40 columns along the midline, two C30x50 on the edges, and several C25x50 that spread across the rest the building. Even though the as-built beams were rectangular, beams are modeled as T-beams calculated using effective slab width as noted in Eurocode. Floor slabs were also modeled to simulate diaphragm effect, using 20cm x1000cm RC sections. Only the support nodes were restrained in every direction and rotation, except for the dynamic time-history analysis, where the software requires freeing the support nodes in the direction of applied force/acceleration. Every other node is free in every direction and rotation.

5.3.3 Alaköy school building

Alaköy school building was modeled according to the article by Taşkın et. al (2014). Using the 2D plan they have published, the building was modeled with the same notion that was applied for the Gedikbulak building, as in figure 5.16.
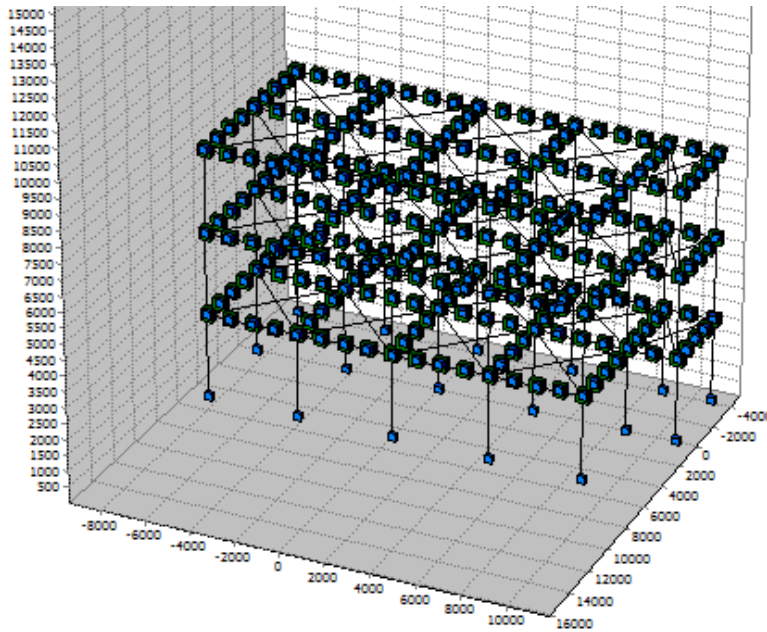
Figure 5.16:   ZEUS-NL model of the Alaköy school building.

Concrete and steel classes were C12 and S220, respectively. Load configuration was calculated and distributed among connection nodes, as well as partitioning nodes, in the form of lumped masses. Confinement effects were neglected due to insufficient hook angle of stirrups. Beams were modeled as T-beams according to Eurocode 8. Details of beam model are given in section 6.4. Floor slabs were modeled using thin elements with 20cm by 1000 cm RC sections.

Only the support nodes were restrained in every direction and rotation, except for the dynamic time-history analysis, where the software requires freeing the support nodes in the direction of applied force/acceleration. Every other node is free in every direction and rotation.

5.4 Modeling Principles

The building models have been generated using a similar approach that was used by Oyguc et. al (2017). The beam elements were separated by nodes, at every 0.35L and the two from 0.15L away from the beam ends. In order to account for P-delta effects the weight of the structures were applied onto respected columns for pushover, adaptive pushover, and dynamic time-history analyses. The mass of the structures; however, were distributed onto each node.

For both models, the beam cross-sections were modeled as T-beams. The web acts as the beam itself, and the flange acts as the floor slab. Slab effective width was calculated using Eurocode effective flange formula as shown in figure 5.17. Floors were assumed to have diaphragm behavior. In order to model that, floor slabs were built with a very low depth to width ratio. 15cm x 100cm. And the longitudinal reinforcements were placed 20cm apart. To create the diaphragm behavior, slab elements were placed between corner nodes crossing from side to side.
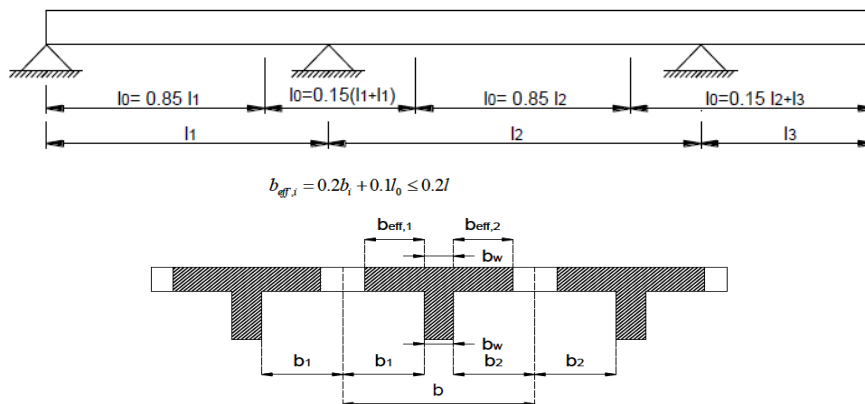
Figure 5.17: Effective slab calculation (Eurocode 8)

5.5 Material Models

Degrading and non-degrading models were used for comparison purposes. Non-degrading models were offered within ZEUS-NL software. Bi-linear steel model with constant strain hardening and constant confinement Mander model were implemented For degrading model, modified Menegotto-Pinto model with added bar-fracture feature was implemented. As depicted by Gomes and Appleton (1997),

material constants R, a1, and a2 were used as 20.0, 19.0, and 0.3, respectively. For degrading concrete model, Lee and Fenves degrading concrete model was used.

5.6 Non-linear Static Analyses

Pushover and force-based adaptive pushover with spectral acceleration were selected for this study for comparison purposes. Earlier studies show adaptive pushover with spectral acceleration results in a 20% lower capacity of buildings. N2 procedure was followed in order to calculate capacities in both pushover and adaptive pushover analyses. Analyses involved P-delta effects with axial loads placed on columns. Only non-degrading models were used in non-linear static analyses, since hysteresis is not a possible outcome.

Non-linear static analyses were conducted in order to determine weaker directions and shear capacities of selected buildings.

5.7 Dynamic time-history Analysis

To account for P-delta effects the weight of the buildings were applied as axial forces initially. Then both buildings were analyzed applying both components of the 7 records in the weak direction of Alaköy and Gedikbulak buildings. Non-degrading and degrading material models were used in the analyses. Therefore, 28 dynamic time-history analyses were conducted. For integration of equation of motion, Newmark's beta method was implemented using 0.5 and 0.25 for gamma and beta, respectively.

6. RESULTS

Prior to conducting any analyses, the building's mode shapes and eigenvectors were investigated and cross checked with the original articles of both subject buildings. The Alaköy building article by Taşkın et. al (2014) mentions their calculation of the natural period; however, Bal et. al (2016) does not. The natural period of Gedikbulak building was crosschecked with the article by Bilgin et. al (2005). Alaköy building verifies the model that is built in this study; however, there is significant difference in between Bilgin et. al and this study. The weight of the structure that was calculated in this study correlate with Bal et. al (2016). Bilgin et al. reports that the weight is 30% lighter and its natural period is 0.1 seconds, which is quite low for a 3-story building. Natural periods that were calculated in this study are given in table 6.1.

Table 6.1 : Natural vibration periods of the x-x and y-y modes and Ω values.

Periods	T1(x-x)	T2(y-y)	Ωx	Ωy
SPEAR	0.67	0.59	1.17	0.95
Alaköy	0.34	0.25	1.22	0.95
Gedikbulak	0.46	0.35	1.02	0.92

According to Fajfar et. al (2005), the ratio of an uncoupled lateral frequency to an uncoupled torsional frequency, called Ω gives an impression of the building's behavior. If the ratio is equal or greater than 1.00, the building behaves translational meaning torsionally stiff. If the ratio is less than 1.00, the building behaves torsionally, meaning torsionally flexible. In addition, the building can be translational in one direction, and torsional in the other direction. Therefore, both Alaköy and Gedikbulak buildings are translational in X-X direction, and torsional in Y-Y direction, which backs the dynamic time-history results.

6.1 Pushover and Adaptive Pushover Analyses

The results of the initial push for X and Y directions are given in the below sections. The lateral push was converted into acceleration units by using the N2 method's conversion into the SDOF system. Where Sa = F* / m*. Then, the resulting graph was compared to the elastic spectrum in ADRS format. Furthermore, adaptive pushover results have been compared with the regular pushover curves. Only the weak directions of the two buildings were evaluated in the adaptive pushover phase. Bi-linearization graphs and details are given in the appendices.

Table 6.2 : Gedikbulak Building's first mode shape and corresponding lateral. forces.
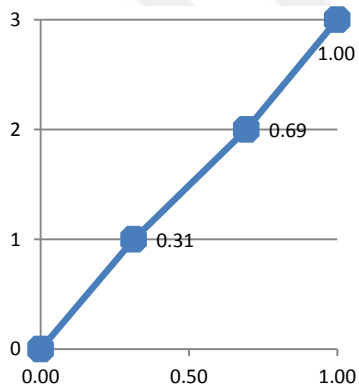
Lat Force Distribution	Force per Story (N)	Node per floor	Force per node (N)
0.50	8,668,708.56	4	2,167,177
0.35	6,012,592.77	4	1,503,148
0.16	2,718,698.66	4	679,675
Total Weight (N)	17,400,000		

Table 6.3 : Alaköy building's first mode shape and corresponding lateral forces.
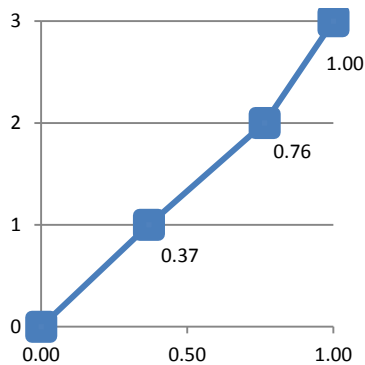
Lat Force Distribution	Force per Story (N)	Node per floor	Force per node (N)
0.47	2,718,490.76	5	543,698
0.36	2,078,614.00	5	415,723
0.17	1,002,895.24	5	200,579
Total Weight (N)	5,800,000		

6.1.1 Gedikbulak school building

Shear capacity and target displacement were calculated as 5234 kN and 0.0762 meters in the −Y direction, respectively. The shear capacity of adaptive pushover was 15% lower than the regular pushover analysis. It was found that adaptive and regular pushover curves were coinciding until the plastic region is reached. Therefore, it is safe to say that adaptive pushover results in a more conservative plasticity.

Plastic hinging occurred at columns as well as beams. Hinging in columns occurred more at top ends than bottom ends by 25 to 46. Beams also encountered plastic hinging, mostly on the first floor and at the far ends in the X direction.
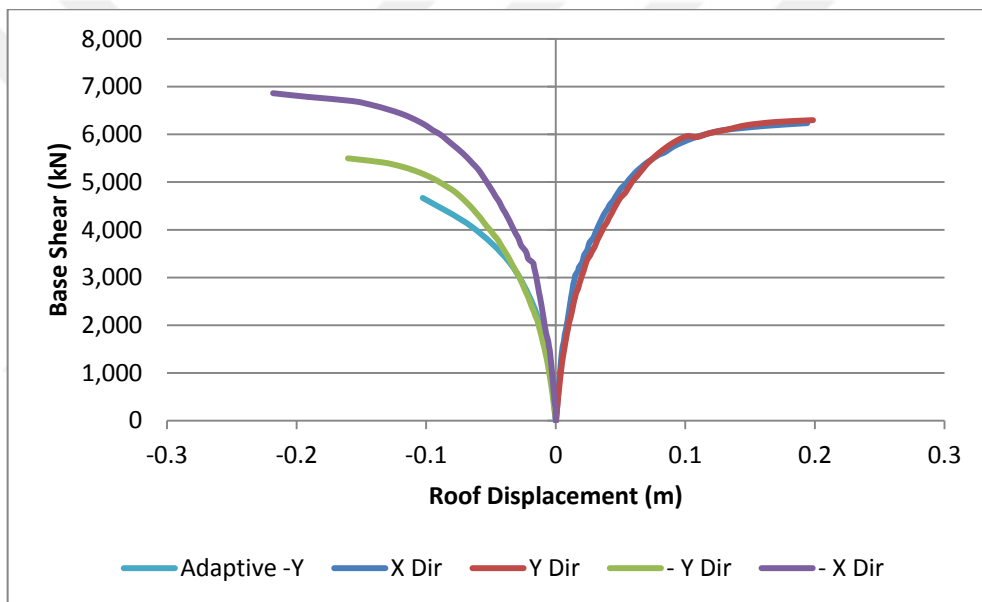
Figure 6.1: Gedikbulak building's pushover curve comparison.

It is worth noting that the +X and +Y directions are almost identical, whereas the −Y direction is much weaker than the −Y direction. It is also noteworthy that the strongest direction is the −X direction, which suggests irregularity.

Plastic hinges in the Y direction is almost the same as the X direction. In columns, 48 hinges occurred on the top end, and 18 hinges occurred on the bottom end. However, the number of nodes in wall members is higher. Since the long shear walls of the building are in the X-X direction, it is evident that much more column-beam connection nodes have yielded in the −Y direction.

Table 6.4 : Number of nodes where hinging occurred in Gedikbulak building. Numbers represent a total of both top and bottom of columns.

Plastic hinges	X	Y	-X	-Y
1st Floor	48	12	27	49
2nd Floor	10	0	18	19
3rd Floor	3	0	0	10

6.1.2 Alaköy school building

The building model has experienced a similar damage distribution to the site investigation. Most of the plastic hinging were evident at the top part of columns at the first floor (second story). Target displacement in the +X direction was found to be 0.061 meters. Target displacement in the –X direction was calculated as 0.070 meters. In the +Y direction the target displacement has been calculated as 0.106 meters, whereas the target displacement of the –Y direction has been found as 0.089 meters. Besides target displacements, the weakest direction of the building can be determined by comparing pushover data of the four directions. The adaptive pushover resulted in a 14% more conservative capacity, 1052 kN at 0.10074 meters of target displacement in the –Y direction. The adaptive and regular pushover capacity curves are identical until the yield point. Figure 7.2 shows the comparison of roof displacement versus base shear for all directions. Bi-linearization curves and response spectra in the ADRS format are presented in the Appendix A.
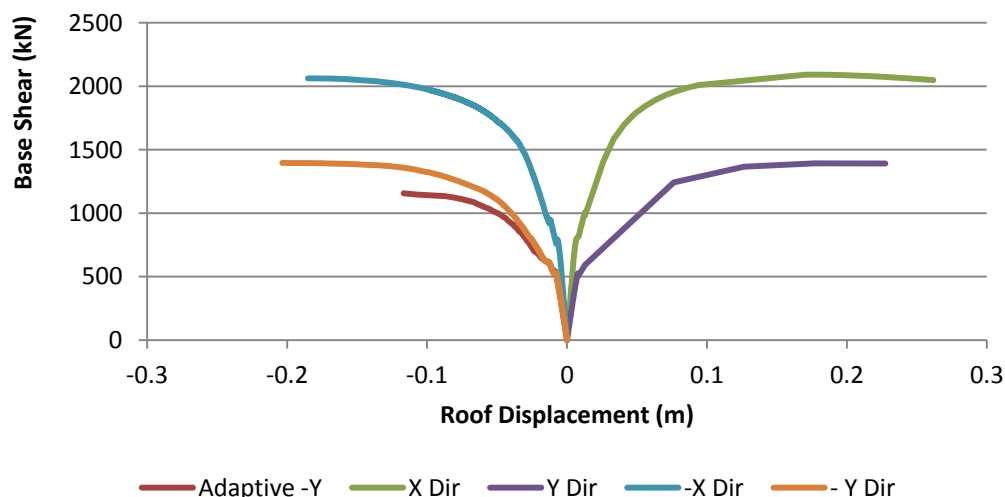
Figure 6.2: Alaköy building pushover capacity curve comparison.

66

Table 6.5 : Number of spots where plastic behavior was observed in Alaköy building. Numbers represent a total of both top and bottom of columns.

Plastic hinges	X	Y	-X	-Y
1st Floor	36	34	17	36
2nd Floor	21	20	24	24
3rd Floor	12	3	5	8

6.2 Dynamic Time-History Analysis

28 analyses were conducted during dynamic time-history analyses. Results from degrading and non-degrading models were compared in overlapping plots and tables. It should be noted that in order to reduce data management efforts, only the strong ground motion components that caused a higher response in the buildings were plotted and tabulated.

6.2.1 Gedikbulak building

Gedikbulak building's members have exceeded the yield strength therefore crossed into plastic hinge region in numerous locations including column-beam connections and in beam sections. Figure 7.3 shows the number of plastic hinging occurring at beams and columns with the respected material model. In both material model it is noteworthy that the columns have reached plastic hinging more than beams, suggesting strong beam-weak column situation. These results are in correlation with the field investigation findings.
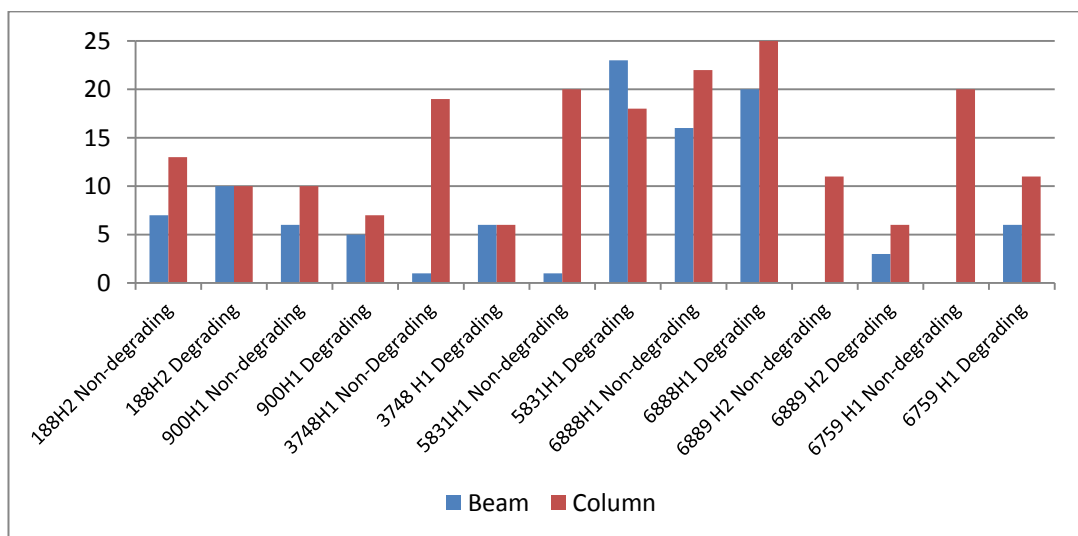
Figure 6.3: Gedikbulak building's total number of plastic hinges.

Table 6.6 : Summary of dynamic time-history results of Alaköy building.

	Non-Degrading				Degrading			
	Roof Drift (%)		Base Shear (kN)		Roof Drift (%)		Base Shear (kN)	
138H2	1.02%	Exceeding	5634	Exceeding	1.14%	Exceeding	7540	Exceeding
900H1	1.22%	Exceeding	7908	Exceeding	1.29%	Exceeding	7818	Exceeding
3748H1	2.02%	Exceeding	8445	Exceeding	1.14%	Exceeding	7215	Exceeding
5837H1	1.10%	Exceeding	6101	Exceeding	1.05%	Exceeding	6954	Exceeding
6888H1	0.92%	Exceeding	6398	Exceeding	1.00%	Exceeding	6094	Exceeding
6889H1	0.99%	Exceeding	5548	Exceeding	0.99%	Exceeding	6583	Exceeding
6952H1	1.06%	Exceeding	7332	Exceeding	2.07%	Exceeding	6627	Exceeding

Furthermore, all of the records have caused exceedance of allowable roof drift of 0.5% and base shear capacity. As in table 6.6, degrading materials have been shown to cause a higher amount of exceedance with two exceptions.
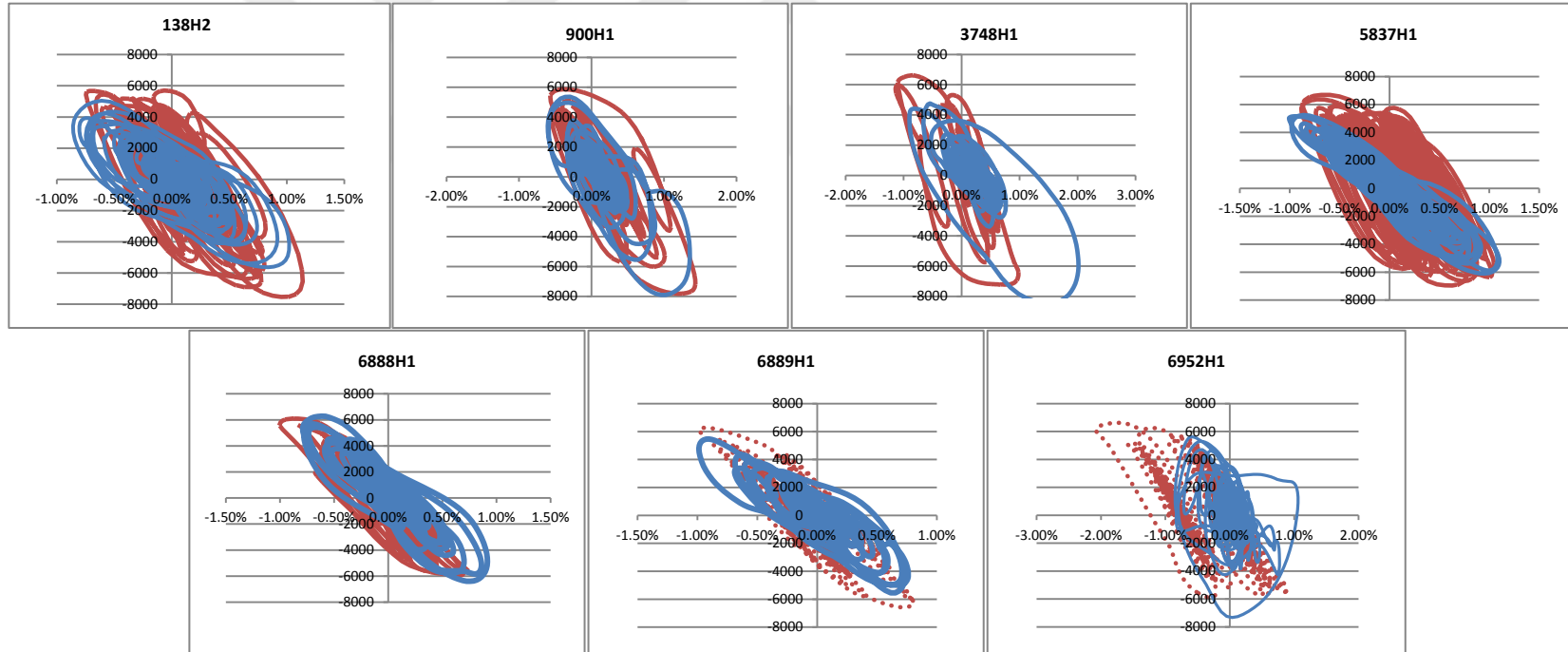
Figure 6.4: Base shear (kN) versus roof drift (%) of Gedikbulak building. Degrading material model (red), non-degrading material model (blue).

Table 6.7 : Residual displacement of Gedikbulak building.

	Residual Displacements (mm)	
	Non-degrading	Degrading
138H2	2.2	25.6
900H1	1.1	18.3
3748H1	5.1	17.1
5837H1	0.7	50.4
6888H1	3.2	3.4
6889H1	3.1	13.2
6952H1	2.9	56.6

Residual displacements have occurred during analyses. Permanent deformations given in table 6.7 can be seen on time plots in the appendices.

6.2.2 Alaköy building

Alaköy building have experienced plastic hinging in beams in 9 cases, whereas, columns experienced plastic hinging more in 5 cases. Degrading and non-degrading models have similar results prooving correct correlation between them.
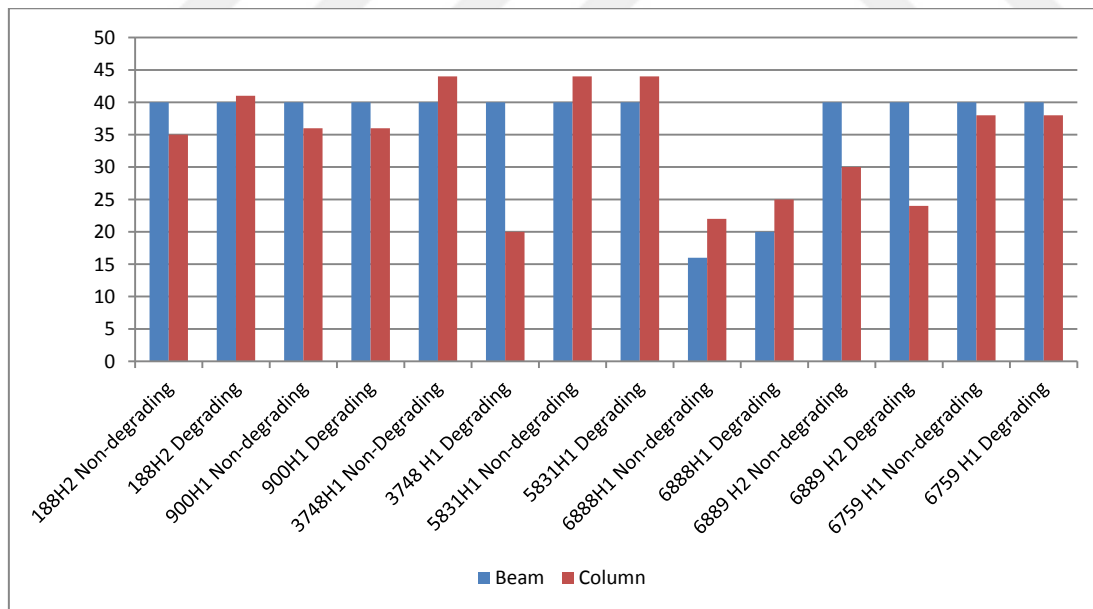
Figure 6.5: Number of plastic hinges that occurred in Alaköy building.

Table 6.8 : Summary of dynamic time-history results of Alaköy building.

	Non-Degrading				Degrading			
	Roof Drift (%)		Base Shear (kN)		Roof Drift (%)		Base Shear (kN)	
138H2	0.85%	Exceeding	1353	Exceeding	1.24%	Exceeding	1622	Exceeding
900H2	1.87%	Exceeding	1569	Exceeding	1.83%	Exceeding	1564	Exceeding
3748H1	2.12%	Exceeding	1634	Exceeding	1.84%	Exceeding	1572	Exceeding
5837H1	0.61%	Exceeding	1186	Exceeding	0.75%	Exceeding	1467	Exceeding
6888H1	0.69%	Exceeding	1487	Exceeding	0.71%	Exceeding	1599	Exceeding
6889H2	0.91%	Exceeding	1367	Exceeding	0.77%	Exceeding	1543	Exceeding
6952H2	1.35%	Exceeding	1429	Exceeding	1.75%	Exceeding	1289	Exceeding
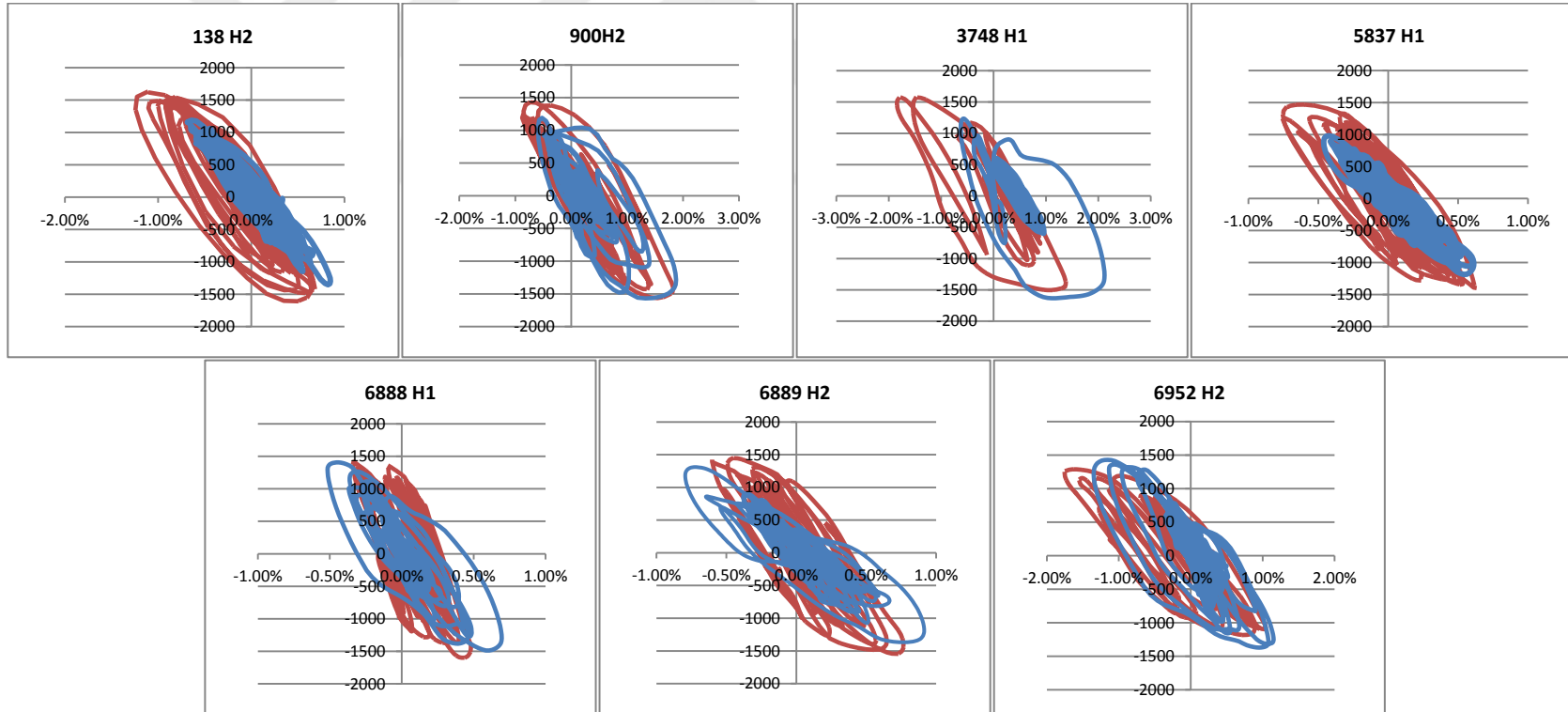
Figure 6.6: Base shear (kN) versus roof drift (%) of Alaköy building. Degrading material model (red), non-degrading material model (blue).

Table 6.9 shows residual displacement occurred during analyses. Analyses of records 5837 H1 and 6888 H2 were stopped due to convergence issues; however, the results are satisfactory besides residual displacements.

Table 6.9 : Residual displacement of Alaköy building.

	Residual Displacements (mm)	
	Non-degrading	Degrading
138H2	5.84	14.69
900H2	33.4	22.3
3748H1	24.1	20.8
5837H1	3.01	--
6888H1	4.49	--
6889H1	7.96	7.77
6952H2	0.72	0.82

6.3 Discussion of Results

Degrading models have resulted in greater absorbed energy, which is visible through visual inspection of figures 6.6 and 6.4. According to Di Sarno et. al (2015), high damage indicates high energy absorption, which occurs through permanent deformations. That means higher damage is indicated by a greater area covered by the base shear versus roof drift graphs. The area under the curve equals total absorbed energy. Higher absorbed energy can also be seen on story drift versus time graphs, in the form of residual deformations. For example, in case 6952 H1 of Gedikbulak building, the final displacement has reached 56.6 millimeters when degrading materials were used. At time 30.9s, the roof displacement's baseline shifts 40 millimeters. That is explained in part by P-delta effect's contribution to degraded cross sections.
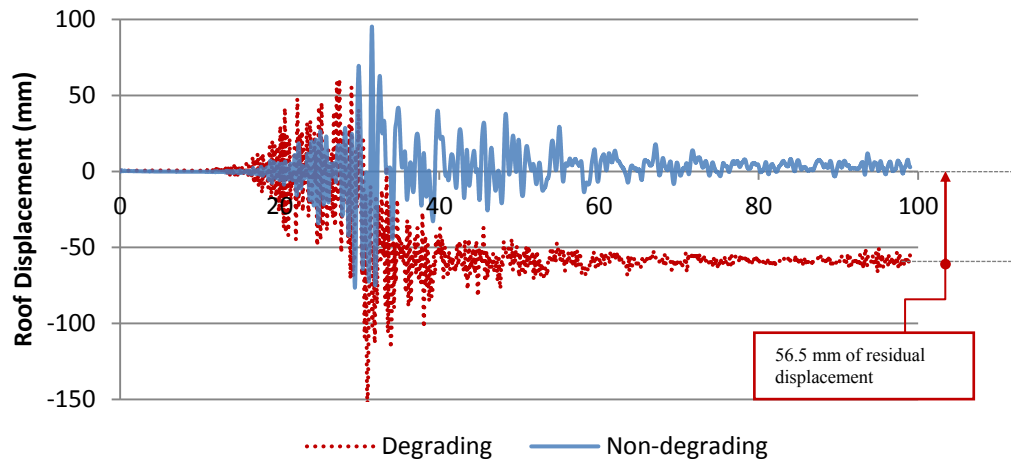
Figure 6.7: Gedikbulak building's roof displacement versus time plot for case 6952 H1.

Generally, after reaching 0.5% drift, analyses yielded large areas under drift versus base shear graphs,, in figures 6.4 and 6.6. This finding resonates with the fact that damage is expected when story drift exceeds 0.5%.

Story drifts and roof displacements give valuable information about building's dynamic behavior. Case 6952 H1 of Gedikbulak building shows significant difference between non-degrading and degrading material models as shown in figures 6.8 and 6.9. Furthermore, figure 7.8 shows the behavior of first floor and its contribution to roof drift when degrading effects are enabled.
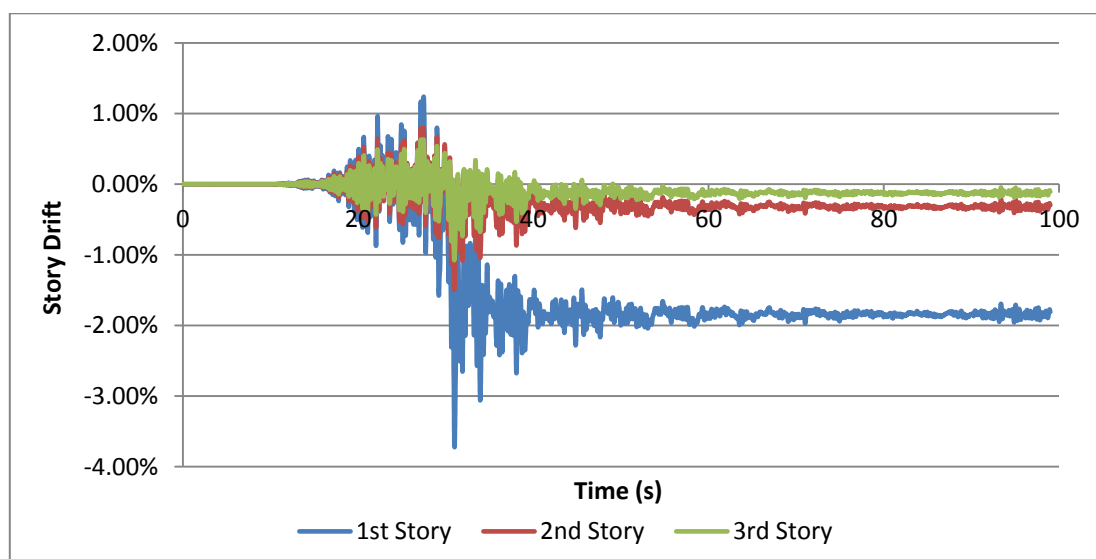
Figure 6.8: Story drift results from degrading model of case 6952 H1 of Gedikbulak building.

74
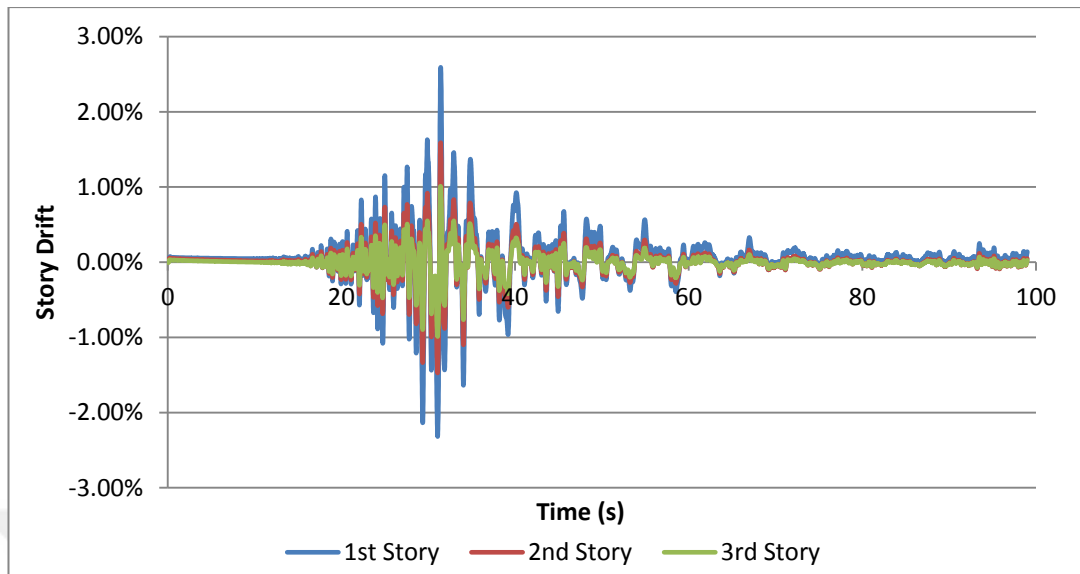
Figure 6.9:   Story drift results from non-degrading model of case 6952 H1 of Gedikbulak building.

Figures 6.8 and 6.9 present the strongest evidence for the difference between degrading and non-degrading models. Non-degrading model has reached a high story drift as well; however, despite present P-delta effects the building show insignificant permanent deformations.

There are cases where response of non-degrading materials exceeded degrading material cases. Non-degrading cases 900 H2 and 3748 H1 of Alaköy building have experienced significant permanent deformation, as shown in figure 7.10. After largest excursions in cases 3748 H1 and 900 H2, Alaköy building becomes permanently deformed possibly due to P-delta effects. According to Abdelnaby (2013), stiffness of the non-degrading model depends solely on maximum displacement. Following maximum displacement, stiffness of the system reaches its lowest value, and stays constant until the end of strong ground motion record. Abdelnaby (2013) adds that P-delta effects have minimal role on stiffness reduction; however, some cases in his study have experienced permanent deformations.

Number of plastic hinging varies greatly between earthquakes. That verifies the effect of earthquake characteristics on dynamic response.
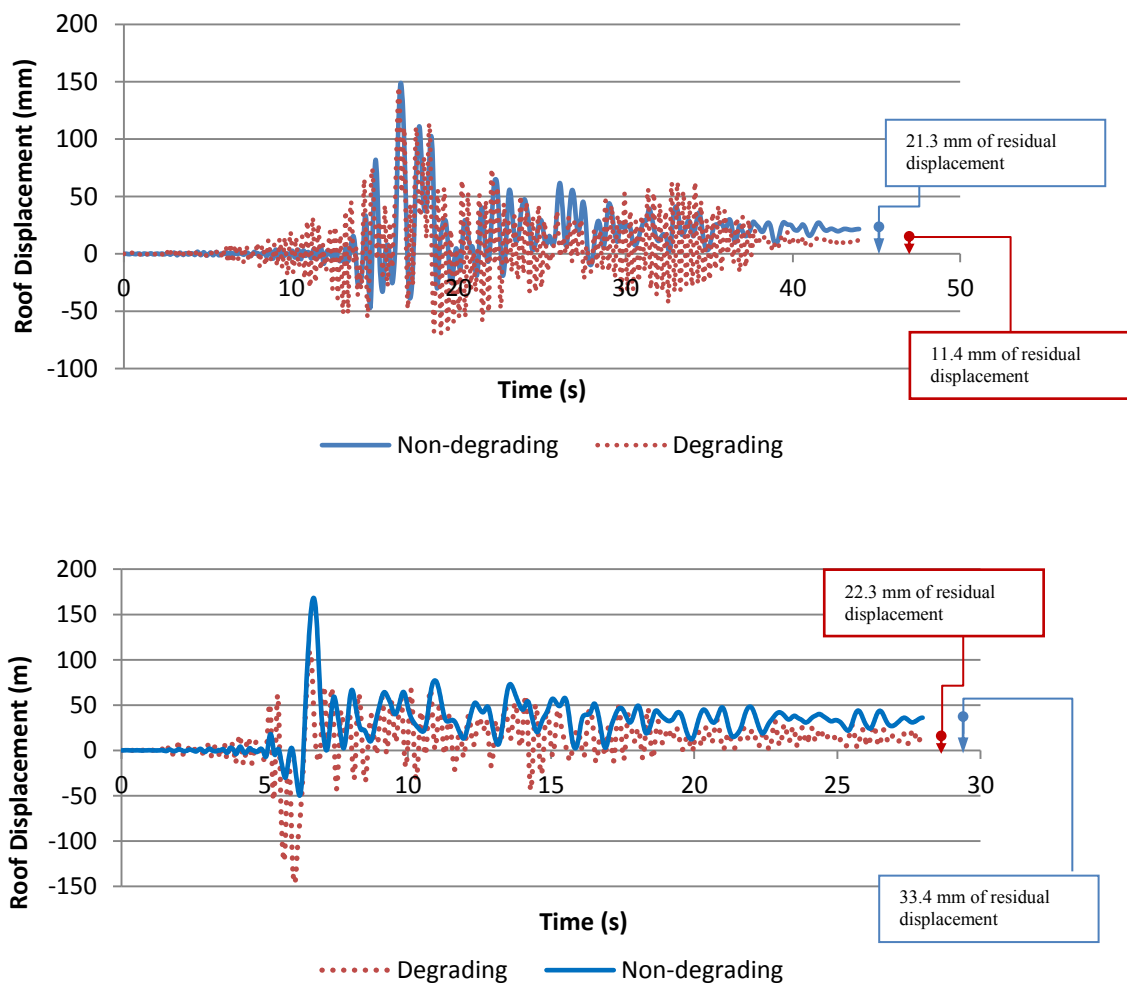
Figure 6.10: Alaköy building's roof displacement versus time (s) plots for cases 900H2 (top) and 3748 H1 (bottom).

7. CONCLUSION

In this study two reinforced concrete school buildings have analyzed in an attempt to simulate their behavior in Van Earthquake of 2011. The results are in good correlation between themselves, such as pushover analyses and dynamic time-history analyses. The results also represent the in-situ damage that has occurred during the Van Earthquake. It can be seen from the analyses that irregularity can affect a building's seismic behavior. Torsionally flexible directions were the weak directions of both buildings, as shown on pushover analyses. Also adaptive pushover results indicate irregularity where Alaköy building 14% and Gedikbulak building 15% more conservative results than conventional pushover analysis.

Dynamic time history analyses resulted in good correlation with in-situ conditions of both buildings. About an equal amount of plastic hinges have occurred between beams and columns in Alaköy building, explaining why the building have taken serious damage but have not collapse. On the contrary, Gedikbulak building have had more damage in the columns than in beams, explaining why the building have collapsed catastrophically. Gedikbulak building is a government-designed building; however, there was significant design flaws in the construction where the contractor skipped some of the shear walls was in the original design. Conclusions of the study are given below:

- Both buildings have behaved in-elastically in all earthquake cases.

- Even carefully selected hazard-compatible earthquakes have had drastic differences between each other in terms of damage mechanism, prooving the necessity of using a set of earthquake records when simulating strong ground motion.

- Degrading models have had much more permanent deformation than non-degrading models. Also degrading models have greater base shear to roof drift ratio, showing that degrading models have dissipated more energy, indicating more occurred damage.

•Story drift threshold ratio of 0.5% was exceeded in al cases. Shear capacity was exceeded in all cases as well.

REFERENCES

[1] **Abdelnaby, A.E.,. and Elnashai, A.S.** (2014). Performance of degrading reinforced concrete frame systems under the Tohoku and Christchurch earthquake sequences. *Journal of Earthquake* (2014), (18), 1009-1036

[2] **Fahjan, Y.M.,** (2008). Selection and scaling of real earthquake accelerograms to fit the turkish design spectra. *Teknik Dergi,* (19)3, 4423-4444

[3] **Taşkın, B., and Tuğsal, U. M.** (2014). Inspection and Modeling of the Observed Damage in an RC Building after 2011 Van Earthquakes. *ACE 11ᵗʰ International Congress on Advances in Civil Engineering 2014 Conference*).

[4] **Bal, İ. E., and Smyrou, E.** (2017). Simulation of the earthquake-induced collapse of a school building in Turkey in 2011 van earthquake. *Bulletin of Earthquake Engineering,* (2016)., (14), 3509-3528

[5] **Papanikolaou, V. K., Elnashai, A.S., Pareja, J.F.,**. (2005). Limits of applicability of conventional and adaptive pushover analysis for seismic response assessment, *Mid-America Earthquake Center University of Illinois at Urbana-Champaign. Retrieved from:*

http://mae.cee.illinois.edu/publications/reports/Report05-02.pdf

[6] **Oyguc, R., Toros, C., Abdelnaby, A.E.,** (2018). Case study on seismic behavior of aseismically designed reinforced concrete frame structures *Bull Earthquake Eng.* (16), 3057

[7] **Reyes, J.C, and Chopra, A.K,.** (2010). Three-dimensional modal pushover analysis of buildings subjected to two components of ground motion, including its evaluation for tall buildings. *Earthquake Engng Struct. Dyn.*(2011), (40), 789-806.

[8] **EUROCODE 8** (2004). *Design of structures for earthquake resistance,* Europoean Standard EN 1998-1:2004

[9] **Lee, J., and Fenves, G.** (1998). Plastic damage model for cyclic loading of concrete structures. *Journal of Engineering Mechanics,* (124)8, 829-900.

[10] **Menegotto, M., and Pinto, P.** (1973). Method of Analysis for Cyclically Loaded RC Plane Frames Including Changes in Geometry and Non-elastic Behavior of Elements Under Combined Normal Force and Bending, *Symp. Resistance and Ultimate Deformability of Structures Acted on by Well Defined Repeated Loads, IABSE Reports Vol 13, Lisbon.*

[11] **Bilgin, H., and Özmen, H.B., İnel, M.,** (2005). Kamu yapılarının performanslarının doğrusal ötesi davranış modelleriyle değerlendirilmesi. *Deprem Sempozyumu March 2005, Kocaeli, Turkey*

[12] **Oyguc. R., Oyguc, E., Tönük, G.,** (2017). Case study on seismic behavior of aseismically designed reinforced concrete frame structures. *Bull Earthquake Eng (2018), (16), 3057–3080*

[13] **Yazgan, U., Oyguc R., Erguven., M. E., Celep, Z.,** (2016). Seismic performance of buildings during 2011 Van earthquakes and rebuilding efforts. *Earthq Eng & Eng Vib* (2016), 15, 591-606

[14] **Di Sarno, L., Yenidogan, C., Erdik, M.,** (2013). Field evidence and numerical investigation of the Mw=7.1 October 23 Van, Tabanli and the Mw > 5.7 Novermber earthquakes of 2011. *Bull Earthquake Eng* (2013), 11, 313–346

[15] **Abrahamson, N. A., and Silva, W. J.,** (2008). Summary of the Abrahamson & Silva NGA Ground-Motion Relations. *Earthquake Spectra* (2008), 24, 67-97

[16] **Abrahamson, N. A., and Silva, W. J.,** (2008). Empirical Response Spectral Attenuation Relations for Shallow Crustal Earthquakes. Seismological Research Letters, 68 (1), 94–127

[17] **Boore, D.,M.,** (2003). Simulation of ground motion using the stochastic method. *Pure Applied Geophysics,* (2003), 160, 635-676

[18] **Mert. A., Fahjan, Y., Pinar, A., Hutchings, L.,** (2014). Strong ground motion simulations around Prince Islands fault. *Digest 2014* (December 2014), 1757-1783

[19] **Douglas, J., Bungum, H., Scherbaum, F.,** (2006). Ground-motion prediction equations for southern Spain and southern Norway obtained using the composite model perspective. *Journal of Earthquake Engineering* (2006), 10, 33-72

[20] **Hutchings, L., and Viegas, G.,** (2013). Application of empirical Green's functions in earthquakesource, wave propagation and strong ground motion studies in earthquake research and analysis. Retrieved from:

https://www.researchgate.net/publication/285026107_Application_of_empirical_Green's_functions_in_earthquake_source_wave_propagation_and_strong_ground_motion_studies_in_earthquake_research_and_Analysis/citations

[21] **Erberik, M. A., and Kurtman, B.,** (2010). A detailed evaluation on degrading behavior of structural systems. *Proceedings of the 9th U.S. National and 10th Canadian Conference on Earthquake Engineering* (2010), Paper no: 369

[22] **Lee, J., and Fenves, G. L.,** (1998), Plastic-damage model for cyclic loading of concrete structures. *Journal of Enginering Mechanics* (1998), 124(8), 898-900

[23] **Mander., J. B., Priestley, M. J. N., Park, R.,** (1988), Theoretical stress-strain model for confined concrete. *Journal of Structural Engineering* (1988), 114(8), 1804-1826

[24] **T. Takeda, M. A. Sozen, and N. N. Nielsen**, (1970). Reinforced concrete response to simulated earthquake, *Journal of Structural Division,* 96(12), 2257–2273

[25] **Kappos, A.J., Lekidis, V., Panagopoulos, G., Sous, I., Theodulidis, N., Karakostas, C., Anastasiadis, T., Salonikios, T., and Margaris, B**. (2007) Analytical estimation of economic loss for buildings in the area struck by the 1999 Athens earthquake and comparison with statistical repair costs. *Earthquake Spectra,* 23, 333-335

[26] **Chopra, A. K. and Goel, R. K.** (2004), A modal pushover analysis procedure to estimate seismic demands for unsymmetric-plan buildings. *Earthquake Engng. Struct. Dyn.,* 33, 903-927

[27] **Shakeri, K., Shayanfar, M. A., Kabeyasawa, T.,** (2010). A story shear-based adaptive pushover procedure for estimating seismic demands of buildings. *Engineering Structures* (2010), (32)1, 174-183.

[28] **Montes-Hernandez, E., Kwon, O., Aschheim, M. A.,** (2004). An energy-based formulation for first-and multiple-mode nonlinear static (pushover) analyses. *Journal of Earthquake Engineering,* (2004), (8)1, 69-88.

[29] **Papanikolaou, V. K., Elnashai, A.S., Pareja, J.F.,** (2005*). Limits of applicability of conventional and adaptive pushover analysis for seismic response assessment.* Mid-America Earthquake Center, University of Illinois at Urbana-Champaign, CD Release 05-02, April. Retrieved from:

https://www.researchgate.net/publication/32962446_Limits_of_Applicability_of _Conventional_and_Advance_Pushover_Analysis_for_Seismic_Response_Asse ssment

[30] **Reyes, J.C., and Chopra, A. K.,** (2010) Three-dimensional modal pushover analysis of buildings subjected to two components of ground motion, including its evaluation for tall buildings. *Earthquake Engineering and Structural Dynamics,* (2011), 40, 789-806.

[31] **Fajfar, P.,** (2000) A nonlinear analysis method for performance based seismic design. *Earthquake Spectra,* (2000), (16)3, 573-592.

[32] **Deierlein, G. G, Reinhorn, A. M., Willford, M. R.** (2010) *Nonlinear structural analysis for seismic design.* NEHRP Seismic Design Technical Brief No: 4, NIST GCR 10-917-5, National Institute of Standards and Technology, Gaithersburg, MD .

[33] **Priestley, M. J. N.,** (2000). Performance based seismic design. *Bulletin of the New Zealand Society for Earthquake Engineering,* (33)3, 325-346

[34] **Papanikolaou, V. K.,** (2000). *Development and Verification of Adaptive Pushover Analysis Procedures* (Master's thesis). Imperial College of Science, Technology and Medicine.

[35] **Antoniou, S., and Pinho, R.** (2004). Advantages and limitations of adaptive and non-adaptive force-based pushover procedures. *Journal of Earthquake Engineering* ,(8)4, 497-522.

[36] **Zengin, E., and Cakti, E.,** (2004). Ground motion simulations for the 23 October 2011 Van, Eastern Turkey earthquake using stochastic finite fault approach. *Bulletin of Earthquake Engineering* (2014), 12, 627–646

[37] **Applied Technology Council** (2009), *FEMA P440A effects of strength and stiffness degradation on seismic response.* Prepared for Federal Emergency Management Agency.

[38] **Applied Technology Council** (2009), *FEMA P-1051 recommended seismic provisions: design examples.* Prepared for Federal Emergency Management Agency.

[39] **Gomes, A., and Appleton, J.,** (1997). Nonlinear cyclic stress-strain relationship of reinforcing bars including buckling. *Engineering Strcutures* ,19(10), 822-826.

[40] **KOERI** (2011). The October 23, 2011 Van, Turkey earthquake (Mw=7.2). Retrieved from: http://www.koeri.boun.edu.tr/depremmuh/deprem-raporlari/Van_Eq_SM_31102011.pdf

[41] **Konca, O.,** (2015). Rupture process of 2011 Mw7.1 Van, Eastern Turkey

earthquake from joint inversion of strong-motion, high-rate

GPS, teleseismic, and GPS data. *Journal of Seismology* ,19, 969-988.

[42] **Oyguc, R.,** (2000). *An adaptive 3-D pushover procedure for determining the capacity of existing irregular reinforced concrete (RC) buildings.* (Doctoral dissertation). Istanbul Technical University.

[43] **Jeong, S., and Elnashai, A. S.,** (2004), *Analytical assessment of an irregular RC full scale 3D test structure.* University of Illinois at Urbana-Champagne. Retrieved from: http://mae.cee.illinois.edu/publications/reports/Report04-03.pdf

[44] **Stratan, A., and Fajfar P.,** (2003), *Seismic assessment of the SPEAR test structure.* University of Ljubljana. Retrieved from:

http://library.upt.ro/pub.edocs/69837/index.pdf

[45] **Motazedian, D., and Atkinson, G. M.,** (2008). Stochastic finite-fault modeling based on dynamic corner frequency. *Bulletin of the Seismological Society of America* ,95(3), 995-1010.

[46] **Ansal, A., and Tonuk, G.,** (2007). Source and site effects for microzonation. *Earthquake Geotechnical Engineering* ,Ch. 4, 73-92.

APPENDICES

APPENDIX A.1 : Capacity curves and corresponding response spectra.

Gedikbulak - X

Gedikbulak - X

Gedikbulak +Y

Gedikbulak +Y

Gedikbulak - Y

Gedikbulak - Y

Gedikbulak Adaptive -Z

Gedikbulak Adaptive -Z

Alaköy X Dir

Alaköy X Dir

Alaköy -X Dir

Alaköy -X Dir

Alaköy Z Dir

Alaköy Z Dir

Alaköy -Z Dir

Alaköy -Z Dir

91

Alaköy Adaptive -Z

Alaköy Adaptive -Z
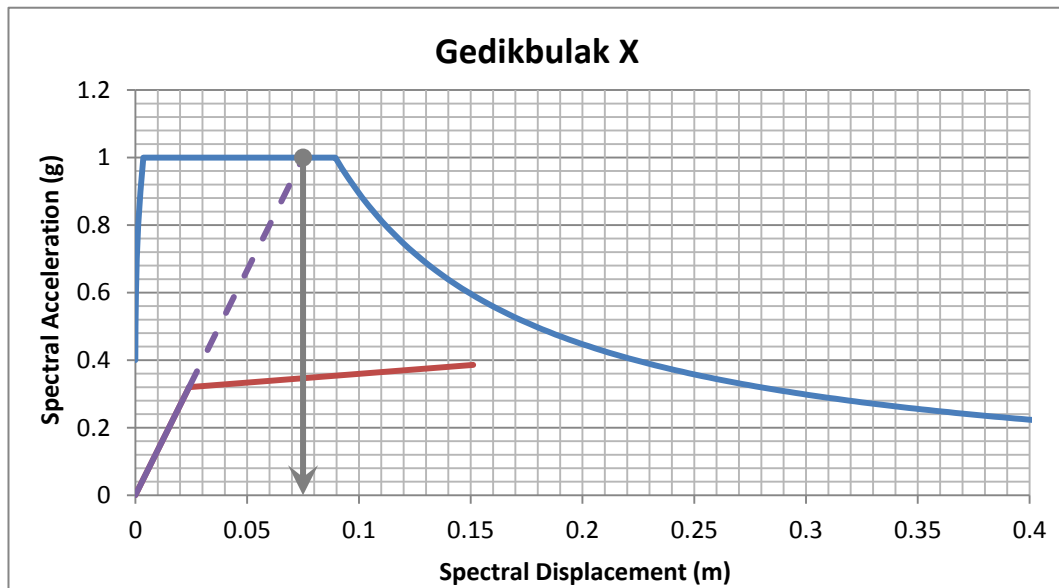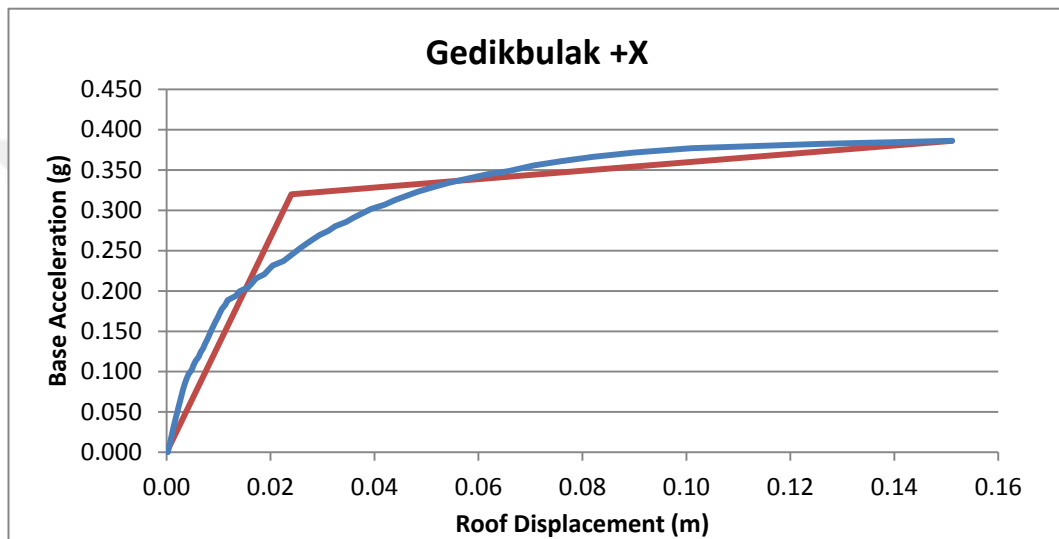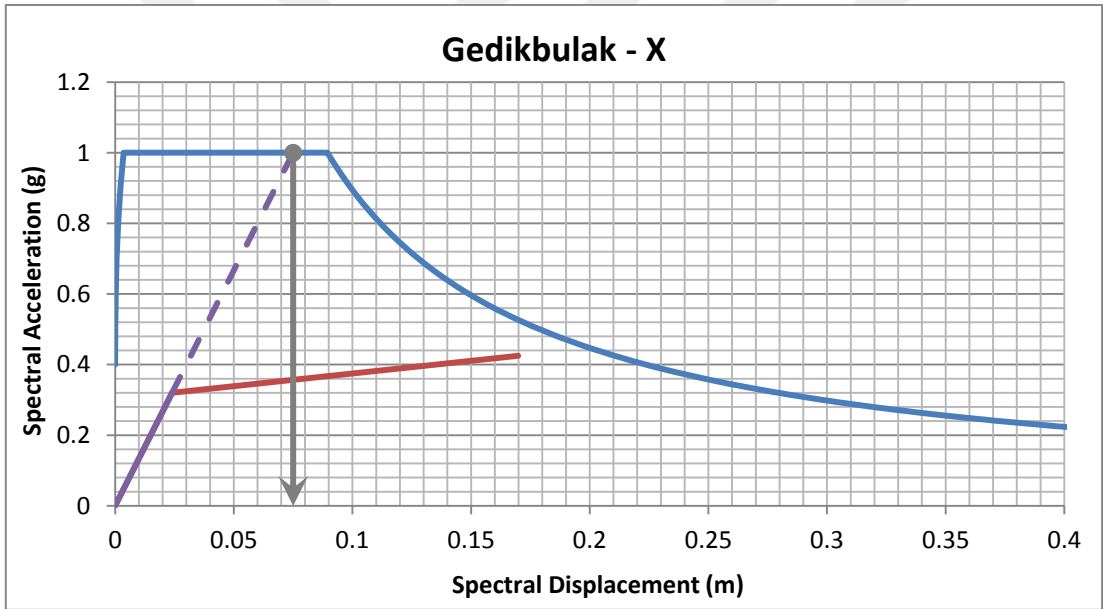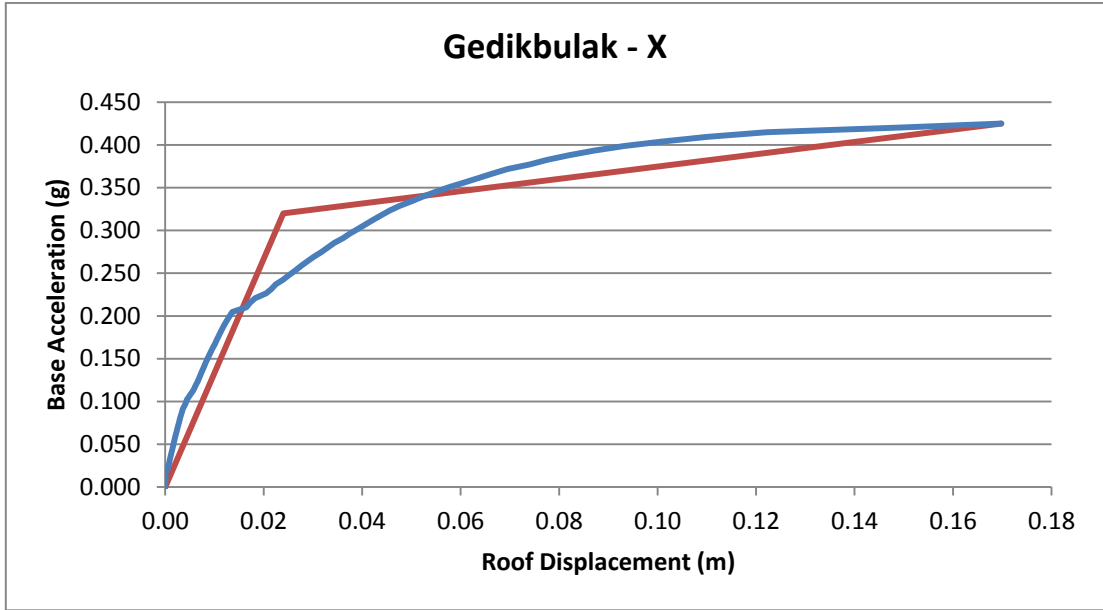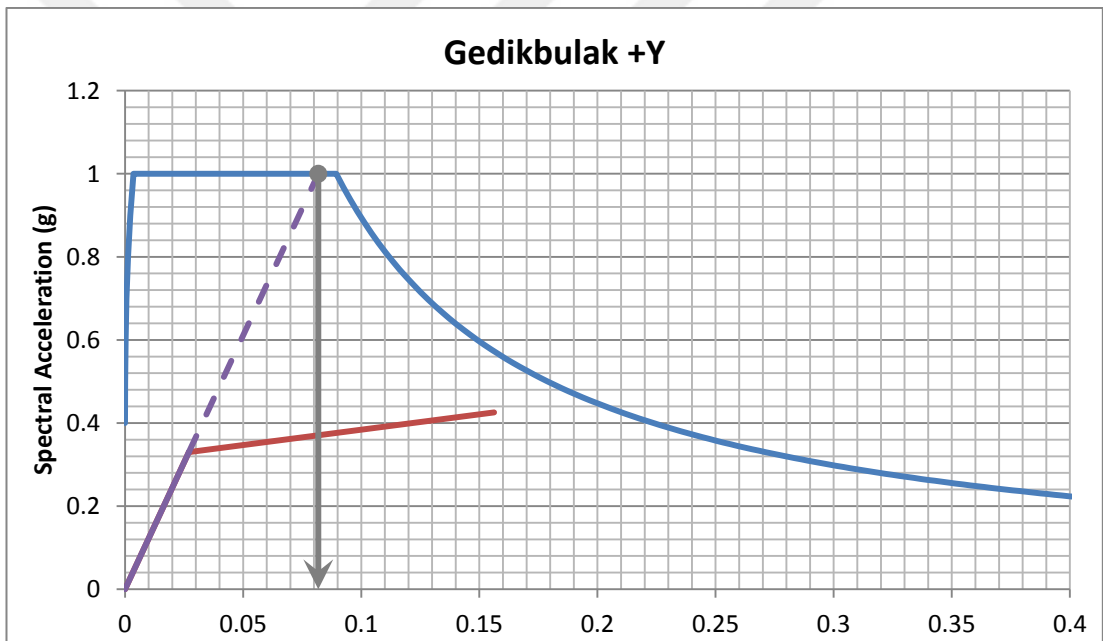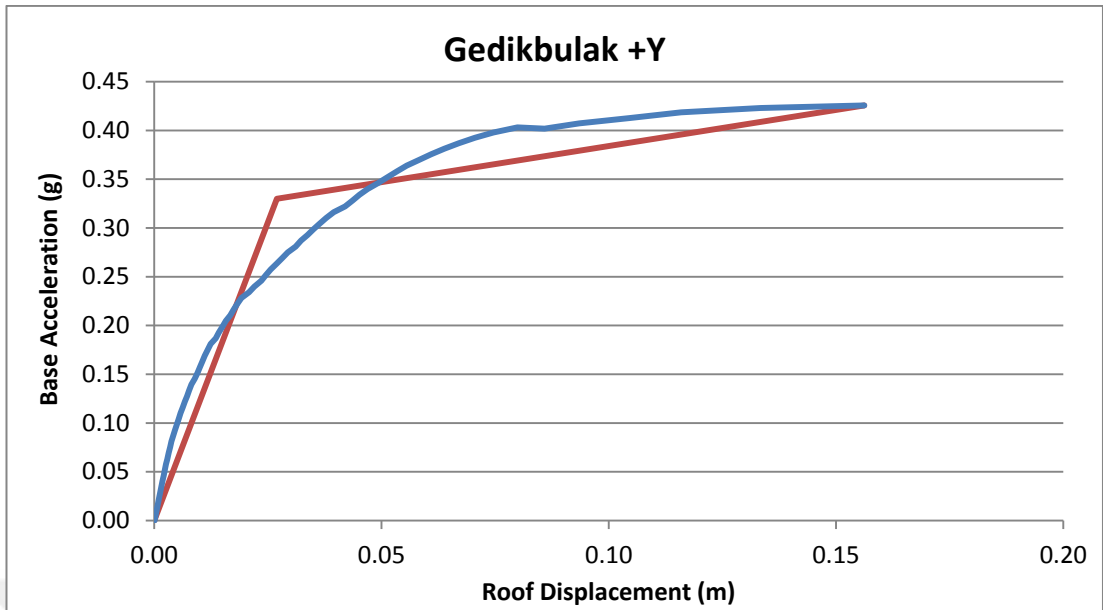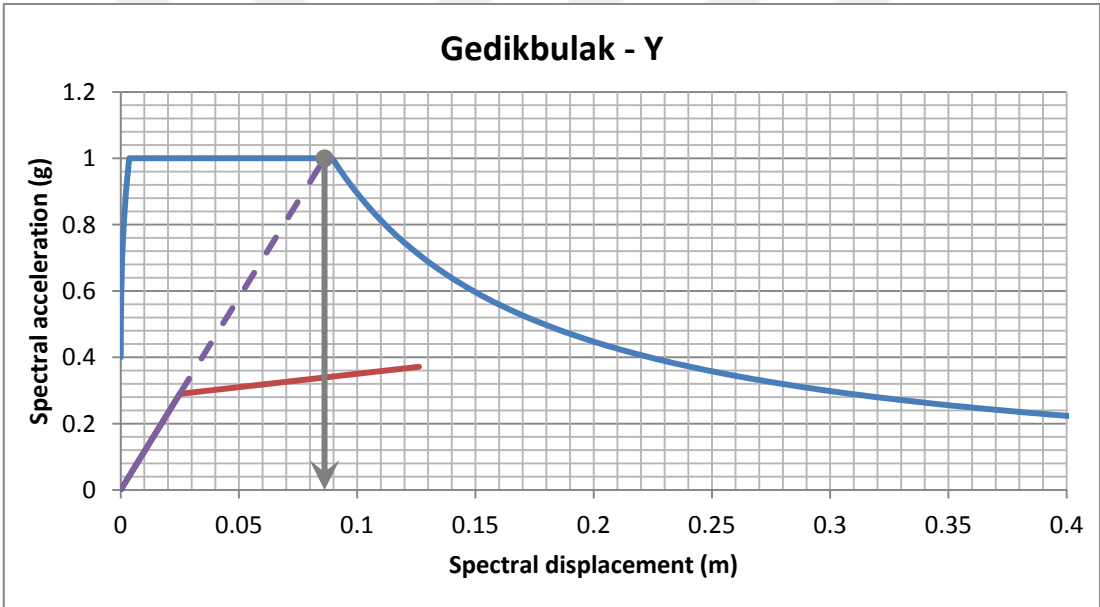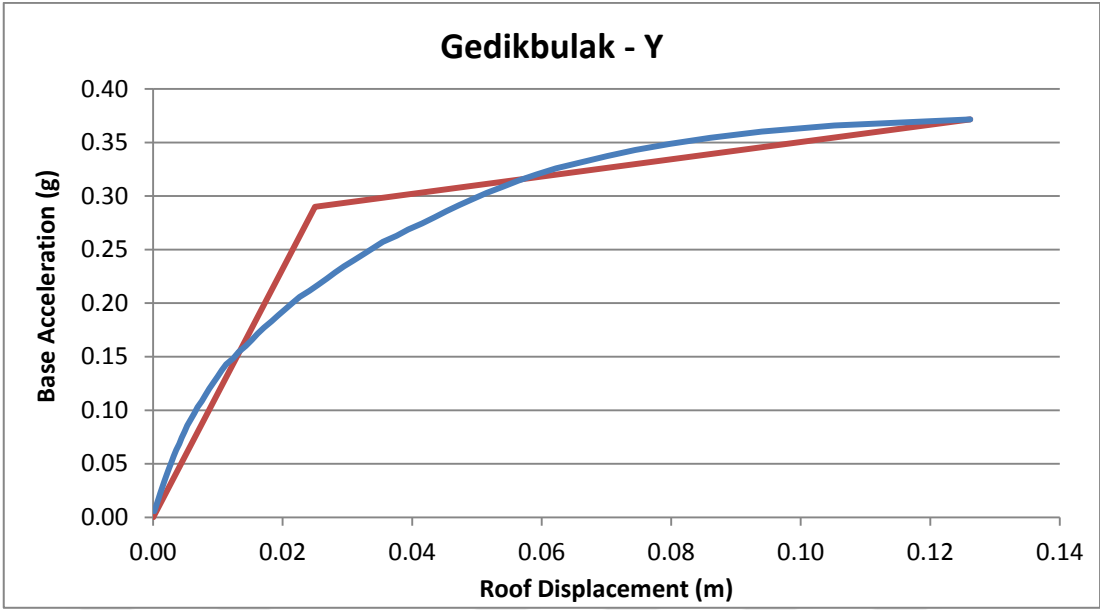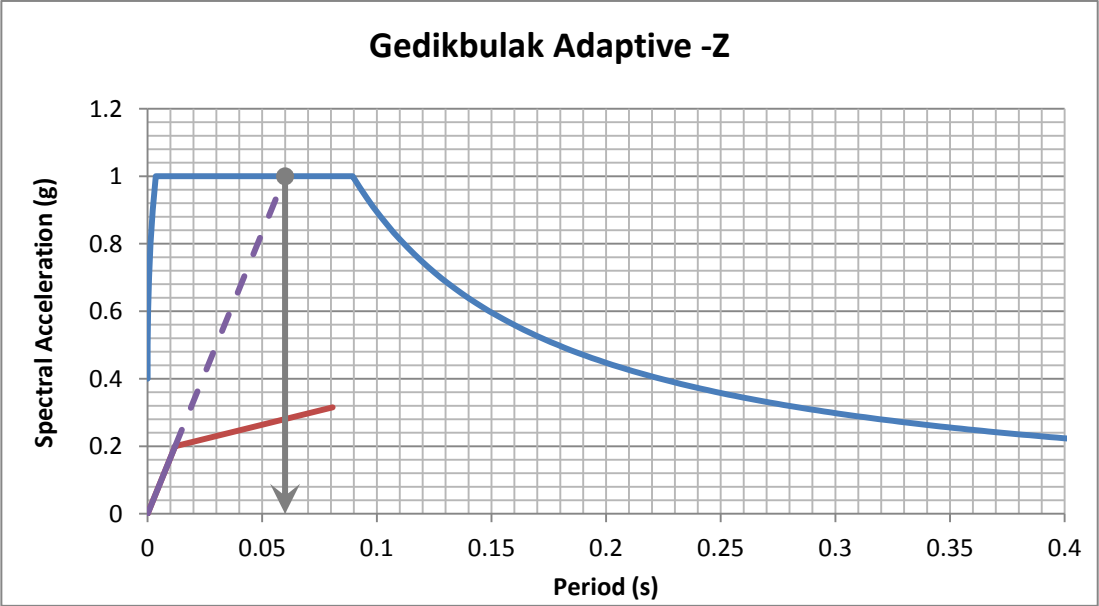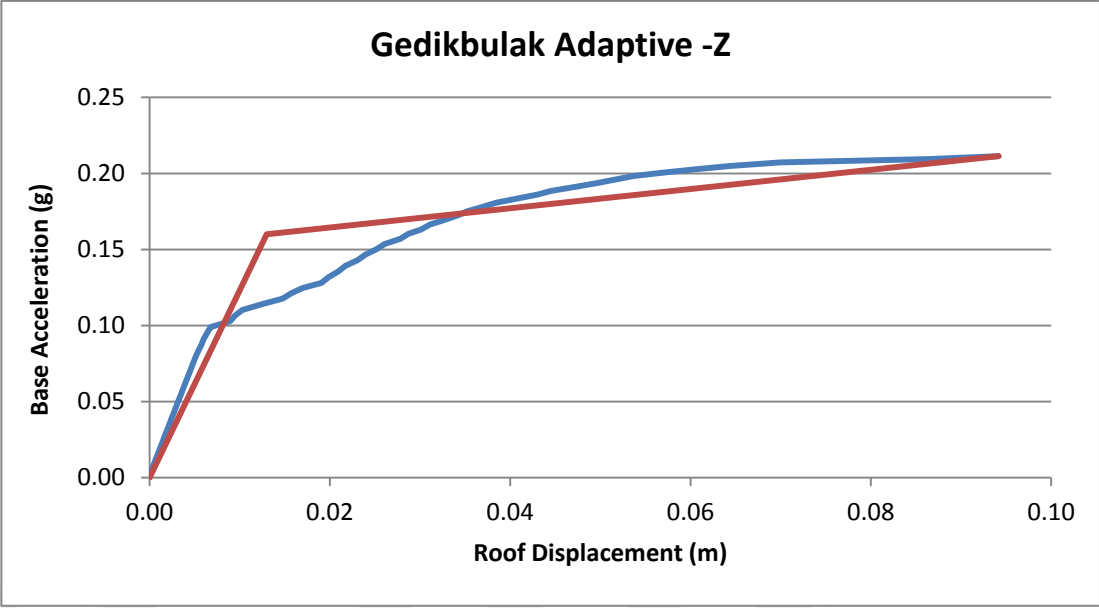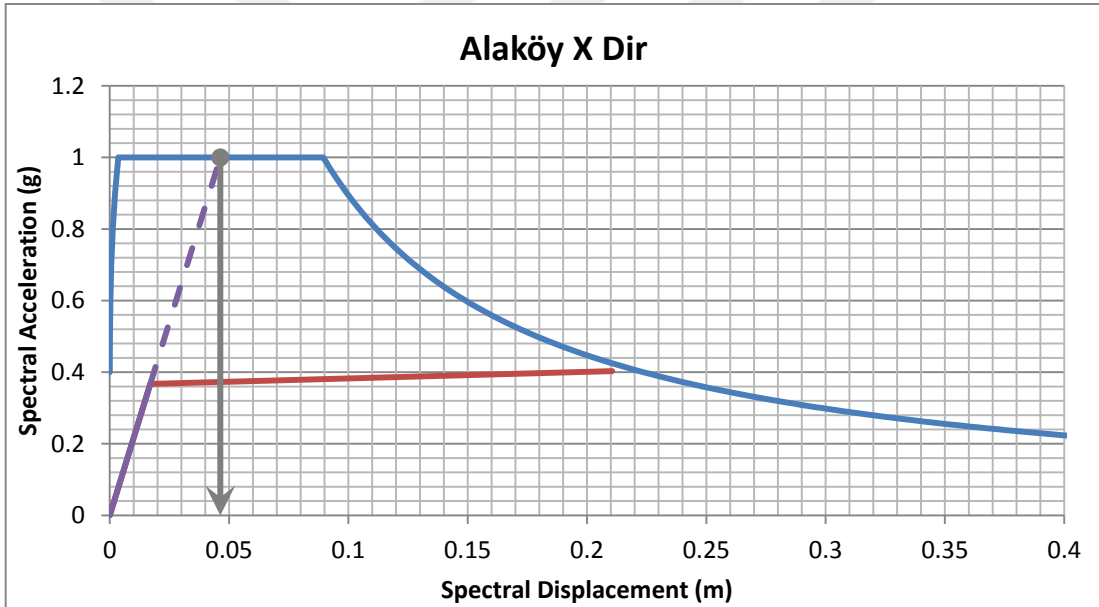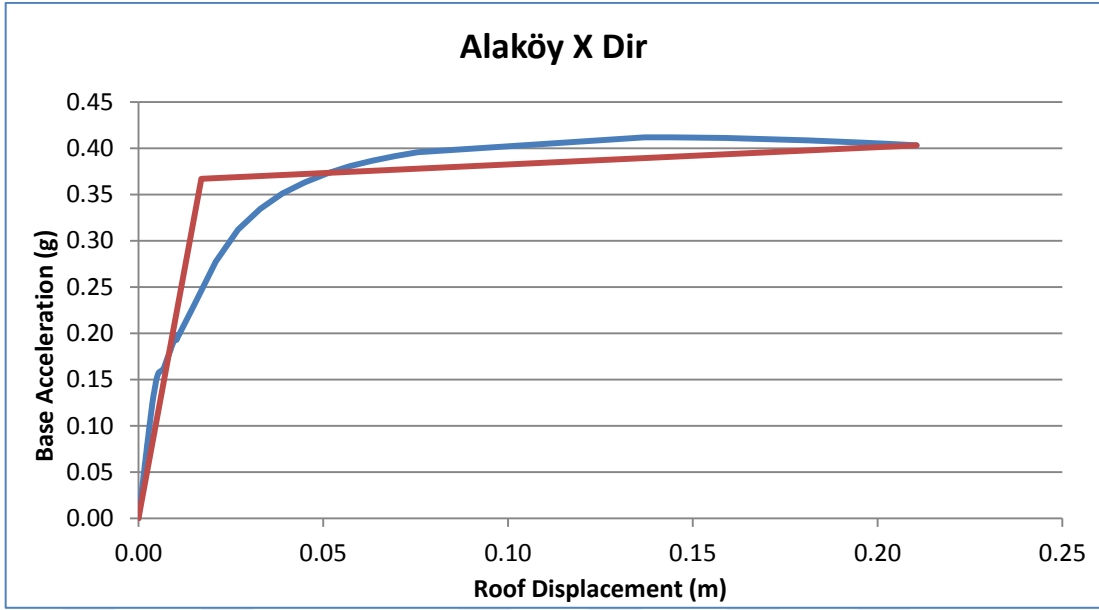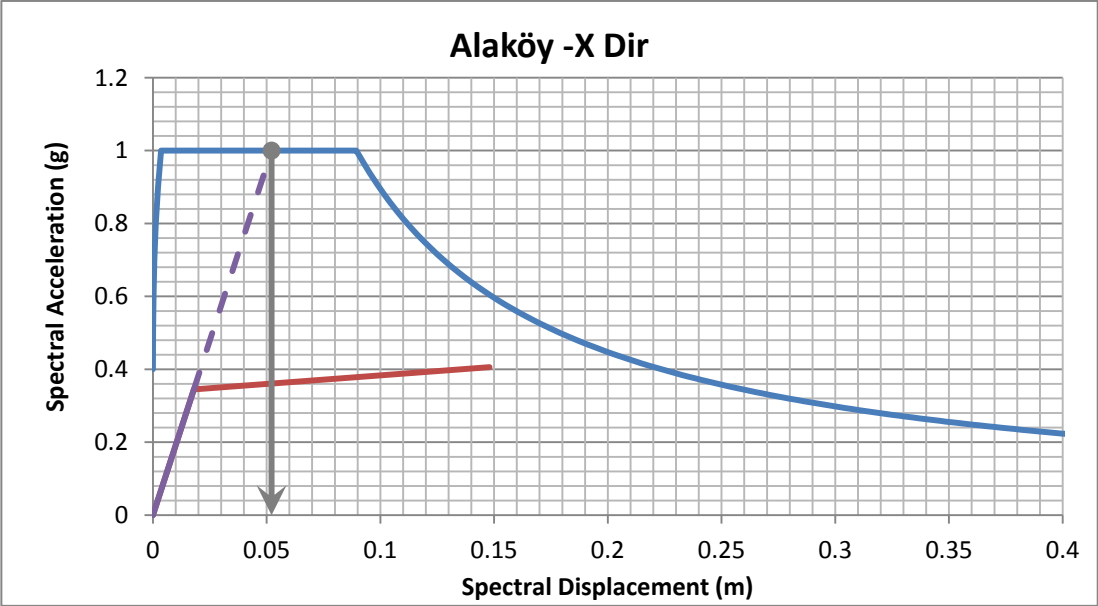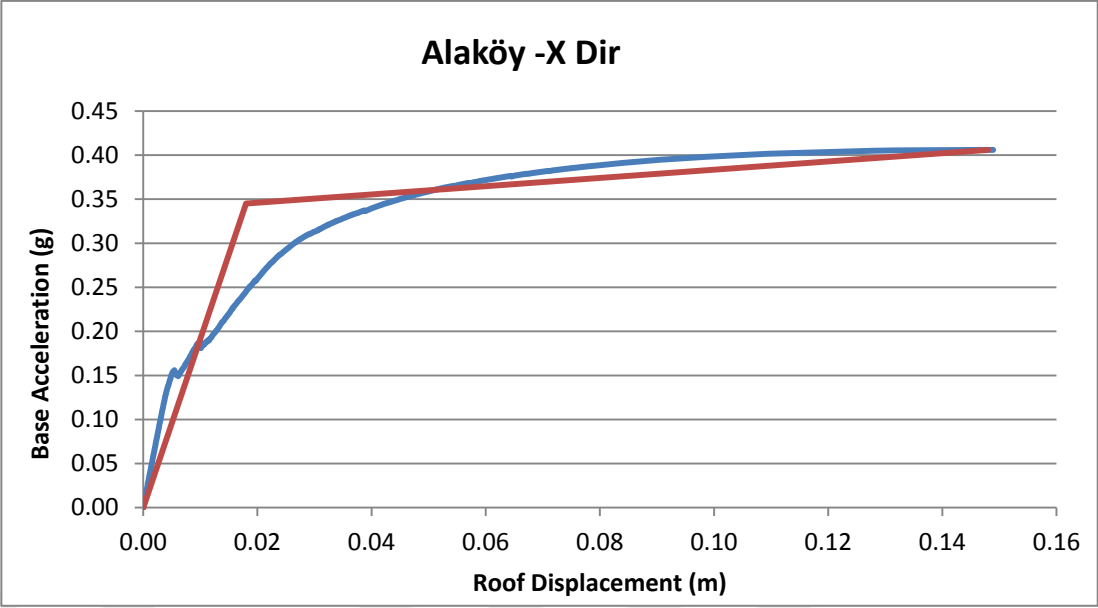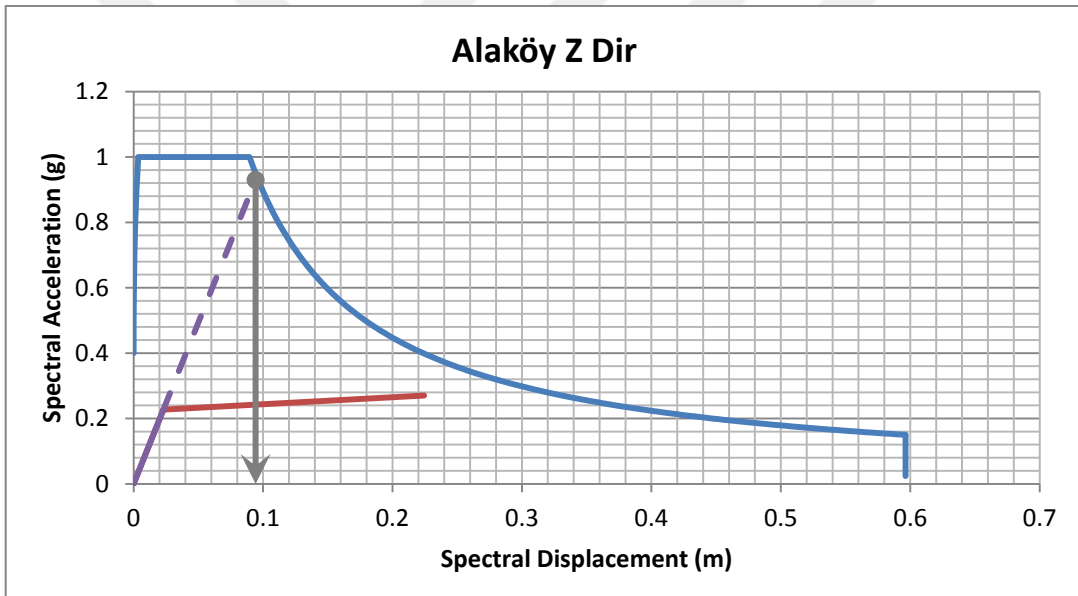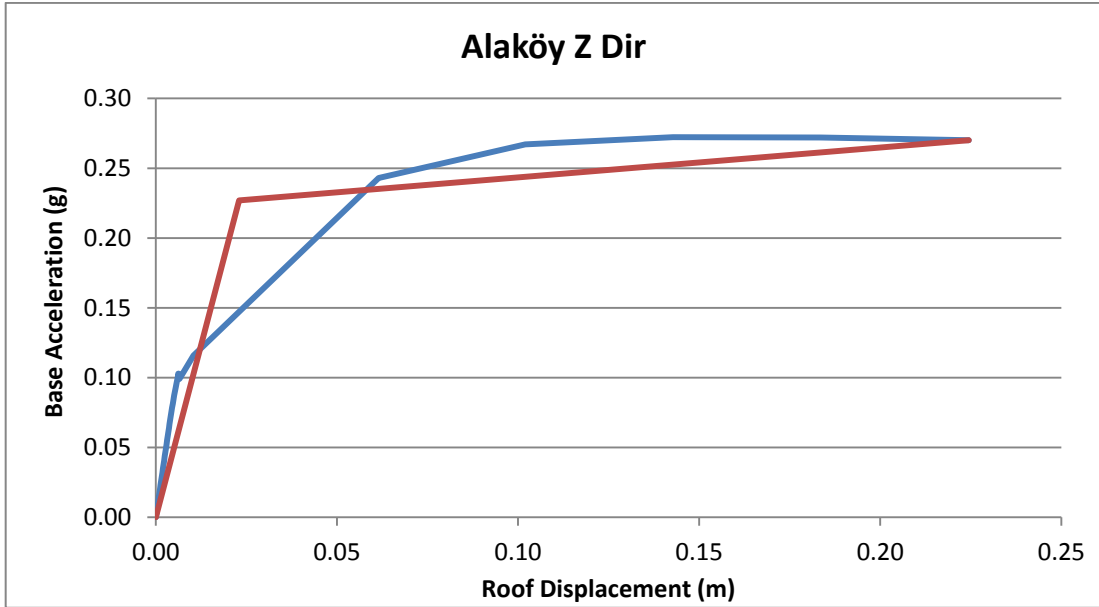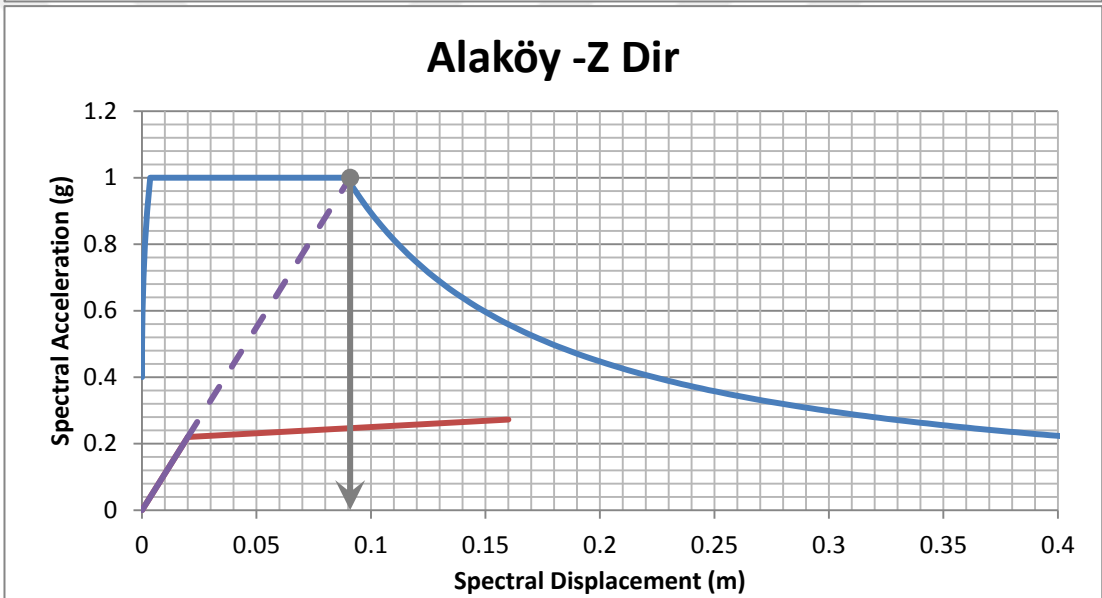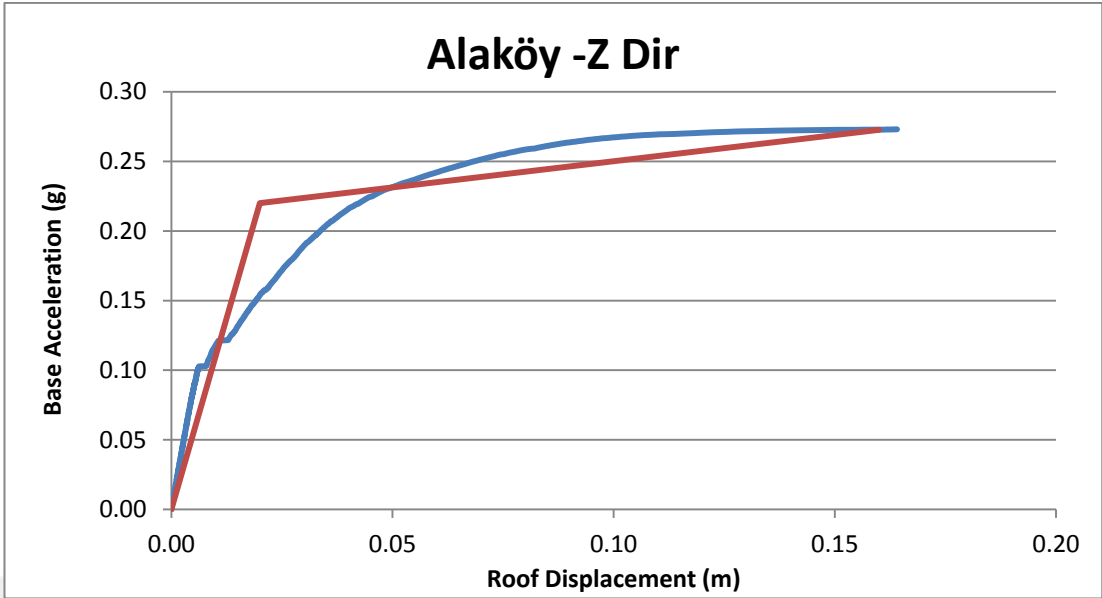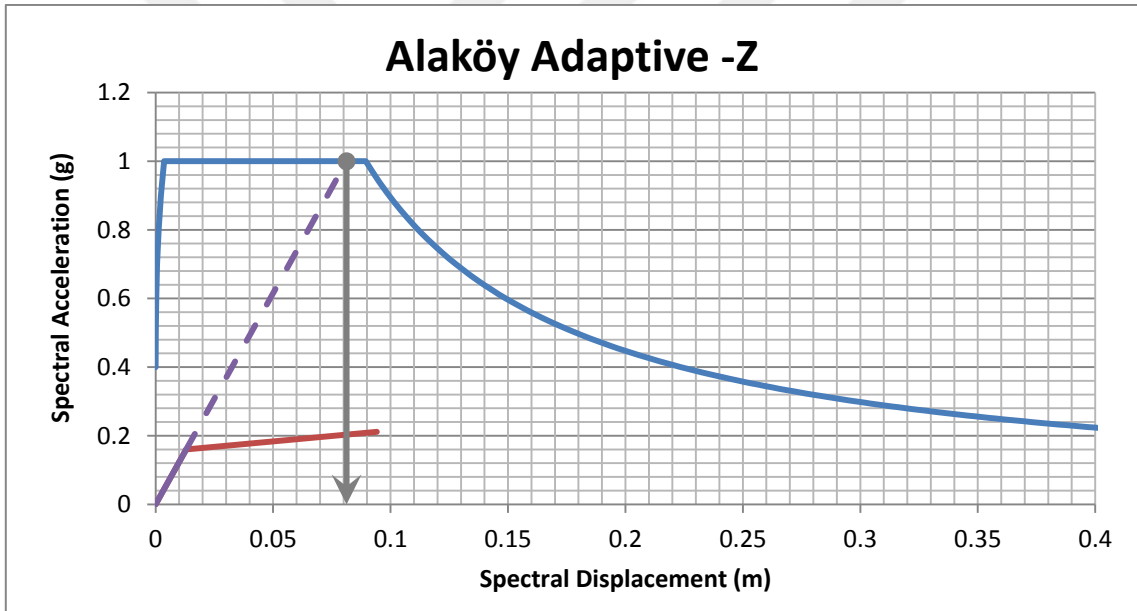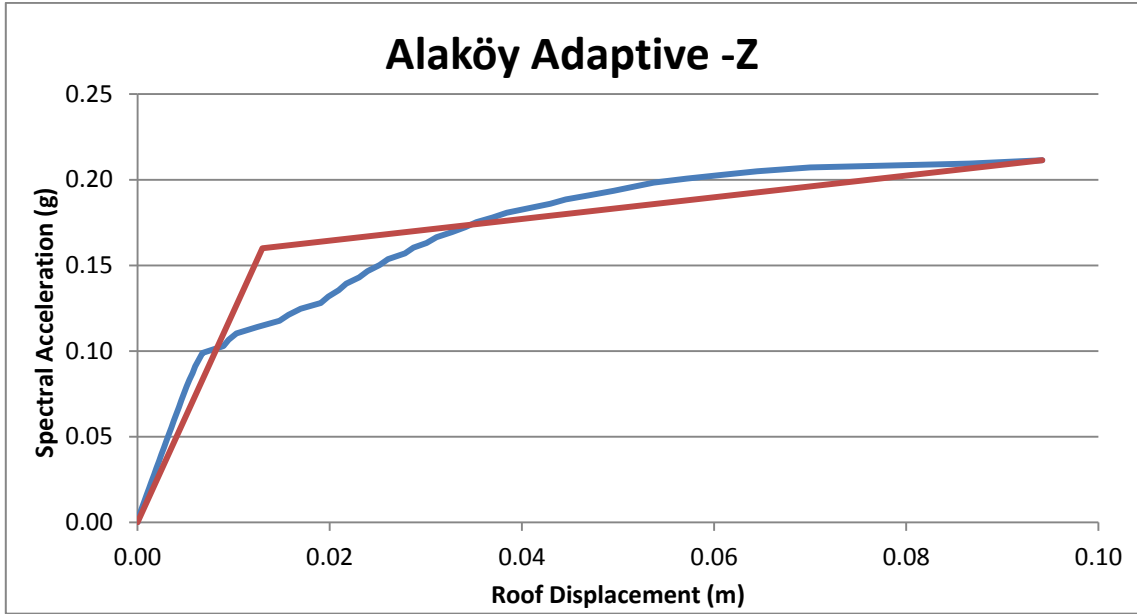
APPENDIX A.2. Gedikbulak Building's Roof displacement versus time (s) plots.

138H2

Roof Displacement (mm)

25.6 mm of residual displacement

—— Non-degrading .... Degrading

900H1

Roof Displacement (mm)

18.3 mm of residual displacement

.... Degrading —— Non-degrading

3748 H2

17.1 mm of residual displacement

Degrading ····· non-degrading

5837H1

50.4 mm of residual displacement

Non-degrading ····· Degrading

13.2 mm of residual displacement

56.5 mm of residual displacement

Legend: ····· Degrading   ──── Non-degrading
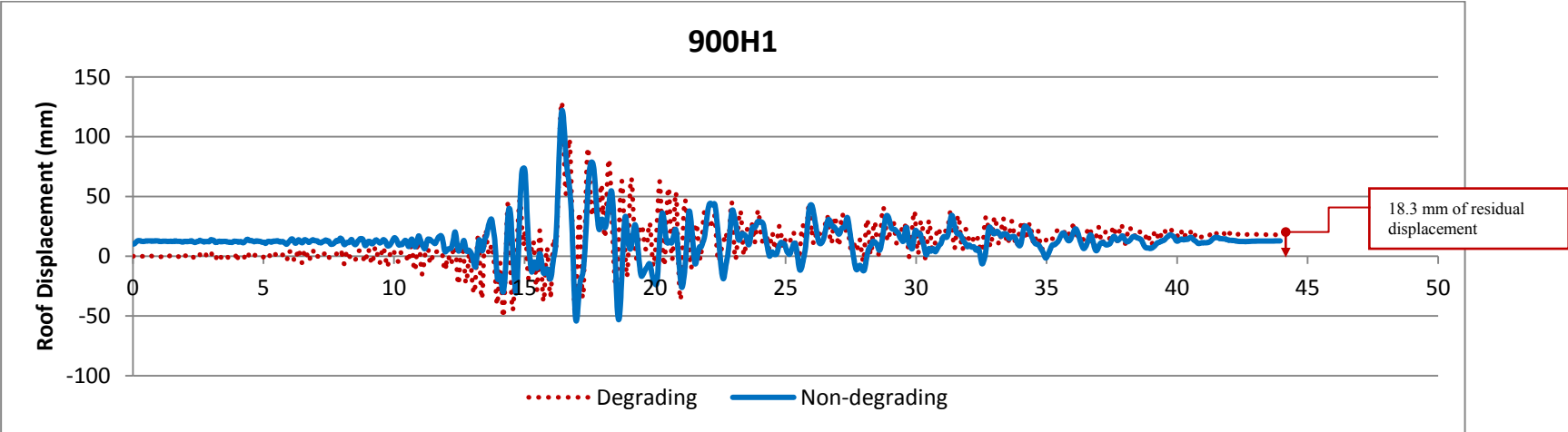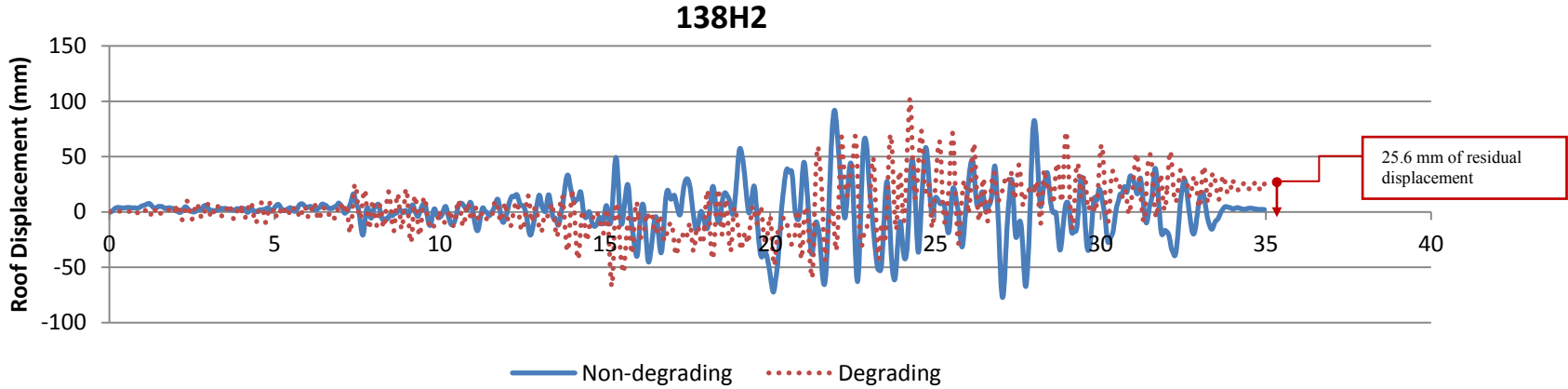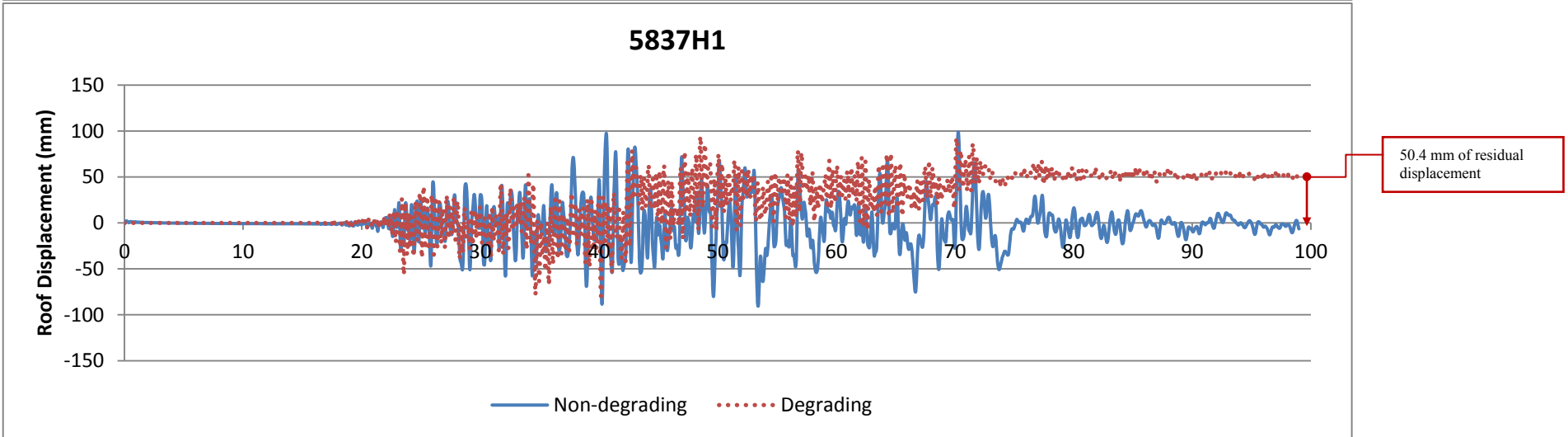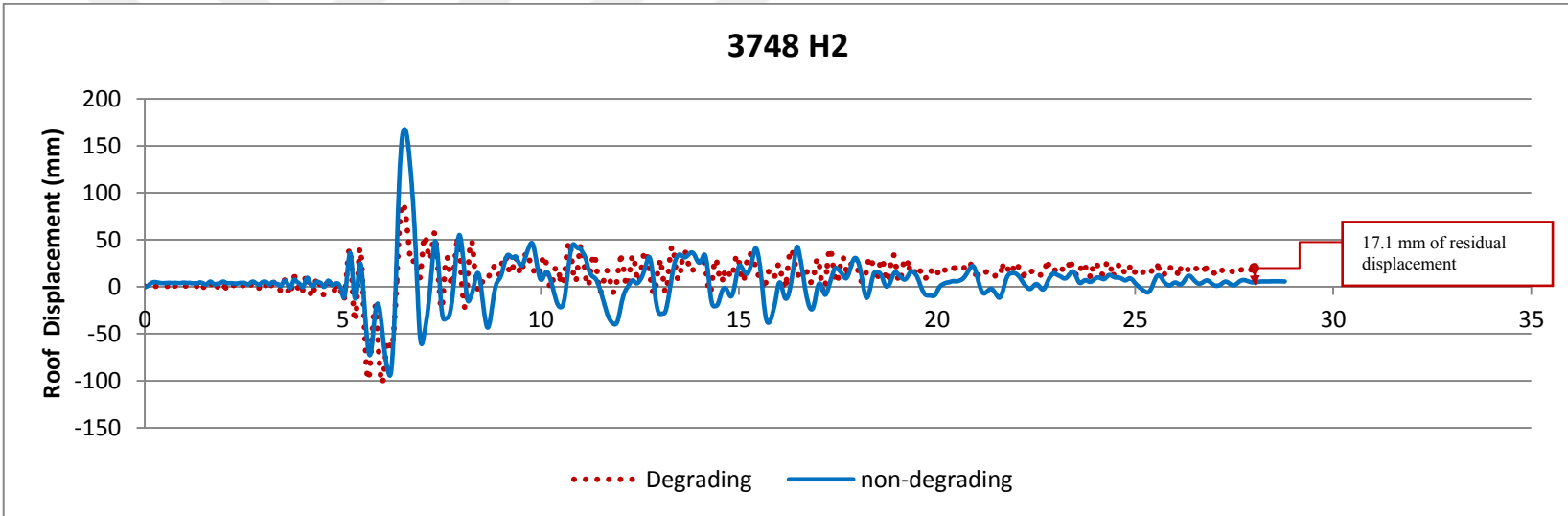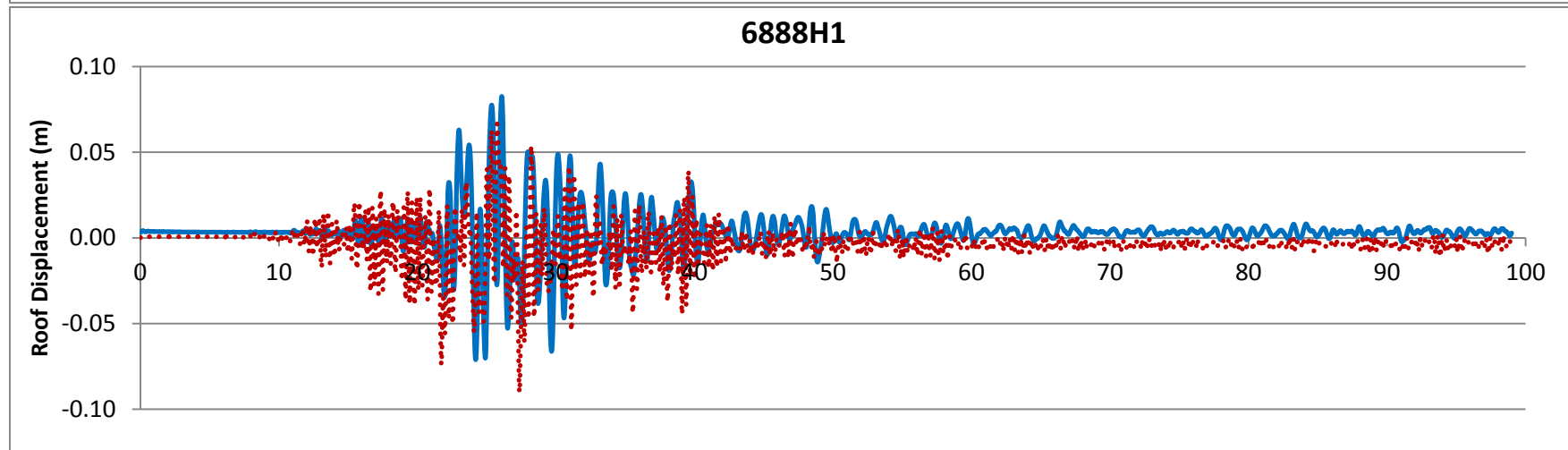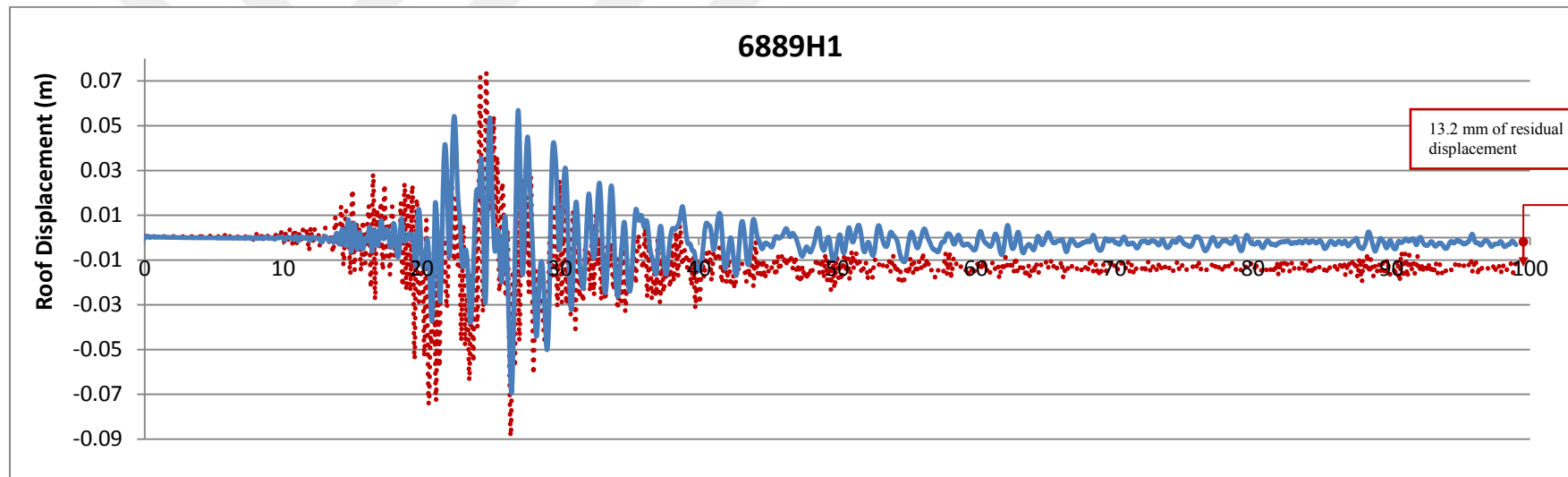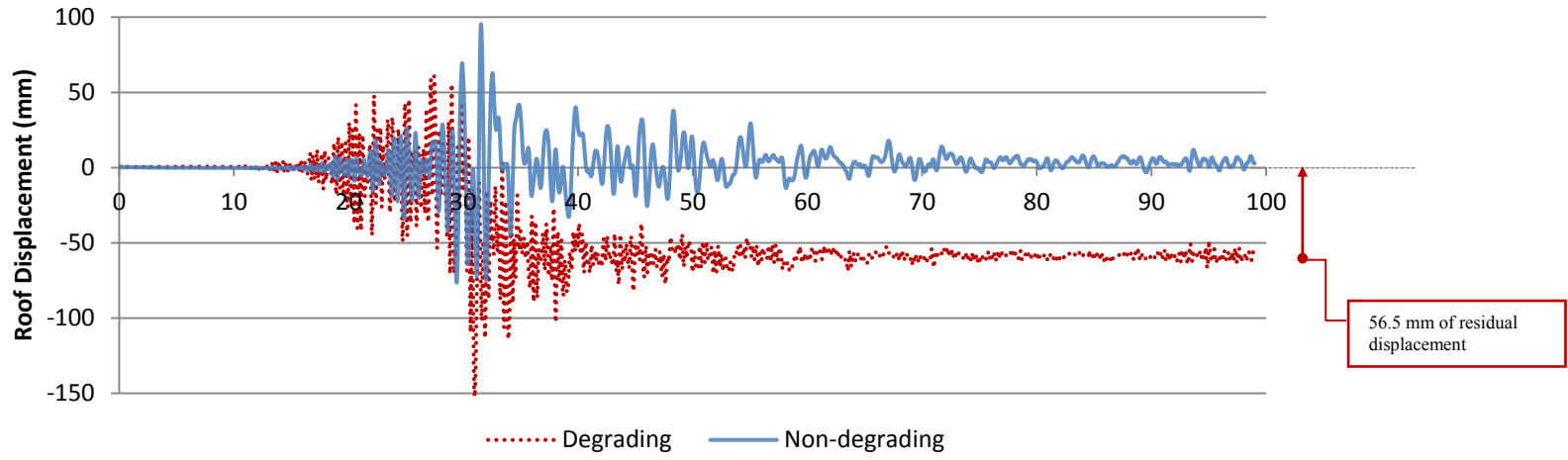
APPENDIX A.3: Alaköy building's roof displacement versus time plots

138H2

14.7 mm of residual displacement

900 H2

11.4 mm of residual displacement

3748 H1

20.08mm of residual displacement

5837H1

6888H1

6889H2

7.77 mm of residual displacement

6952H1
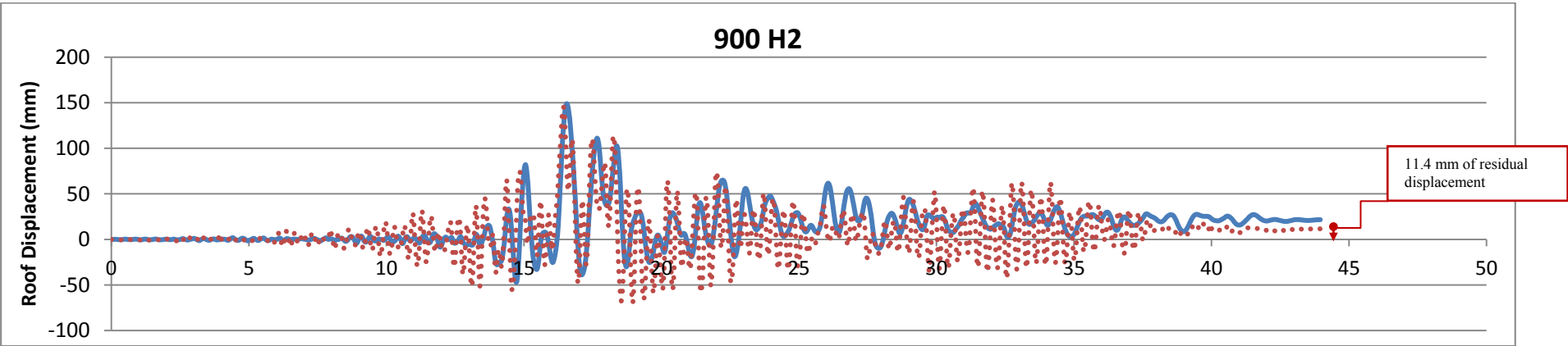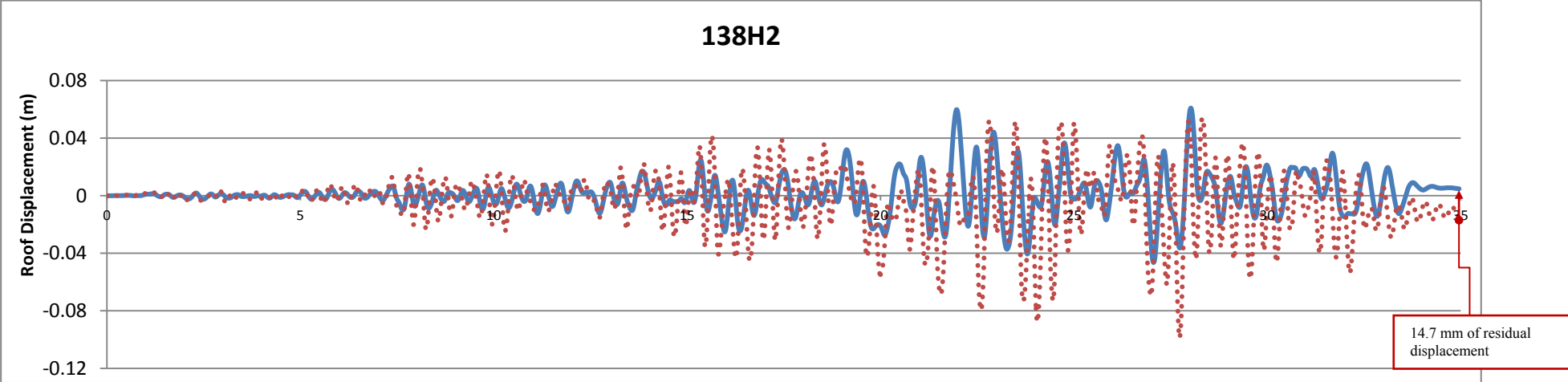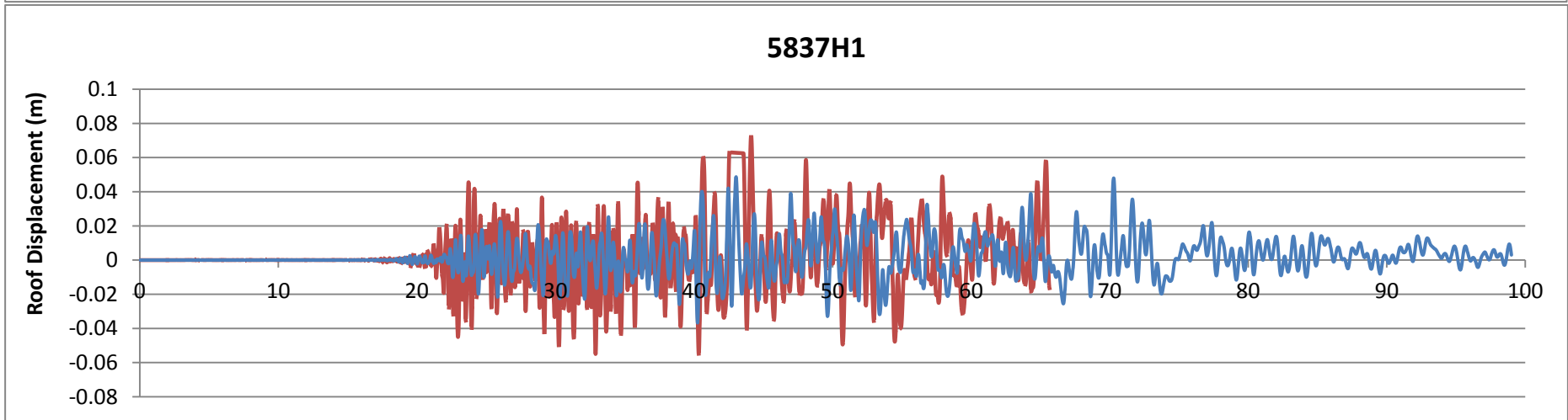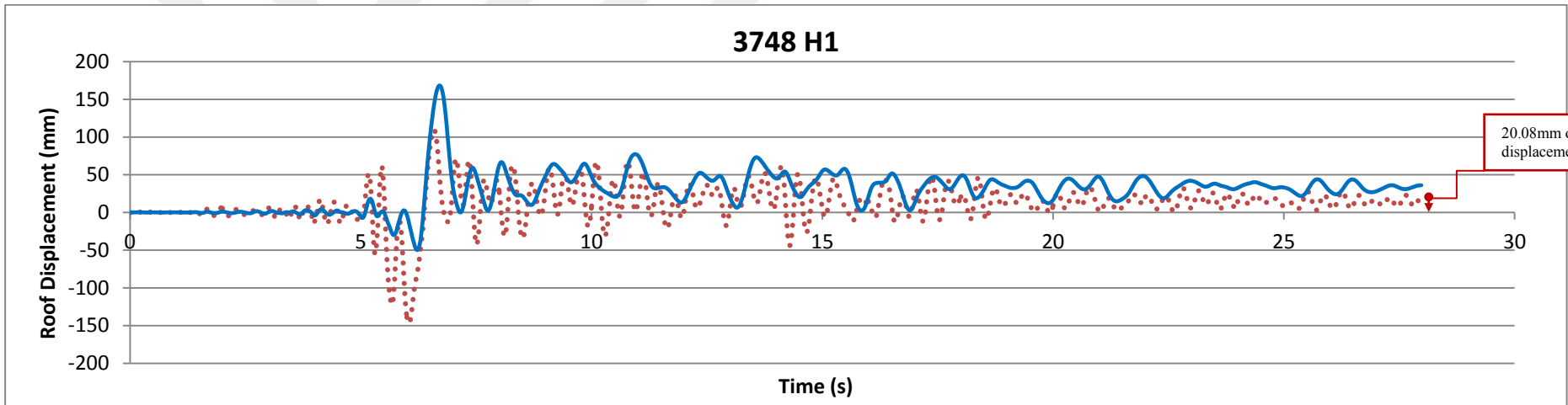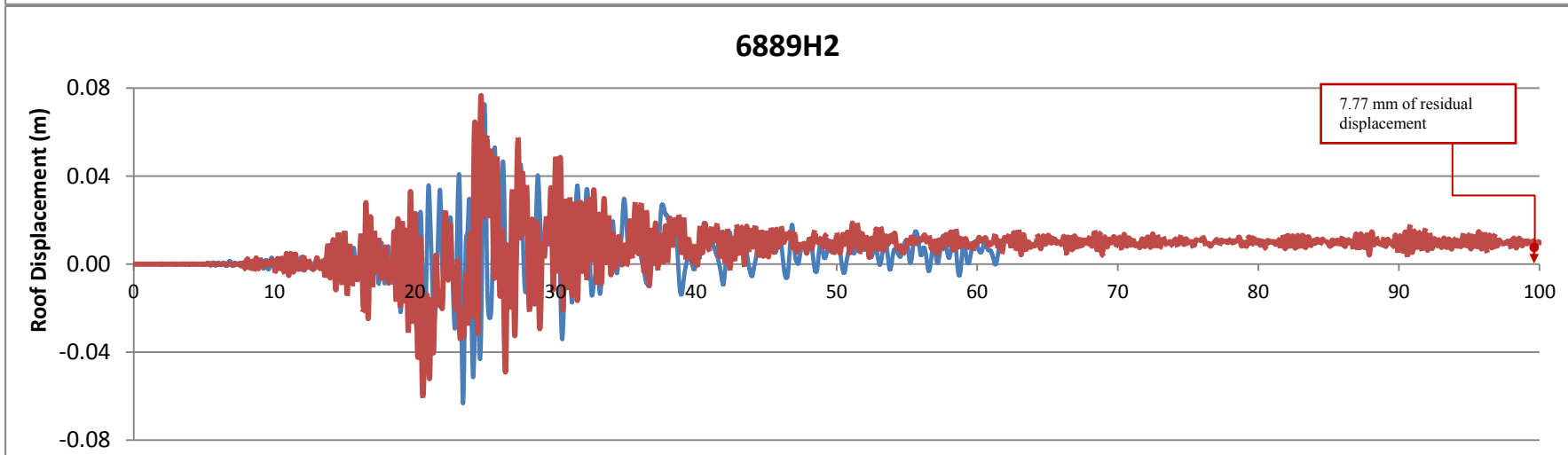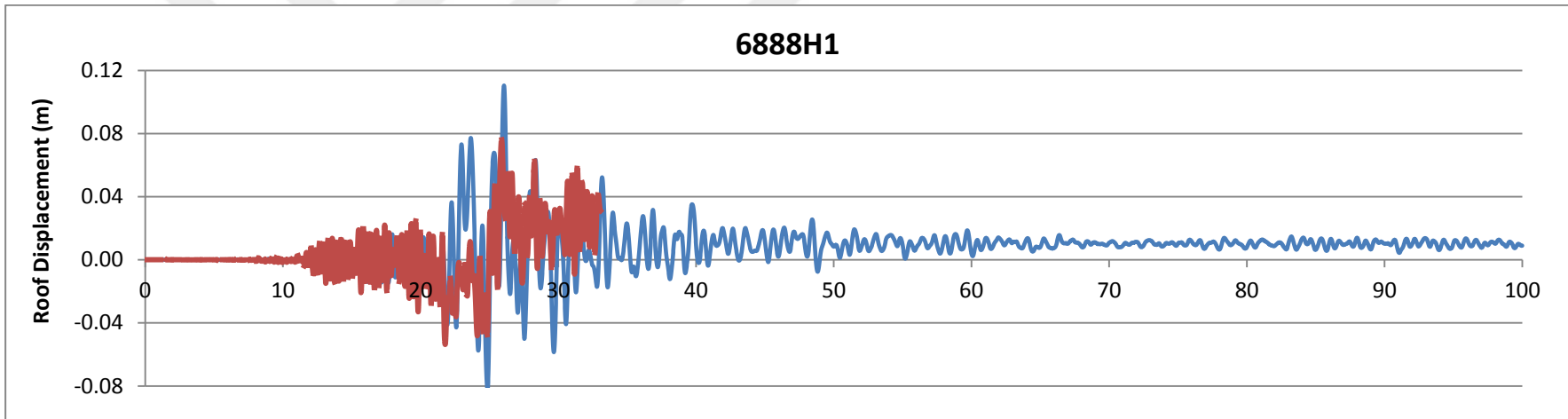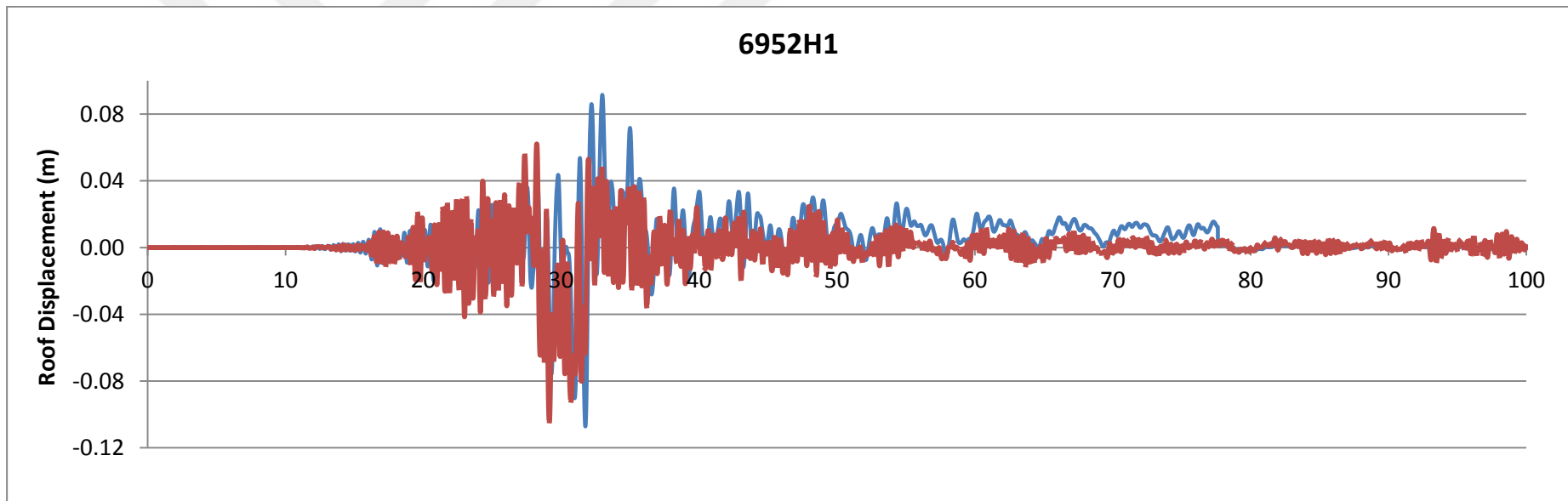
Appendix A4: First Story Drifts of Gedikbulak Building

138 H2

900 H2

3748 H1

5831 H1
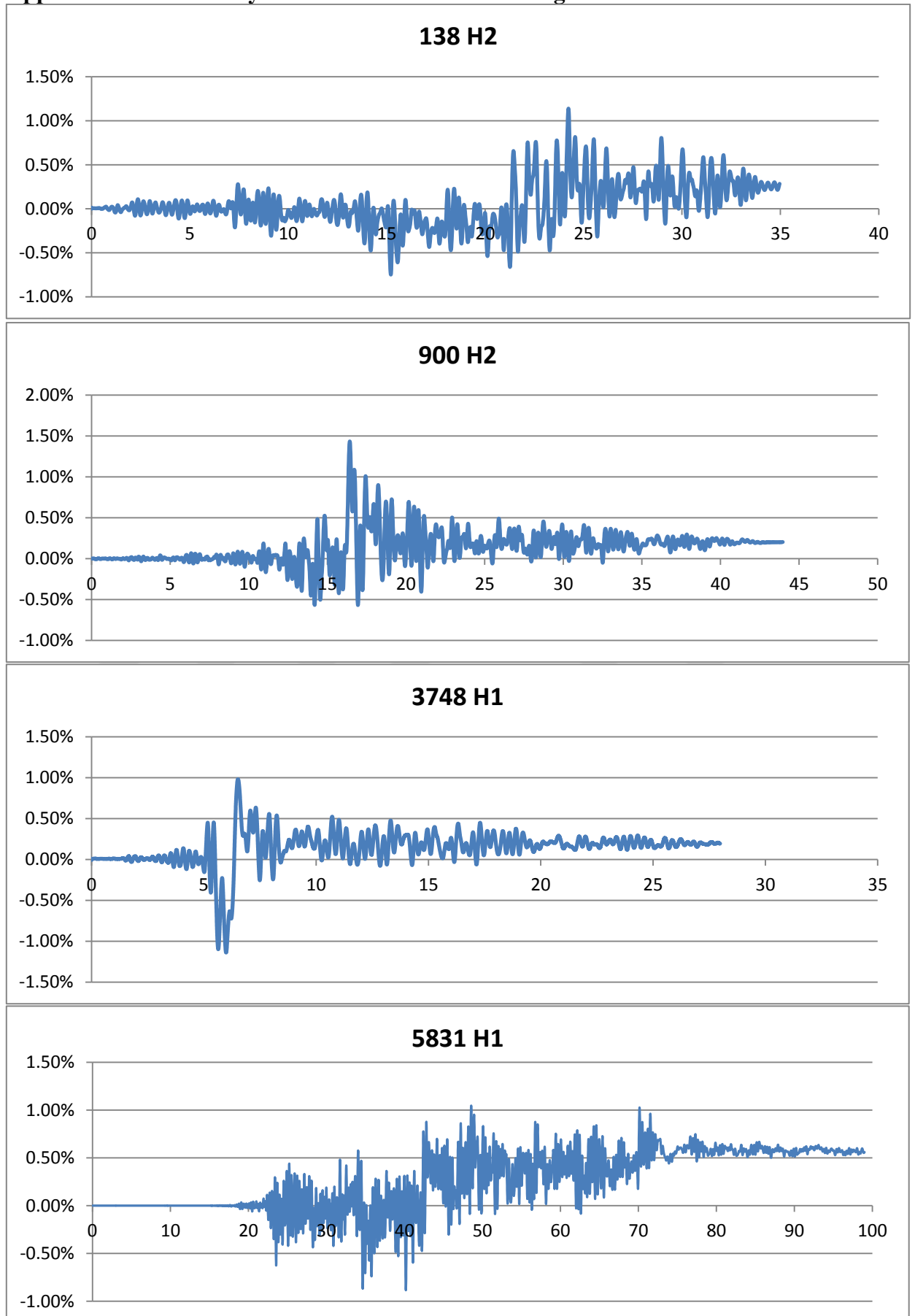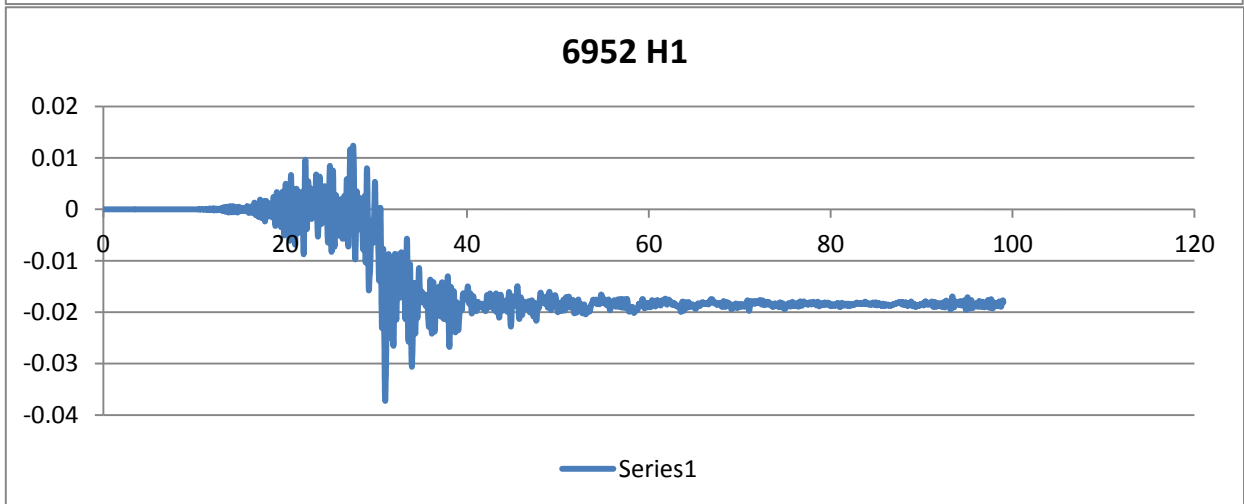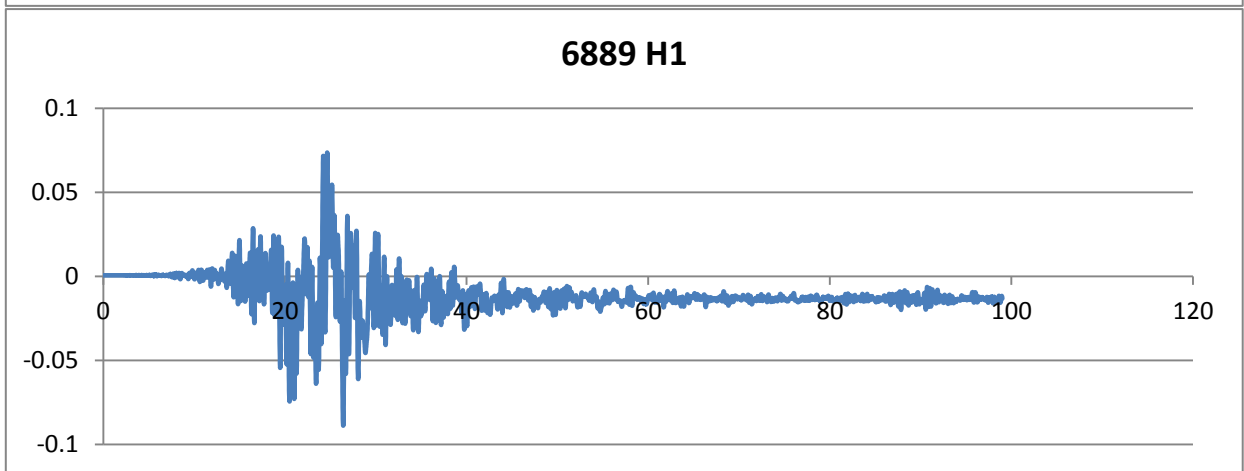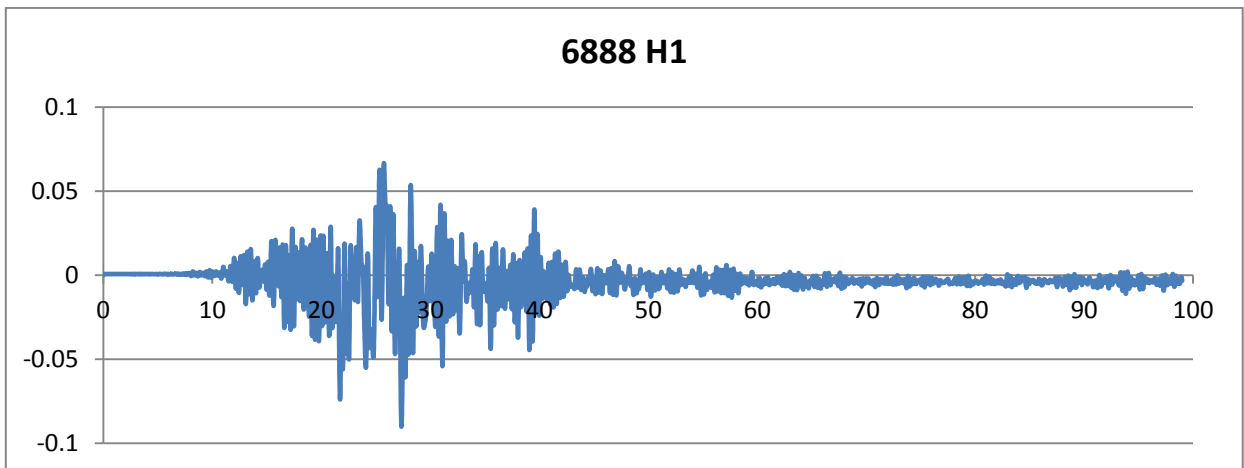
Appendix A5: Story Drifts of Alaköy Building

138 H2

900 H1

3748 H1

5831 H1

6888 H1

6889 H1

6957 H1

104
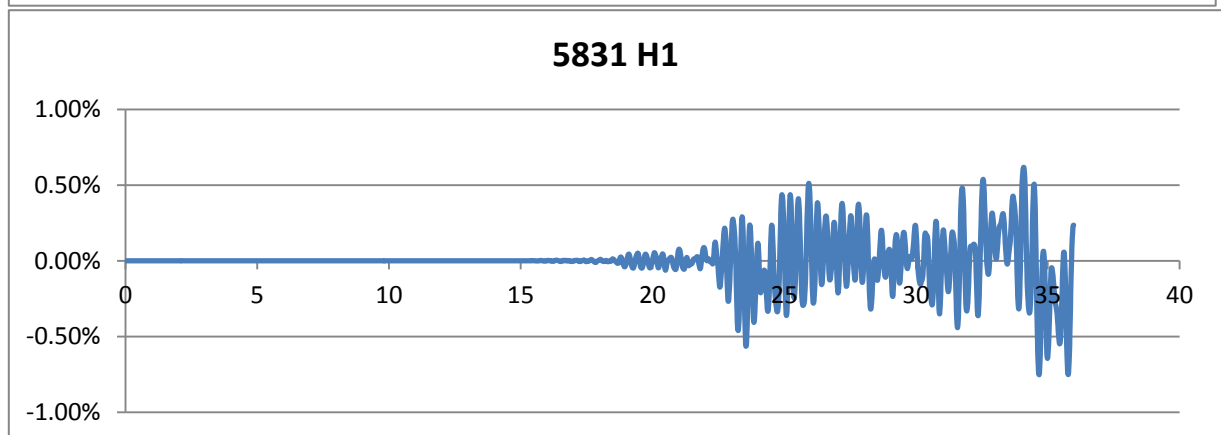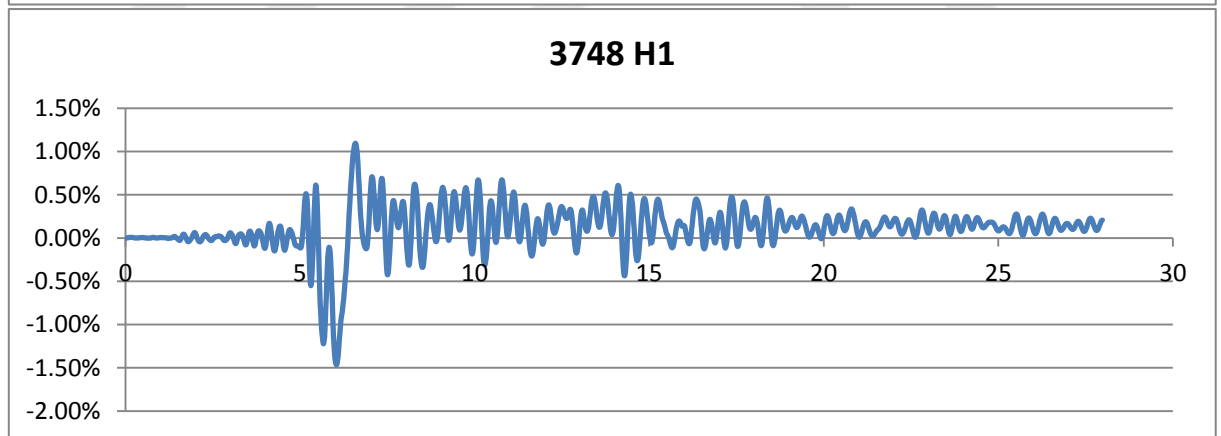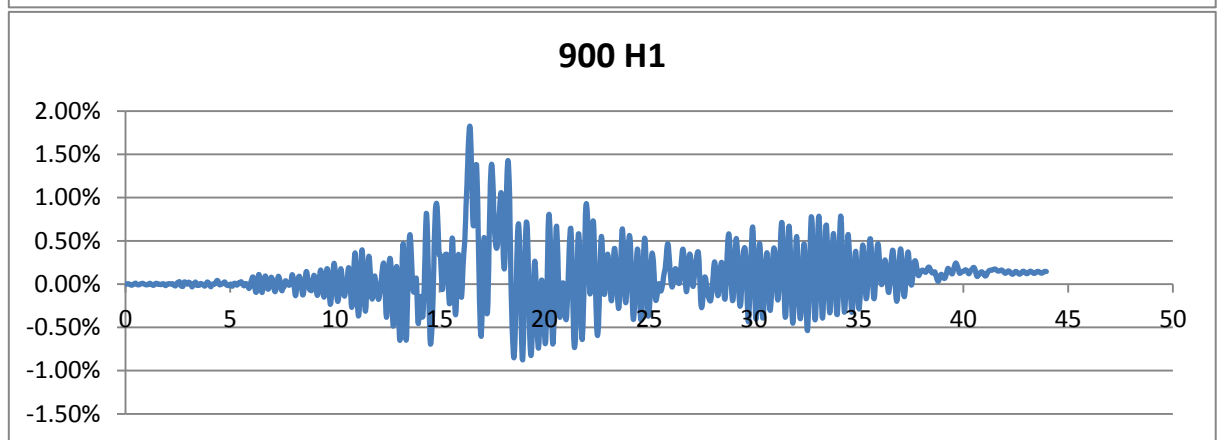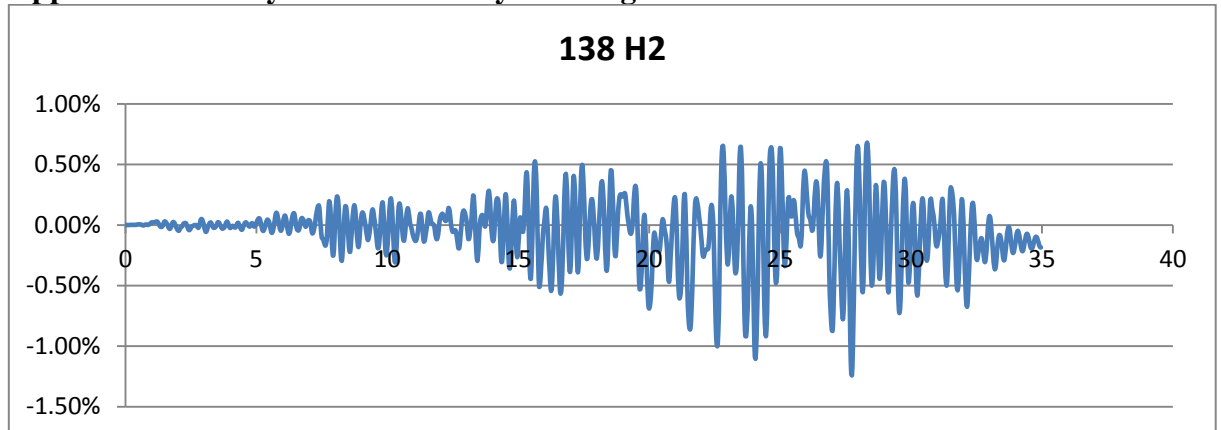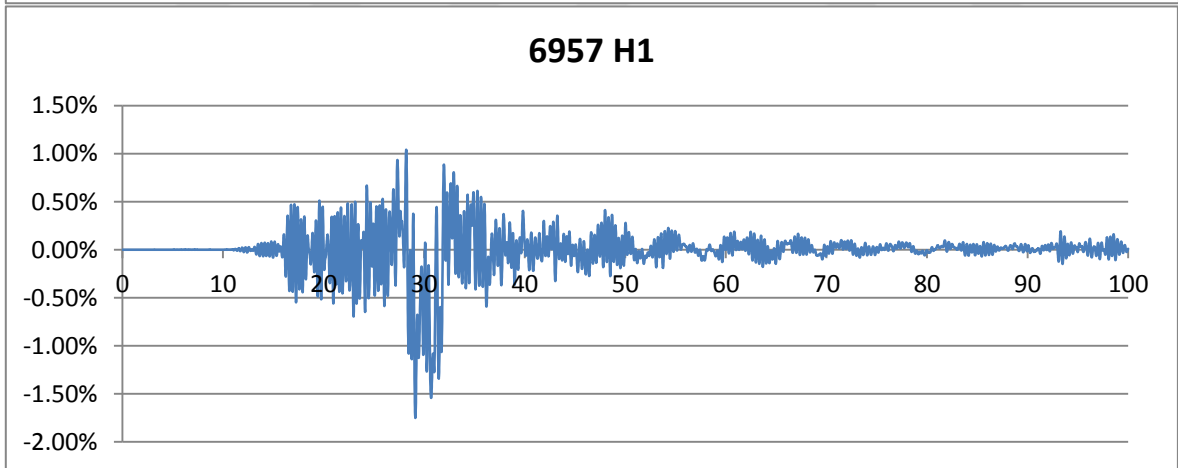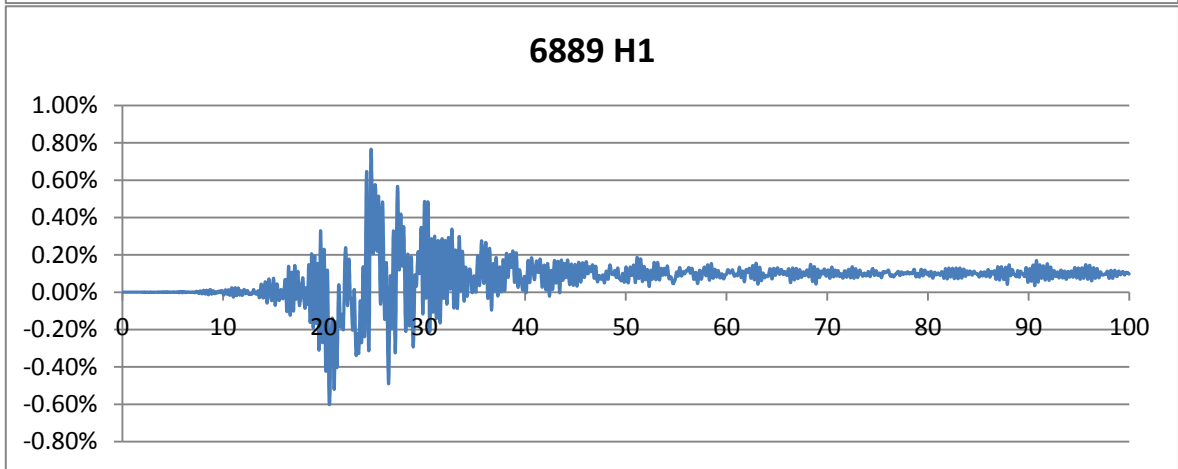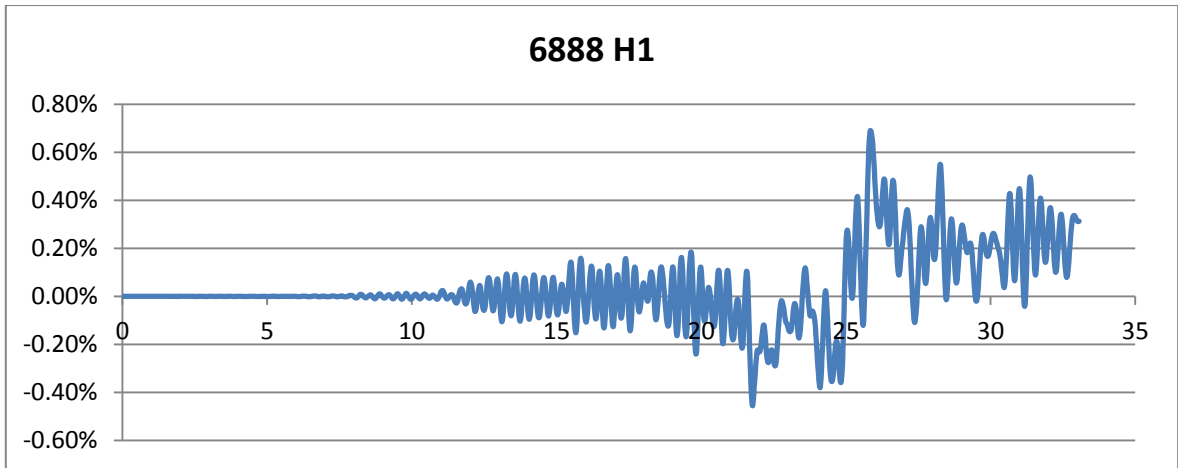
APPENDIX A.6

: Alaköy building's plastic hinge locations. From southern end to northern end.

188H2 Non-degrading
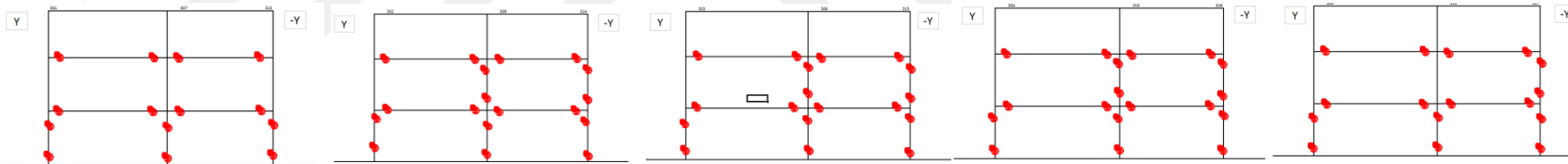
188H2 Degrading

900H2 Non-degrading

900H2 Degrading
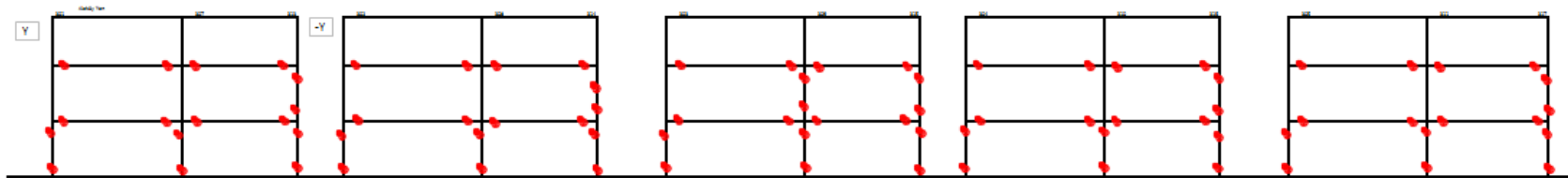
5831H1 Non-Degrading

5831H1 Degrading

6888H1 Non-degrading

6888H1 Degrading
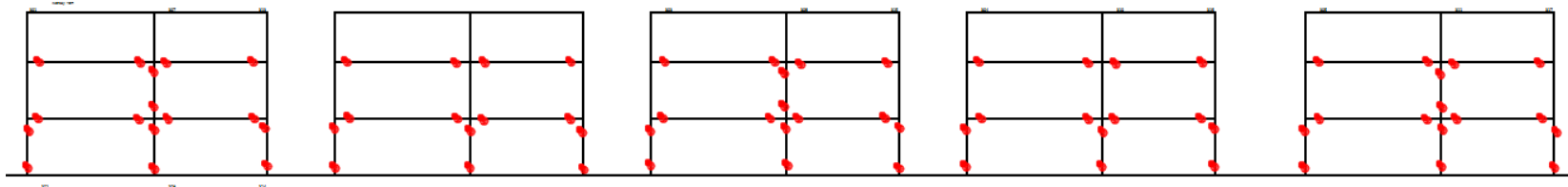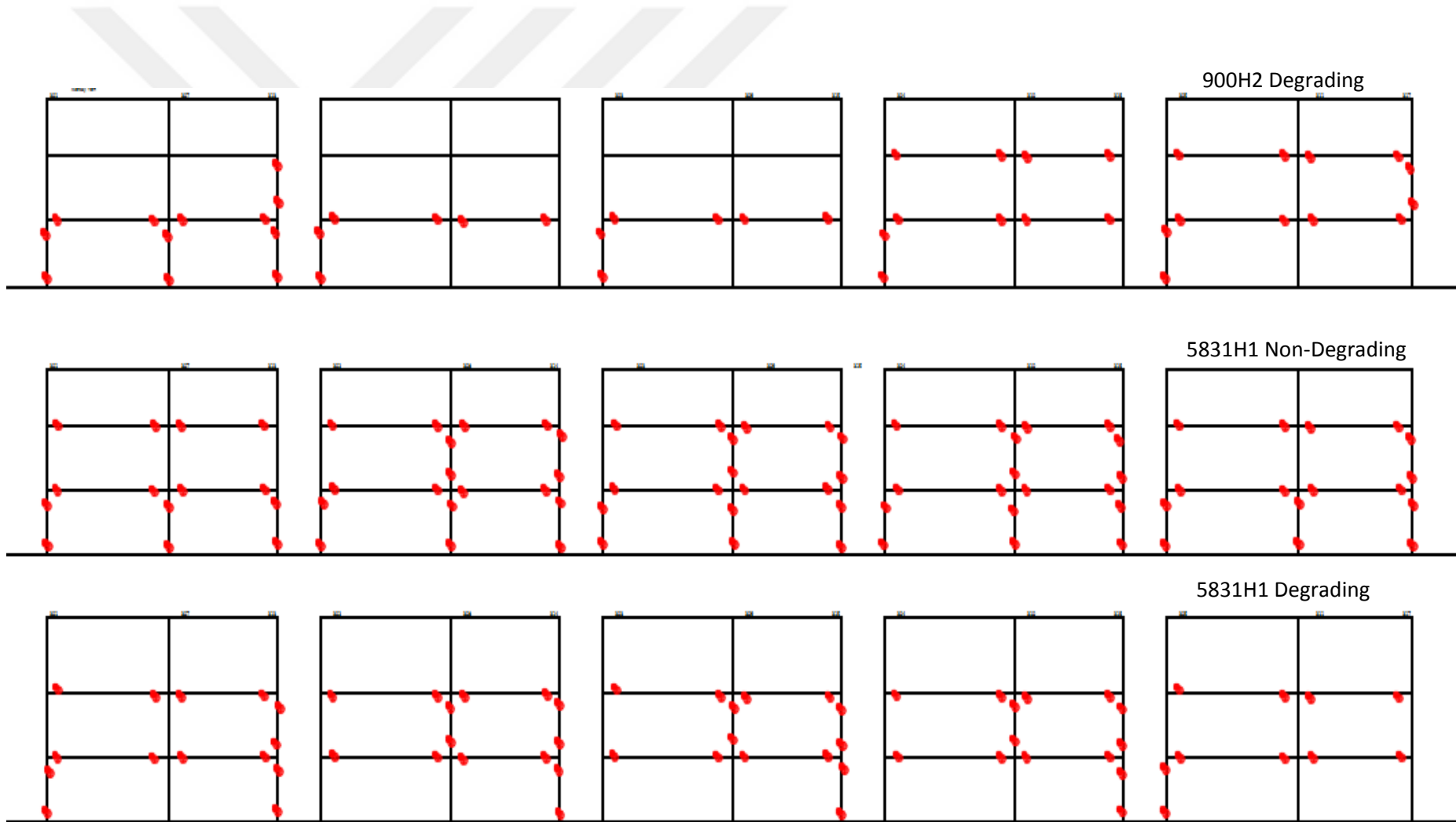
6889H1 Non-Degrading
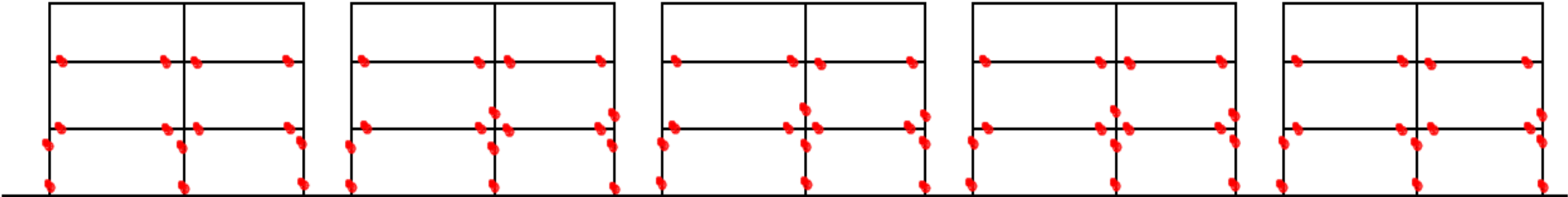
6889H1 Degrading
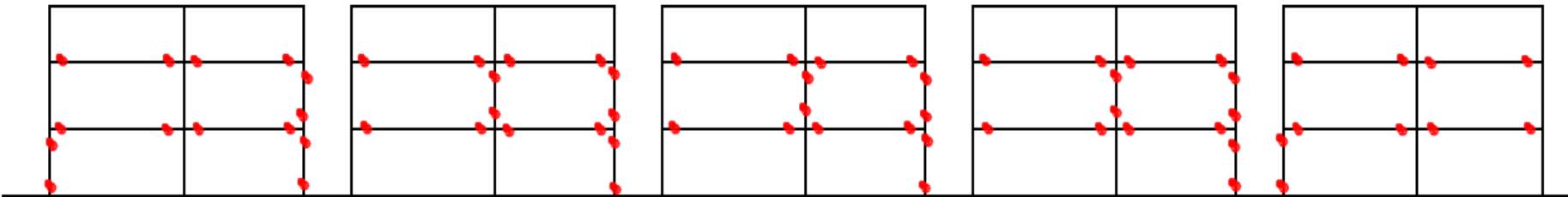
6952H1 Non-degrading
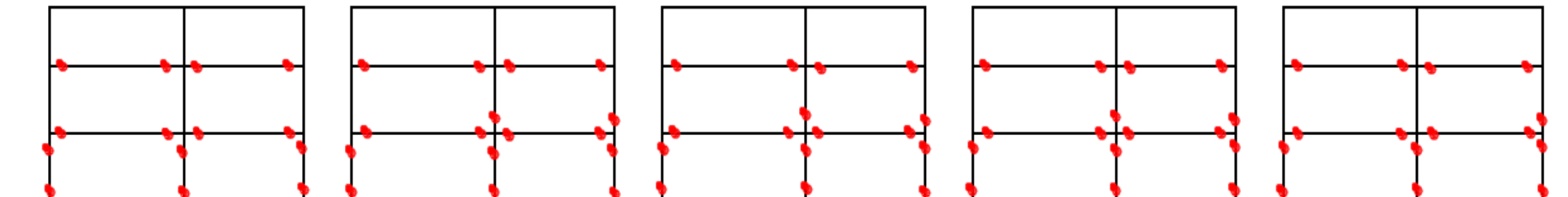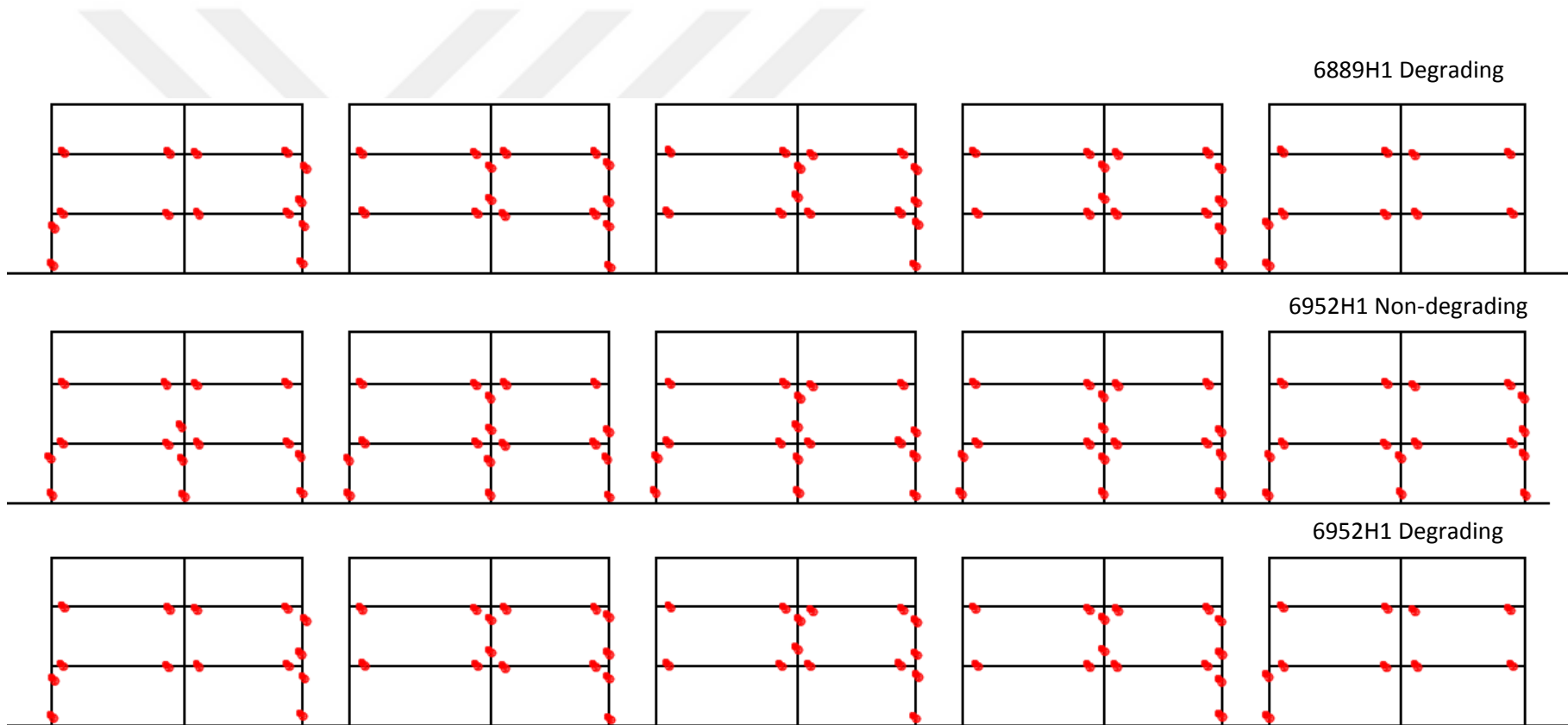
6952H1 Degrading

APPENDIX A.7.: Gedikbulak building's plastic hinge locations.

188H2 Non-degrading
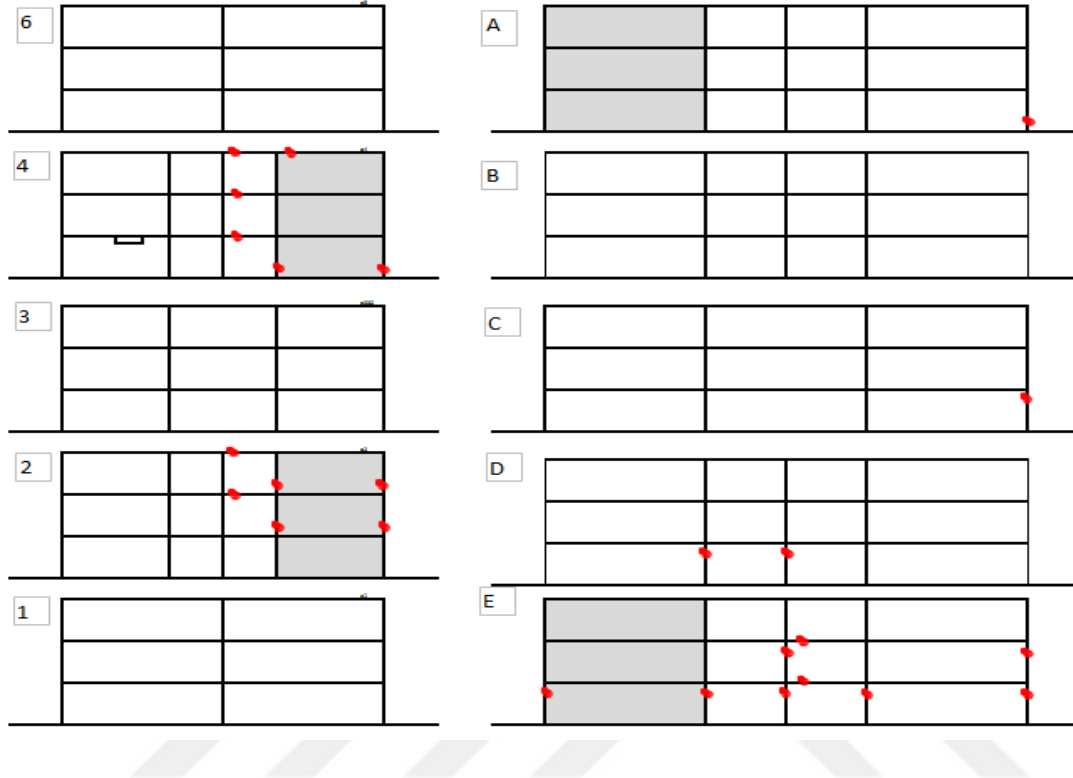
188H2 Degrading
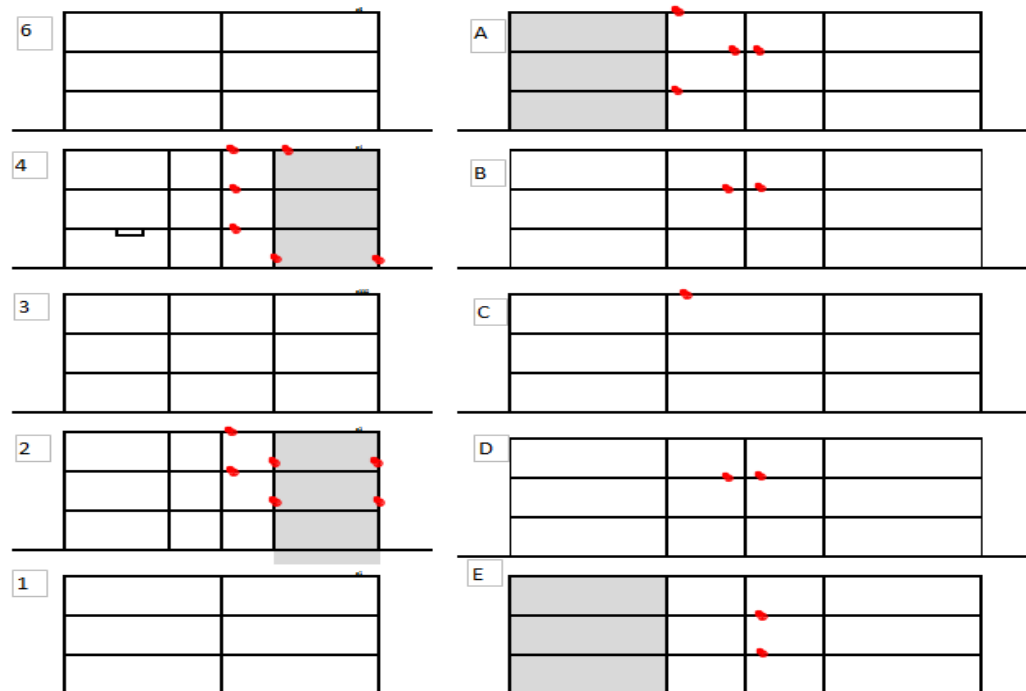
900H1 Non-Degrading

900H1 Degrading

110
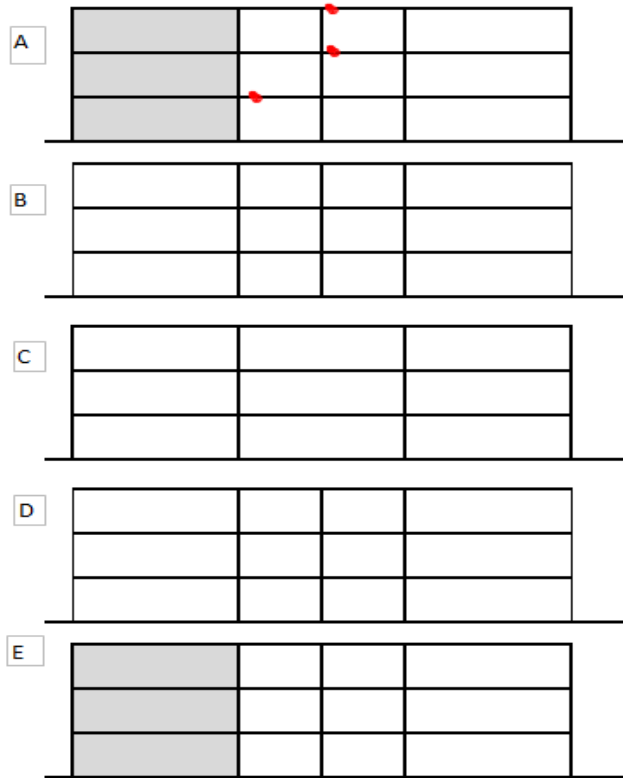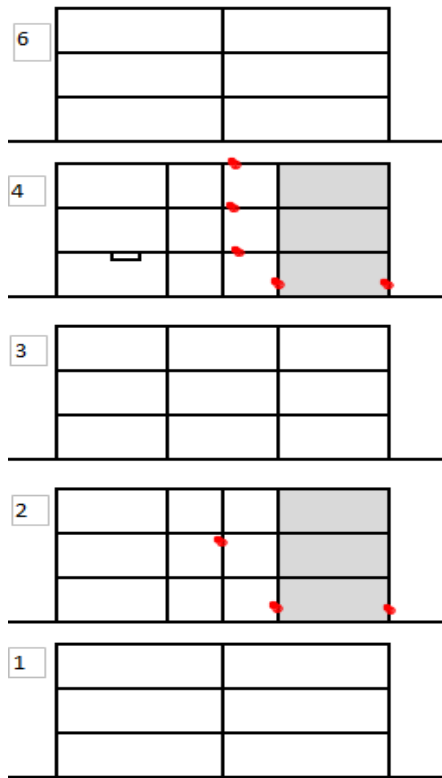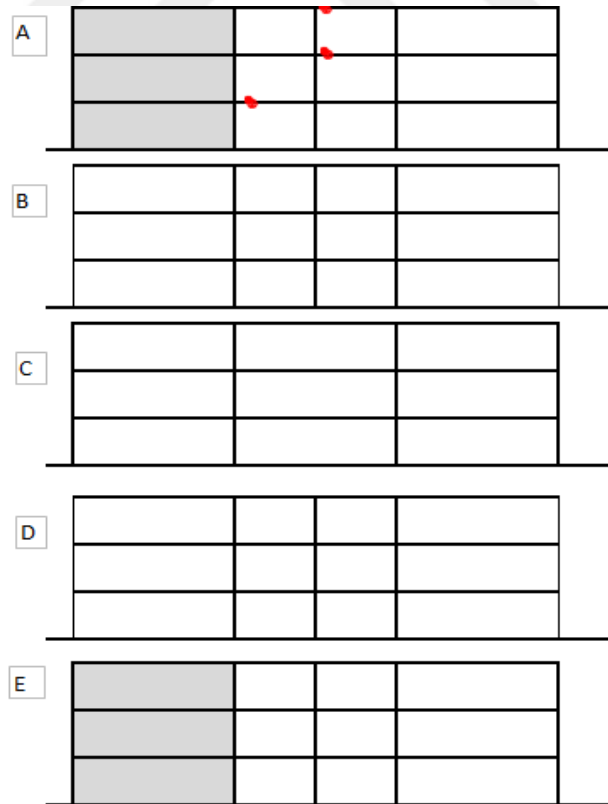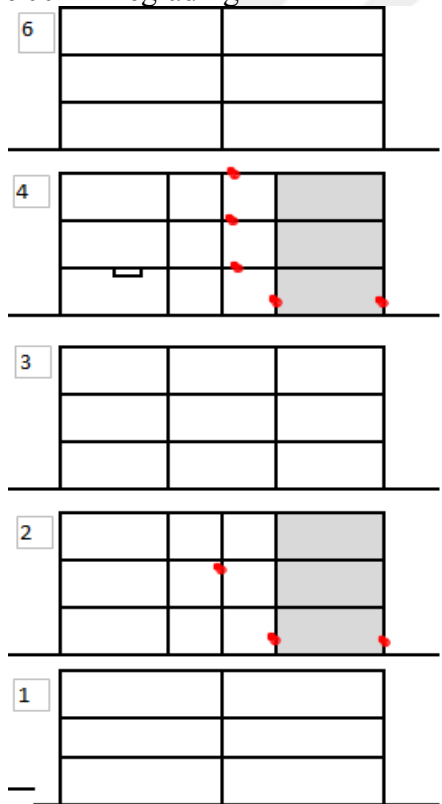
3748H1 Non-degrading
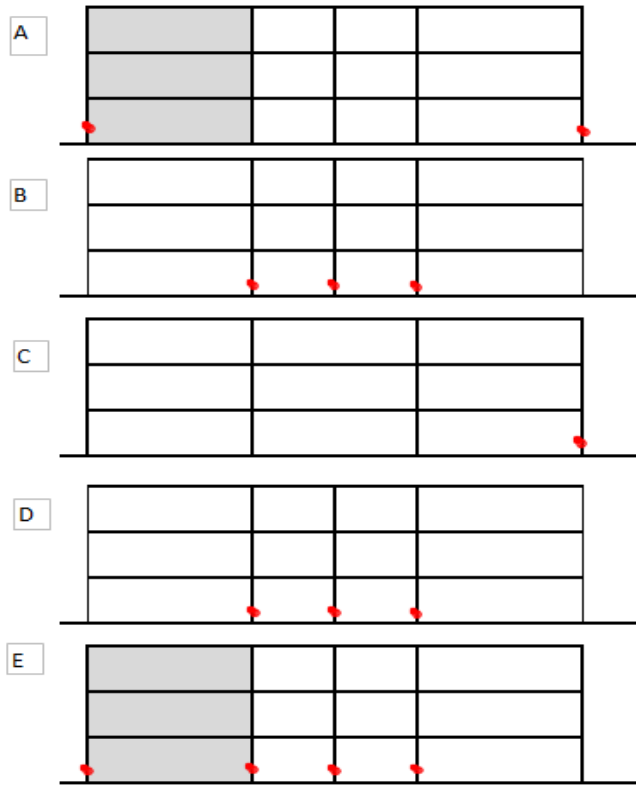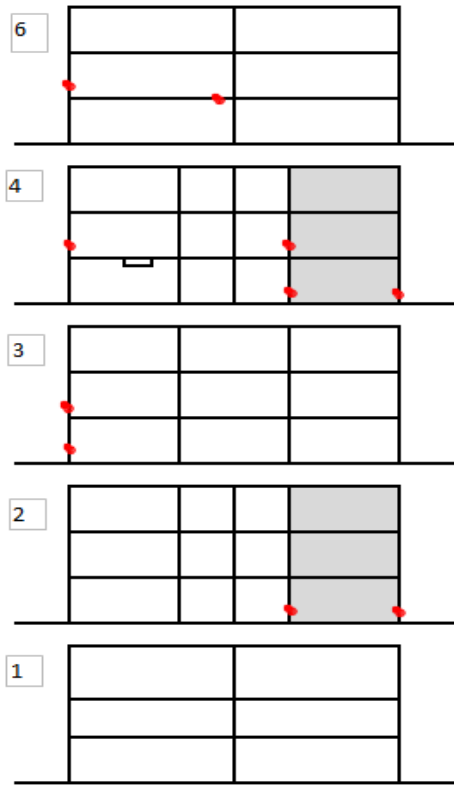
3748H1 Degrading

5831H1 Non-Degrading

5831H1 Degrading

112

6888H1 Non-degrading

6888H1 Degrading

6889H1 Non-Degrading

6889H1 Degrading

114

6952H1 Non-degrading

6952H1 Degrading

115
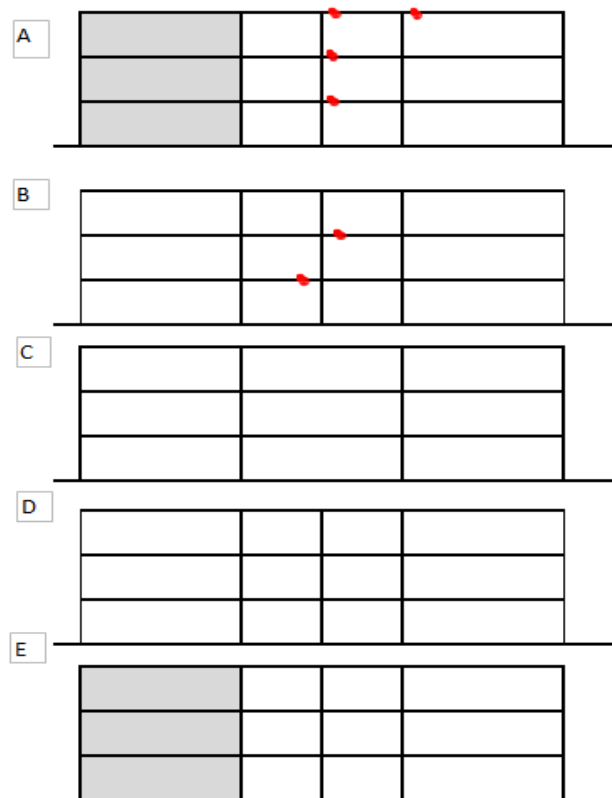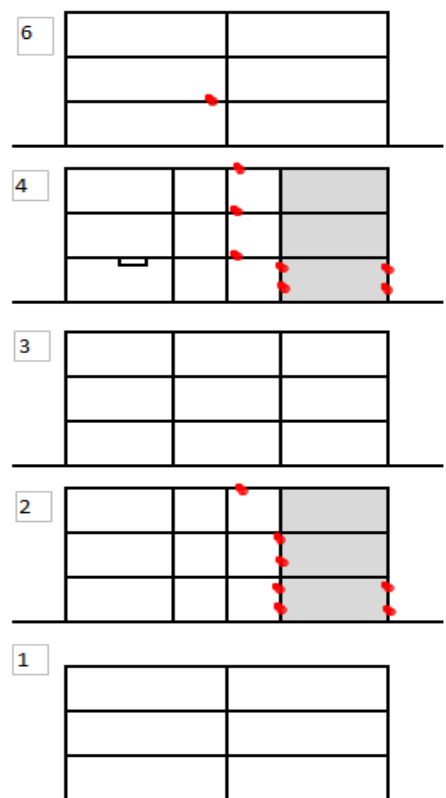
APPENDIX A.7. : Earthquake records that were used in the analyses in g units.

138_H1

138_H2

900_H1

900_H2
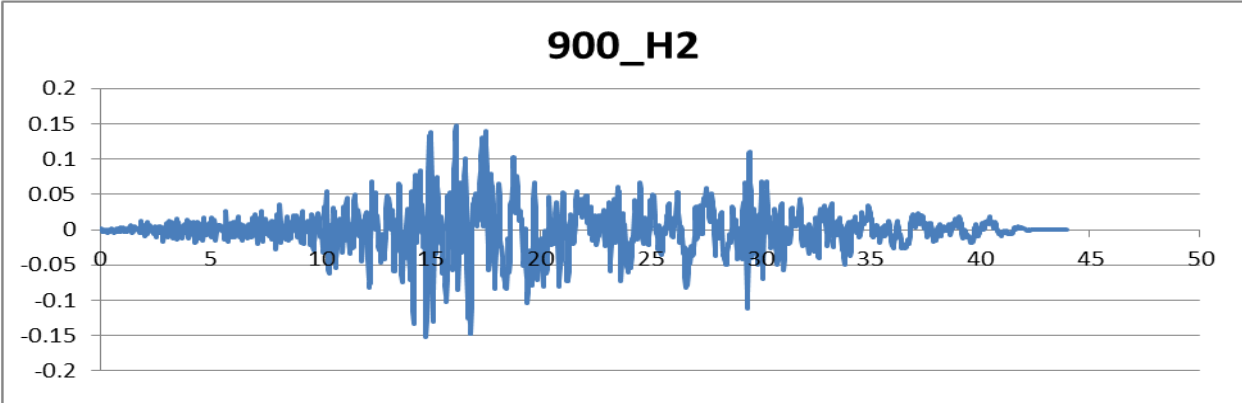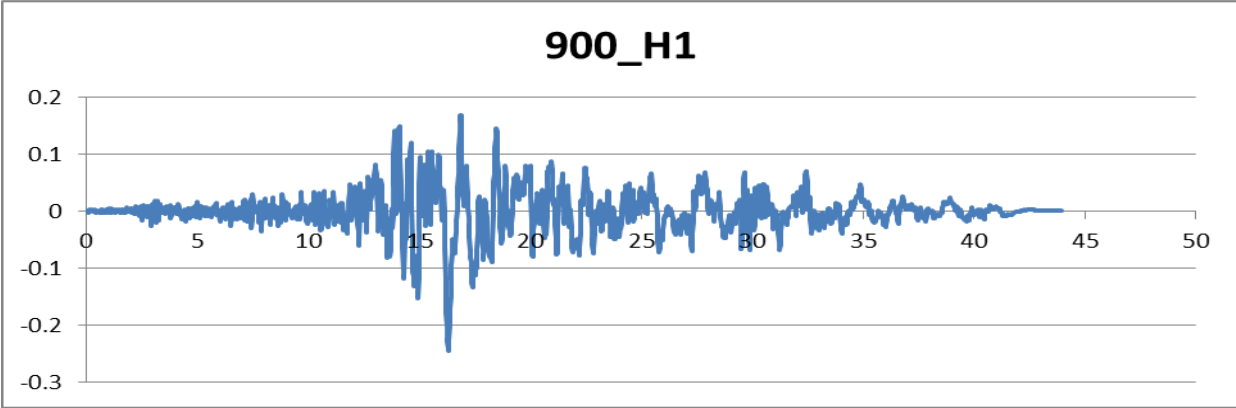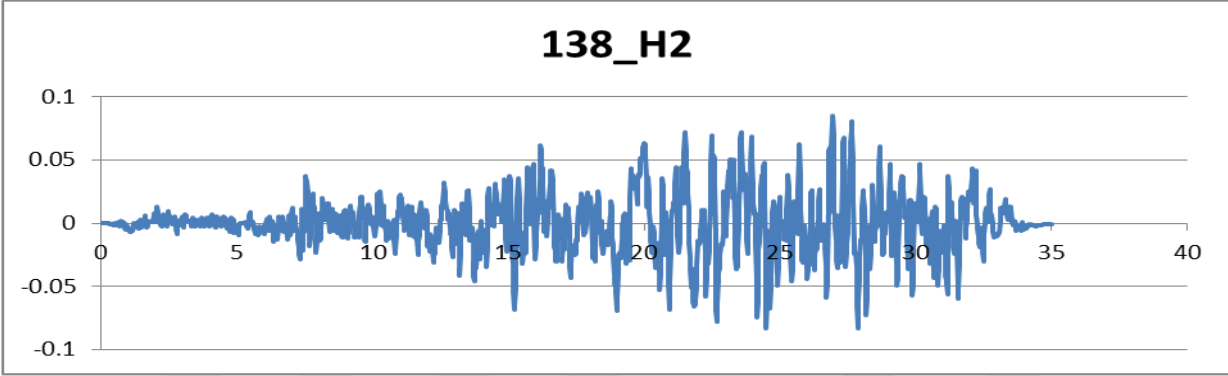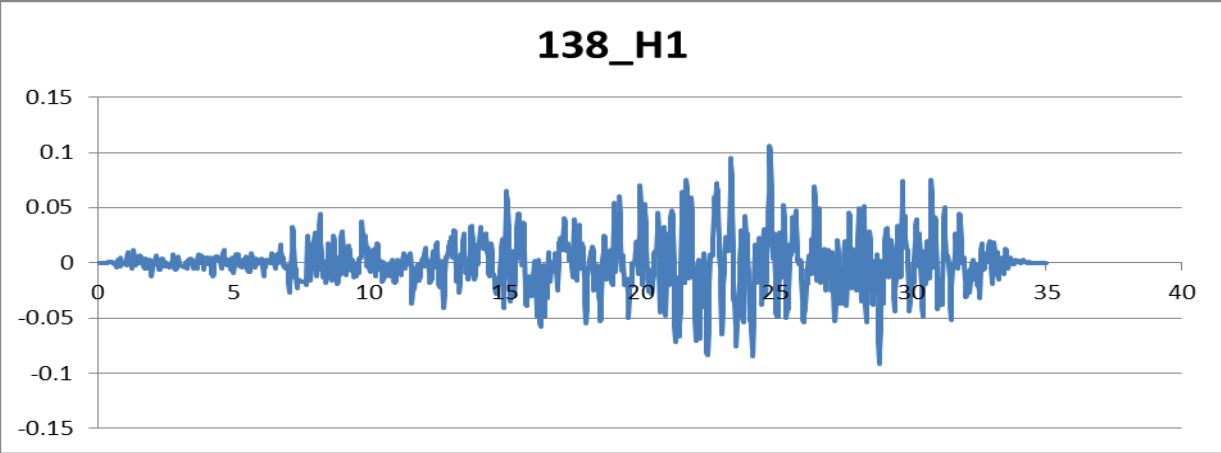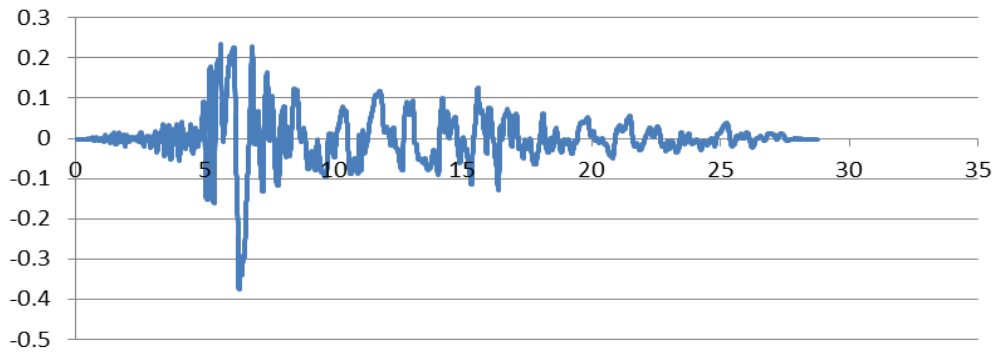
3748_H1

3748_H2
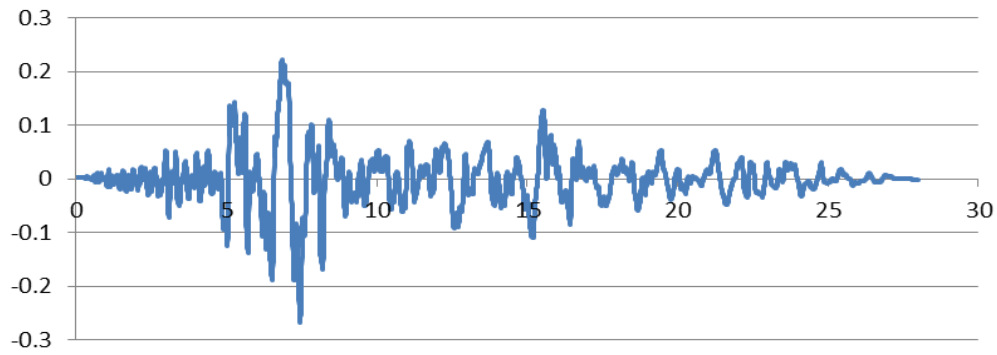
5831_H1
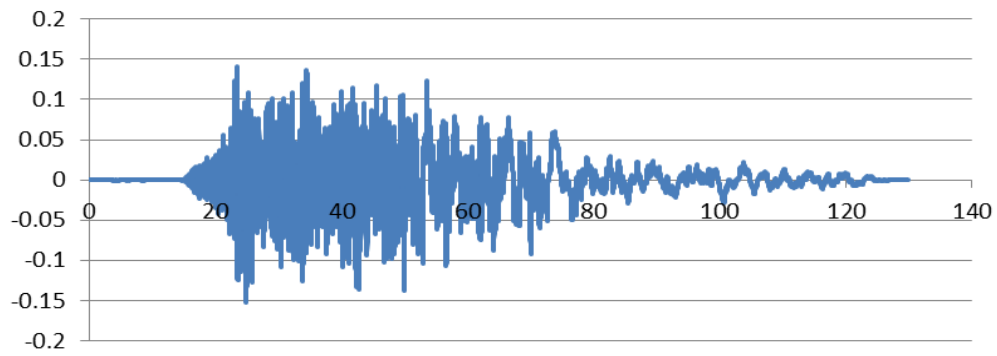
5831_H2
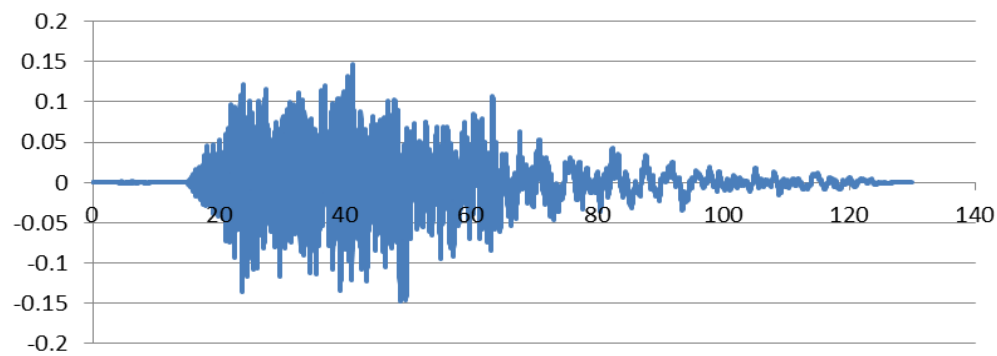
6888_H1
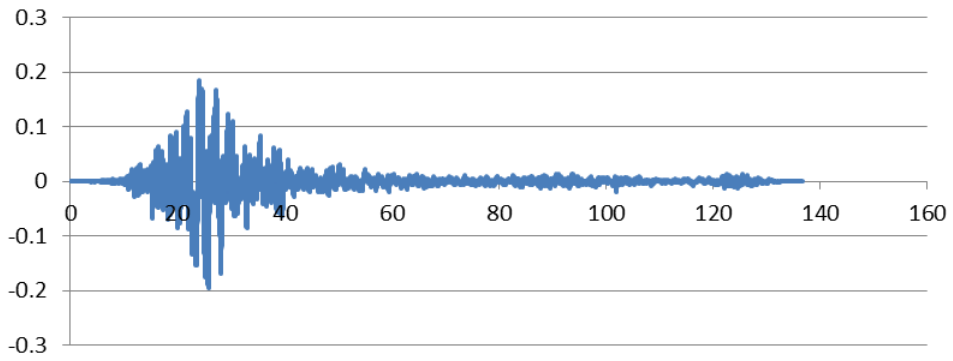
6888_H2

6889_H1
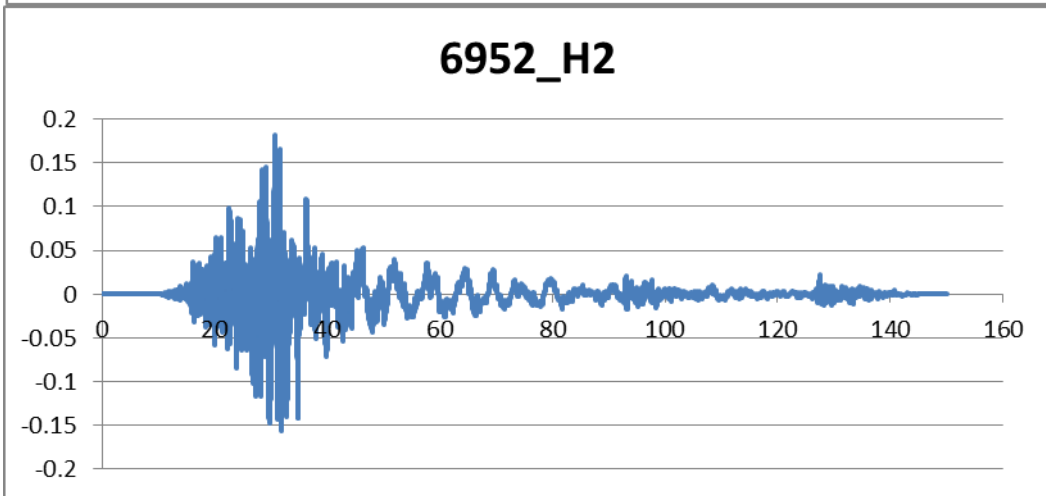
6889_H2

118
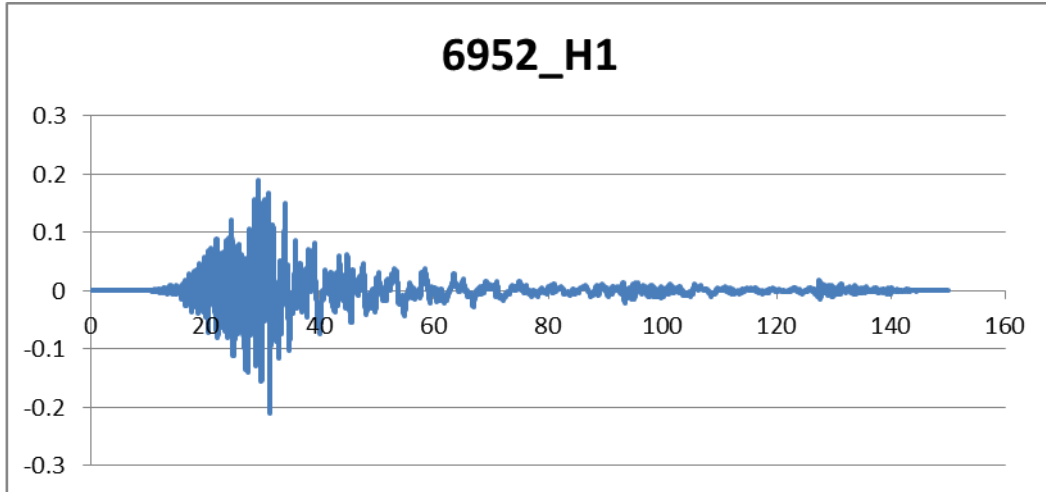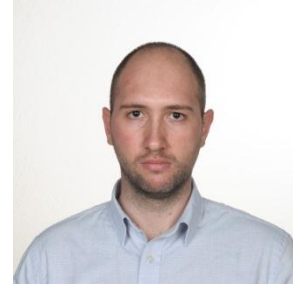
6952_H1
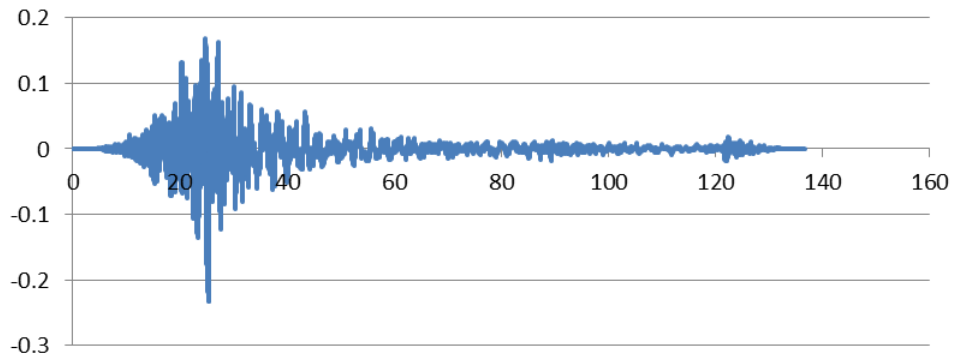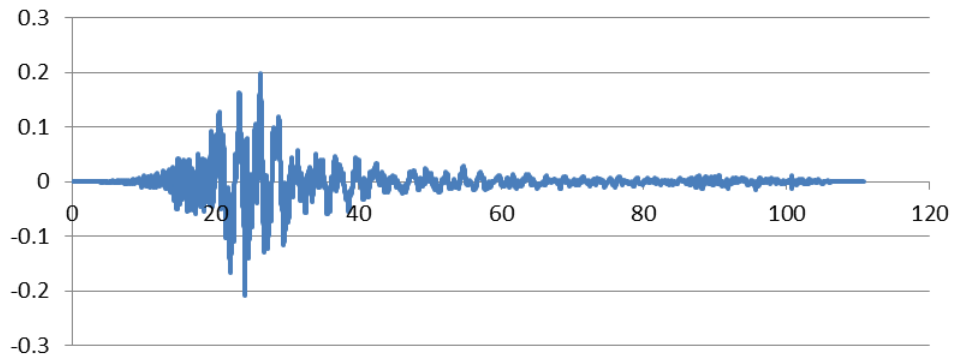
6952_H2
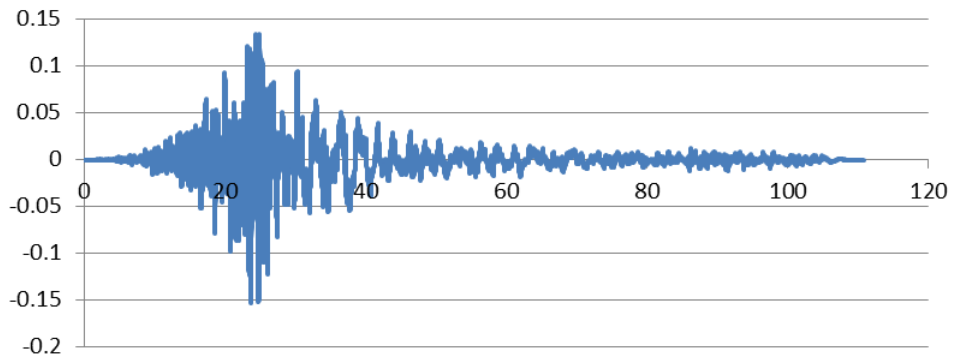
CURRICULUM VITAE

Name Surname: Doruk Uçak

Place and Date of Birth: İstanbul 13.08.1990

E-Mail: dorukucak@live.com

B.Sc.:

2013, University at Buffalo, Civil Engineering, Environmental Engineering (double major)

2012, Istanbul Technical University, Environmental Engineering (dual-degree program)

Professional Experience and Rewards:

2016-Present, Ata GYO, Istanbul, Turkey

2012-2015, PARSONS Corporation, Buffalo, NY

Engineer in Training Certificate, New York State Board of Education, 2014